

CONDUCTION THROUGH THIN
TITANIUM DIOXIDE FILMS

Thesis by

Joseph Maserjian

In Partial Fulfillment of the Requirements

For the Degree of
Doctor of Philosophy

California Institute of Technology

Pasadena, California

1966

(Submitted April 4, 1966)

ACKNOWLEDGMENTS

The author is indebted to his advisor, Dr. C.A. Mead for his inspiration and encouragement and for making this research possible. Sincere appreciation is offered to the California Institute of Technology Jet Propulsion Laboratory for their financial support. In particular, thanks are offered to the author's supervisors at Jet Propulsion Laboratory who have been extremely generous and patient during the course of this work. Special acknowledgment is due to the author's wife Patricia for her many sacrifices during this endeavor and for typing the final manuscript of this thesis.

ABSTRACT

Conduction through TiO_2 films of thickness 100 to 450 \AA have been investigated. The samples were prepared by either anodization of Ti or evaporation of TiO_2 , with Au or Al evaporated for contacts. The anodized samples exhibited considerable hysteresis due to electrical forming, however it was possible to avoid this problem with the evaporated samples from which complete sets of experimental results were obtained and used in the analysis. Electrical measurements included: the dependence of current and capacitance on dc voltage and temperature; the dependence of capacitance and conductance on frequency and temperature; and transient measurements of current and capacitance. A thick (3000 \AA) evaporated TiO_2 film was used for measuring the dielectric constant (27.5) and the optical dispersion, the latter being similar to that for rutile. An electron transmission diffraction pattern of a evaporated film indicated an essentially amorphous structure with a short range order that could be related to rutile. Photoresponse measurements indicated the same band gap of about 3 ev for anodized and evaporated films and reduced rutile crystals and gave the barrier energies at the contacts.

The results are interpreted in a self consistent manner by considering the effect of a large impurity concentration in the films and a correspondingly large ionic space charge. The resulting potential profile in the oxide film leads to a thermally assisted tunneling process between the contacts and the interior of the oxide. A general relation is derived for the steady state current through structures of this kind. This in turn is expressed quantitatively for each of two possible limiting types of impurity distributions, where one type gives barriers of an exponential shape and leads to quantitative predictions in close agreement with the experimental results. For films somewhat greater than 100 Å, the theory is formulated essentially in terms of only the independently measured barrier energies and a characteristic parameter of the oxide that depends primarily on the maximum impurity concentration at the contacts. A single value of this parameter gives consistent agreement with the experimentally observed dependence of both current and capacitance on dc voltage and temperature, with the maximum impurity concentration found to be approximately the saturation concentration quoted for rutile. This explains the relative insensitivity of the electrical properties of the films on the exact conditions of formation.

TABLE OF CONTENTS

I.	Introduction.....	1
II.	Experiments on Anodized TiO_2 Films.....	6
	A. Preparation of Specimens.....	6
	B. Measurements of Anodized Films.....	10
	C. Discussion of Results on Anodized Samples...	29
III.	Experiments on Evaporated TiO_2 Films.....	41
	A. Preparation of Evaporated Specimens.....	41
	B. Measurements of Evaporated TiO_2 Films.....	49
	1. Thickness Measurements.....	49
	2. Optical Measurements.....	53
	3. Photoelectric Measurements.....	58
	4. Electrical Measurements.....	62
	C. Discussion of Results on Evaporated Films...	80
IV	Theory.....	95
	A. The Barrier Potential	95
	1. Impurity-Space-Charge Models.....	95
	2. Image Force Corrections.....	102
	3. Effective Barrier Approximations.....	103
	4. Effect of Statistical Fluctuations.....	104
	B. Transport Theory.....	107
	1. General Equations.....	107
	2. Current for the Intermediate Case.....	110
	3. The Two Barrier Problem.....	112
	4. Formulation in Terms of Proposed Barriers.....	120
	C. Application of the Theory.....	126
	1. General Considerations.....	126
	2. Current Dependence.....	128
	3. Capacitance Dependence.....	139
V	Conclusions.....	146
APPENDIX A.	Properties of Rutile.....	151
APPENDIX B.	Experiments on Rutile.....	157
REFERENCES	163

I. INTRODUCTION

The subject of conduction through thin insulating films has received much attention since the earliest observations of Schuster⁽¹⁾ in 1874 on tarnished copper wire. The underlying theoretical principles have since been well established so that the primary challenge remaining during the last few decades has been to apply these principles to a physical model or mechanism which satisfactorily explains the observed electrical properties. Among the many specialized treatments available in the literature, none has been found directly applicable to the results considered here. However, a theoretical description of the results has been derived in this work which is closely related to some of the earliest ideas.

Two important mechanisms based on relatively simple physical models were first introduced in the "thirties" and remain to this day often the starting point in attempting to explain many experimental observations of thin insulating films. There is the well-known mechanism of quantum-mechanical tunneling of electrons through a narrow potential barrier or insulating region, originally introduced by Frenkel⁽²⁾ in 1930 and developed further by Wilson⁽³⁾, Nordheim⁽⁴⁾, and Frenkel and Joffé⁽⁵⁾, in 1932. Opposite this is the mechanism

involving thermal excitation of electrons over the barrier, developed by Schottky and his collaborators⁽⁶⁾ in the following years. Each of these mechanisms proposed to explain the properties of the early metal-semiconductor rectifiers, but conflicted in their predictions of the direction of rectification and other device properties. A controversy existed for several years over which of these two processes applied to the typical rectifying devices of that era. The thermionic process eventually gained widespread acceptance⁽⁷⁾ primarily because it appeared to conform with the observed direction of rectification, gave the correct order of magnitude for current based on reasonable estimates of barrier thickness, and predicted a temperature dependence in qualitative agreement with experiment. In fact, this acceptance became so strong that little further consideration was given to the tunneling mechanism until recent years when attention focused on semiconductor tunnel diodes, the study of very thin insulating films in connection with cold emission of hot electrons⁽⁸⁾, and tunneling between superconducting films⁽⁹⁾.

The original tunneling theory has most recently been extended by Simmons⁽¹⁰⁾ and Stratton⁽¹¹⁾ to describe more generally the effects of image forces and other departures from a simple rectangular potential barrier. Most attempts

at quantitative comparisons of experimental results with the theory have had relatively poor success. This is not too surprising in view of the simplifying assumptions necessarily involved. At least two recent results can be cited which do give satisfactory quantitative agreement. The work of Hartman and Chivian⁽¹²⁾ on extremely thin aluminum oxide films has provided good agreement but required some arbitrary fitting of unknown properties of the oxide. McCall's results⁽¹³⁾ on extremely thin films of mica cleaved from single crystals demonstrated that it was possible to introduce independently determined properties of mica into the theory and still obtain agreement at least over a limited range of conditions.

The application of a tunneling theory to films thicker than about 50 Å is generally excluded because of the unreasonably small currents predicted. However this is true only if the electrons must tunnel through the entire film thickness. In fact the original theory was used, during the controversy over the mechanism of rectification, to describe tunneling through only a very narrow ionic space charge barrier created at the metal contact on a much thicker semiconducting layer. Relatively thick barriers of this kind at metal-semiconductor interfaces have been extensively considered in connection with the thermionic process ("Schottky emission") that had

been further developed by Mott⁽¹⁴⁾ and Schottky⁽¹⁵⁾ and are commonly referred to as Schottky barriers. Since the original ideas were first introduced, the concept of tunneling through very thin Schottky type barriers appears to have been generally ignored. It will be shown that the experimental results on titanium dioxide (TiO_2) thin films can be explained on the basis of such a physical model. However, the original theory had not been carried sufficiently far to satisfactorily account for the observed electrical properties and temperature dependence. The theory is extended in Chapter IV, considering in some detail the effect of the ionic space charge and the problem of charge transport through the resulting barriers, and leads to relationships that agree with the experimental results.

Although there is little information available on the physical properties of TiO_2 thin films, there have been detailed studies made of rutile (TiO_2) ceramics and single crystals with comprehensive surveys of the literature having been reported by Grant⁽¹⁶⁾, Frederikse⁽¹⁷⁾, and Hollander and Castro⁽¹⁸⁾. Experimental evidence will be given which indicates that the film structure, although highly disordered, retains properties that are similar to that of rutile. Some of the more relevant properties of rutile are discussed in

Appendix A and some experimental results on rutile are given in Appendix B.

Experimental results have been obtained from both anodized and evaporated TiO_2 films. The anodized films, described in Chapter II, exhibited effects that are attributed to ionic migration induced by the applied voltage, making it difficult to obtain reproducible results. These electrical "forming" tendencies were successively avoided with the evaporated films. Therefore most of the detailed results are obtained from the evaporated films described in Chapter III.

II. EXPERIMENTS ON ANODIZED TiO_2 FILMS

A. Preparation of Specimens

The techniques used for fabricating the anodized titanium specimens may be divided into three parts: (1) the preparation of the titanium substrate, (2) the anodization procedure, and (3) the deposition of metal contact.

Two methods were used in preparing titanium surfaces for anodization. The first method started with 20-mil-thick sheets of commercial-grade titanium (99% pure). The sheets were cut into rectangular strips $7/8" \times 3"$ and heat treated under high vacuum for several hours. This was accomplished by passing approximately 100 amps along the length of the strips in order to heat them to slightly below their melting point ($1800^{\circ}C$), while maintaining a slight tension at the contacts to prevent buckling. The heat treatment was performed in a Veeco 400 high-vacuum system equipped with a liquid nitrogen trap. It was possible to maintain vacuums less than 10^{-7} torr during the heat treatment because of the additional gettering action of titanium sublimating from the heated strip. The heat treatment served to purify the titanium by distilling out most of its impurities, as well as crystallize the metal with crystallites measuring the order of one centimeter.

across. Many slippage lines appeared in the individual crystallites. The strips were subsequently cut into smaller rectangles $3/16" \times 1"$ and lapped on one side with #600 SiC paper. The central $3/4"$ of the lapped surfaces were electropolished to a mirror finish using a Buehler electropolisher with the recommended solution. The samples were rinsed repeatedly and boiled in distilled water before anodizing.

The second method of preparing the titanium surface was accomplished by evaporating zone-refined titanium (99.999% pure) onto a glazed alumina substrate $.030" \times 1/2" \times 1"$ (commercially obtained under the name "Smoothstrate"). This substrate was chosen because it is smoother than commonly used glass slides or cover glass. The evaporation was carried out in a Veeco 400 system. The titanium was evaporated from a water-cooled copper crucible by means of electron bombardment. The substrate located 10 cm above the titanium source was heated to 380°C several minutes prior to and during the evaporation of the titanium. A sublimating titanium strip located in the upper part of the bell jar provided additional gettering action as mentioned above, and insured vacuums of less than 10^{-6} torr during evaporation. The evaporation was performed during a period of 5 to 10 seconds while exposing the substrate to the

evaporating source of titanium by means of a movable shutter. Films the order of 1000 Å thick were insured by observing a glass monitor slide located adjacent to the substrate and closing the shutter at the point the slide just became opaque. The rate and thickness of evaporation were so chosen to provide very smooth titanium surfaces. The substrates were placed directly into the anodizing solution after this evaporation process.

The anodization process used an electrolyte of either concentrated ammonium citrate or ammonium borate solution. The choice of either electrolyte had no noticeable effect on the results. The solution was at room temperature and agitated with a magnetic stirring rod during anodization. The substrate was submerged to about three fourths of its length at one side of the vessel with electrical contact made to the exposed titanium. A platinum cathode was inserted at the opposite side of the vessel. The anodization was carried out either at constant current or constant voltage. The constant-voltage method which is normally used⁽¹⁹⁾ was accomplished by applying the desired voltage across the cell until the anodization current dropped to some small constant value (<0.1 ma) during a period of several minutes. The constant-current method was used to gain some comparative

information on the effect of the anodization process. Currents of 0.9, 2.5, and 8 ma were applied until the desired voltage was reached across the cell. After anodizing, the specimens were thoroughly rinsed in distilled water, dried with a jet of pure nitrogen gas, and immediately placed in the vacuum system for the next operation of depositing metal contacts.

Gold was deposited as contacts on all anodized specimens. The gold was evaporated from a tungsten filament through stainless-steel masks. In some cases, a single mask was used having uniformly spaced holes ten mils in diameter. In other cases, two masks were used, one providing thirteen rectangular contacts 20×250 mils spaced uniformly along the substrate, the other with 6-mil holes providing 12 groups of 12 dots each located between the rectangular contacts. The rectangular contacts were designed for photoresponse measurements and required film thicknesses the order of 500 \AA . This was accomplished with a glass monitor slide in a manner similar to that already described. After evaporating the rectangular contacts, the mask was changed using a mechanical jig which provided registration, and the remainder of the gold on the filament evaporated through the second mask providing gold dots at least 1000 \AA thick. The evaporation were performed in a vacuum of less than 10^{-6} torr with the substrate at

room temperature after it had been under high vacuum for a few hours.

B. Measurements of Anodized Films

Electrical measurements of the anodized films were influenced by large hysteresis and time-dependent effects. This was a general characteristic of all the anodized films tested regardless of the method of preparation. Consequently, the results presented in this section are in large part of a qualitative nature, but are useful in supporting the ideas to be applied later.

The electrical measurements were made by contacting a gold dot with a pointed 3-mil gold wire with the aid of a micromanipulator. The pressure applied by the point contact gave no noticeable effect on the electrical characteristics.

The time dependence of current with a relatively large constant positive voltage applied at the gold contact is typified by the result given in Fig. II-1. The measurement was made by applying successively longer pulses at constant voltage from a low-impedance source, while recording the current response on an oscilloscope at correspondingly slower sweeps. A chart recorder was started simultaneously with the slowest sweep on the oscilloscope (5 sec/cm). The discontinuities result from some hysteresis effects even though

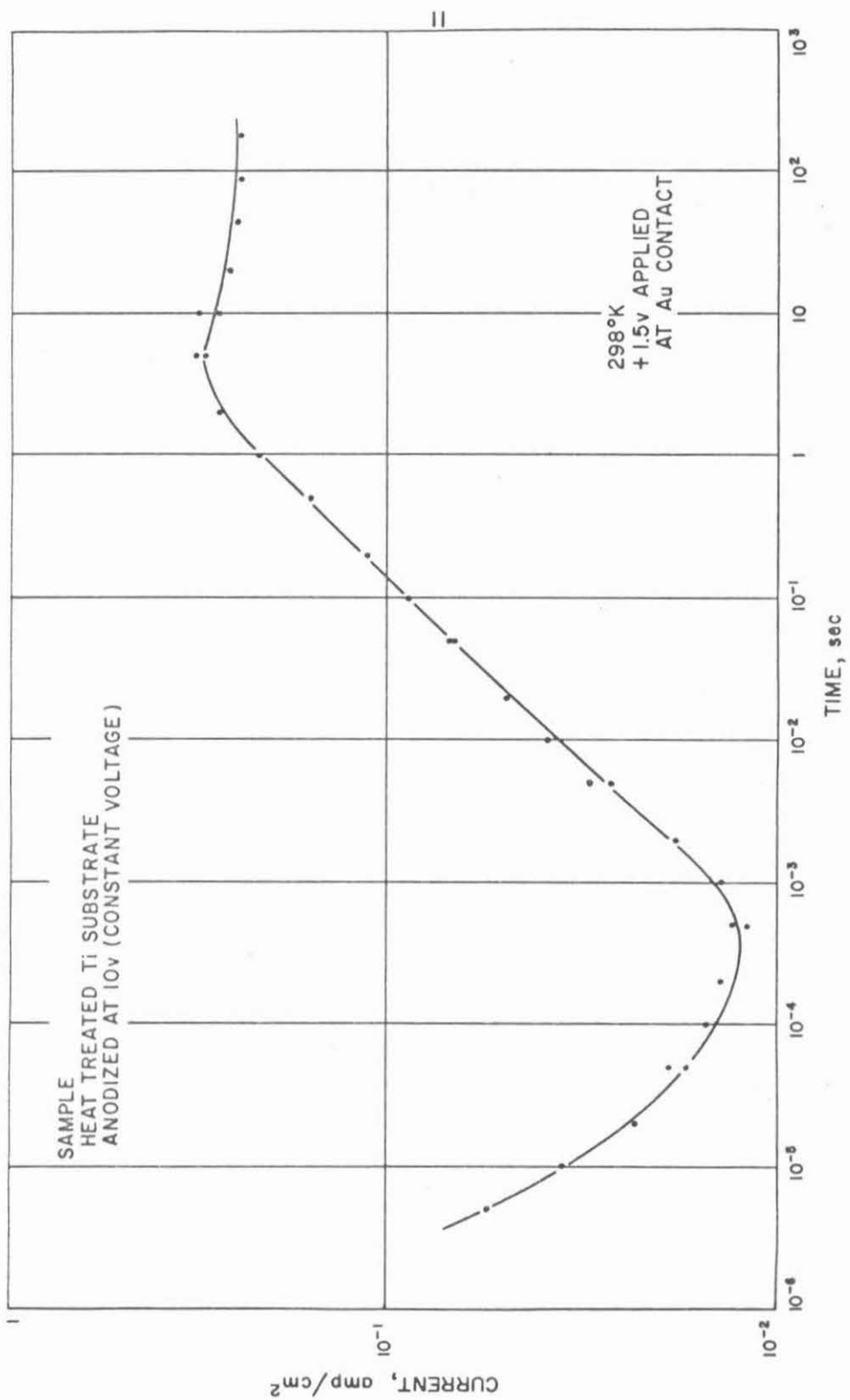


Figure II-1. Current versus time at large positive bias

minimum pulse durations were applied in preceding pulses. Other samples exhibited a similar time dependence at large positive bias, the onset and rate of current rise and the maximum value increasing with positive voltage. The current rise would first appear in the vicinity of 1 volt positive bias at room temperature and at much larger voltages at low temperatures as will be discussed later in this section. The samples undergo large changes in electrical characteristics after being subjected to dc voltages of this magnitude. These characteristics would usually partially recover over periods of hours. For lower positive voltages and for negative voltages (below breakdown), no current rise in the time response was observed and the current would continue to decrease more slowly from the foot of the initial decay to some asymptotic value. At sufficiently large negative voltages an abrupt breakdown (B_d) would occur before a current increase with time could be observed.

The capacitance of the samples was measured at 100 kc on a Boonton 74C capacitance bridge. The sample used in Fig. II-1 measured 595 pf prior to the above measurements, 682 pf immediately afterwards, partially recovering to 658 pf after several minutes. The external series resistance used in the measurements for Fig. II-1 was 100 ohms,

therefore the external time constant of the RC circuit was only $0.06 \mu\text{sec}$. The oscilloscope limited the response to about $1 \mu\text{sec}$. The observed decay time was approximately $100 \mu\text{sec}$ which corresponds to the RC value obtained if one takes R to be the maximum resistance of the oxide occurring at the minimum in the current response. This leads one to suspect that the observed decay may be associated with a redistribution of trapped electrons in the oxide film⁽²⁰⁾.

The dc I-V characteristics were obtained by adjusting the applied current to the desired value and allowing sufficient time for the voltage to reach a nearly constant value. The results given in Fig. II-2 were obtained from a typical sample from the same substrate used for Fig. II-1. A log-log plot is included for comparison with other results. The measurements were made in this case by alternately applying positive and negative currents in decreasing steps starting from the maximum current of 0.03 ma. This sequence of measurements permitted the maximum changes to occur in the sample during the initial measurements. The sample is seen to exhibit a strong rectification property in this case. At larger currents the samples would usually break down or undergo an irreversible change to a lower impedance characteristic.

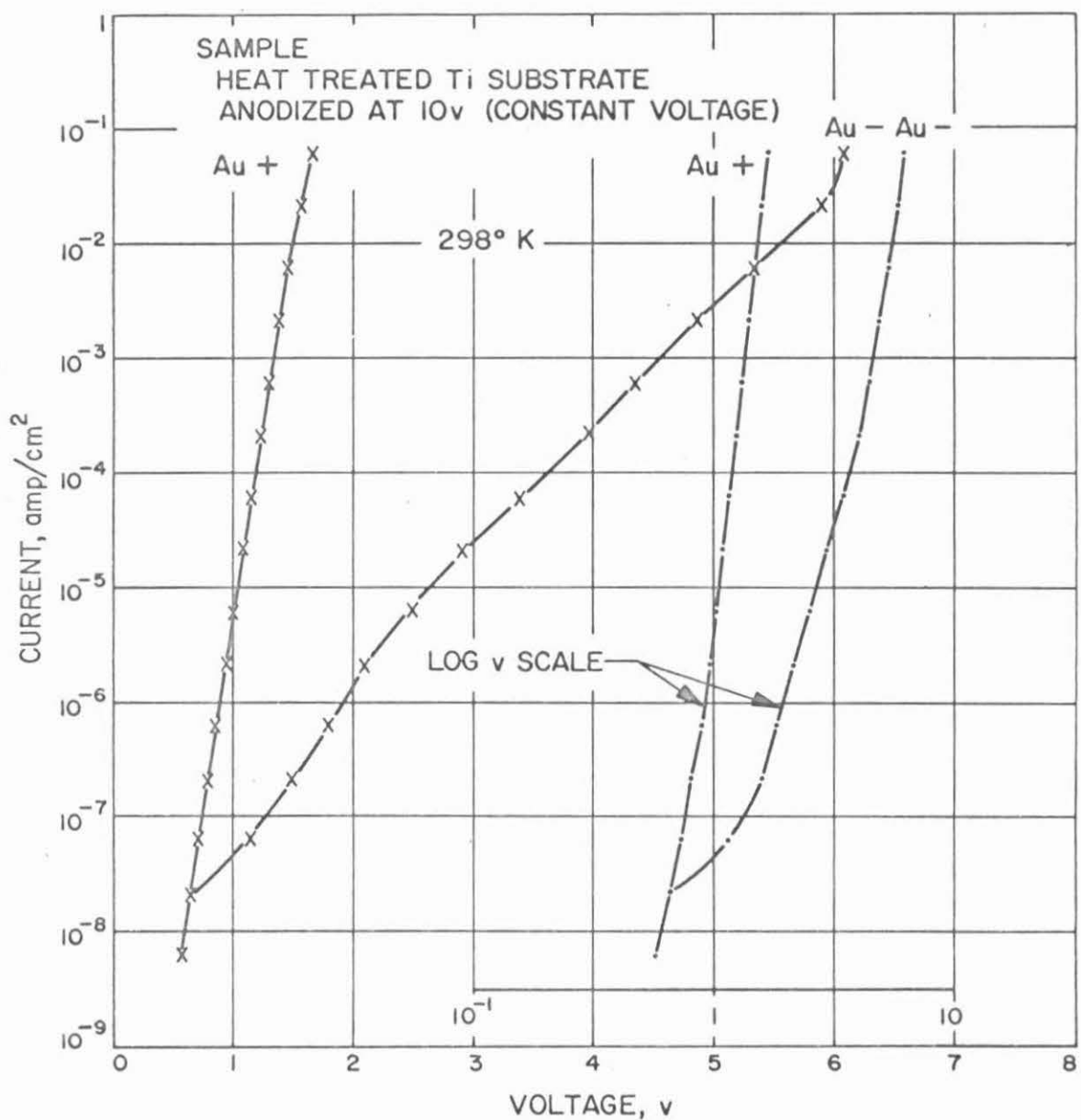


Figure II-2. Current versus dc voltage

The capacitance was observed to vary considerably as a function of dc voltage. Measurements performed on most samples were complicated by the hysteresis effects mentioned above. The result given in Fig. II-3 measured at 100kc typifies the kind of dependence observed and was selected from a sample exhibiting a minimum of hysteresis; that is, its capacitance returned to its initial value at zero bias (C_i) after the positive voltages had been applied. A variation of capacitance with voltage is suggestive of Schottky type barriers. Barriers of this kind exhibit a linear relation between $(1/\text{capacitance})^2$ and voltage, and for this reason the data given in Fig. II-3 were plotted in the form shown; however, the result clearly does not indicate this dependence. The relation arising from exponential barriers as discussed in Chapter IV suggests the plot given in Fig. II-4. In this case a reasonable correspondence with the assumed dependence is obtained.

Samples prepared by anodizing heat-treated titanium sheet at constant current gave characteristics similar to those discussed above except the drift and hysteresis effects were enhanced. For this reason these samples were used to examine the effects further. It was impractical to obtain useful measurements at room temperature because of the complications arising from the tendency of the

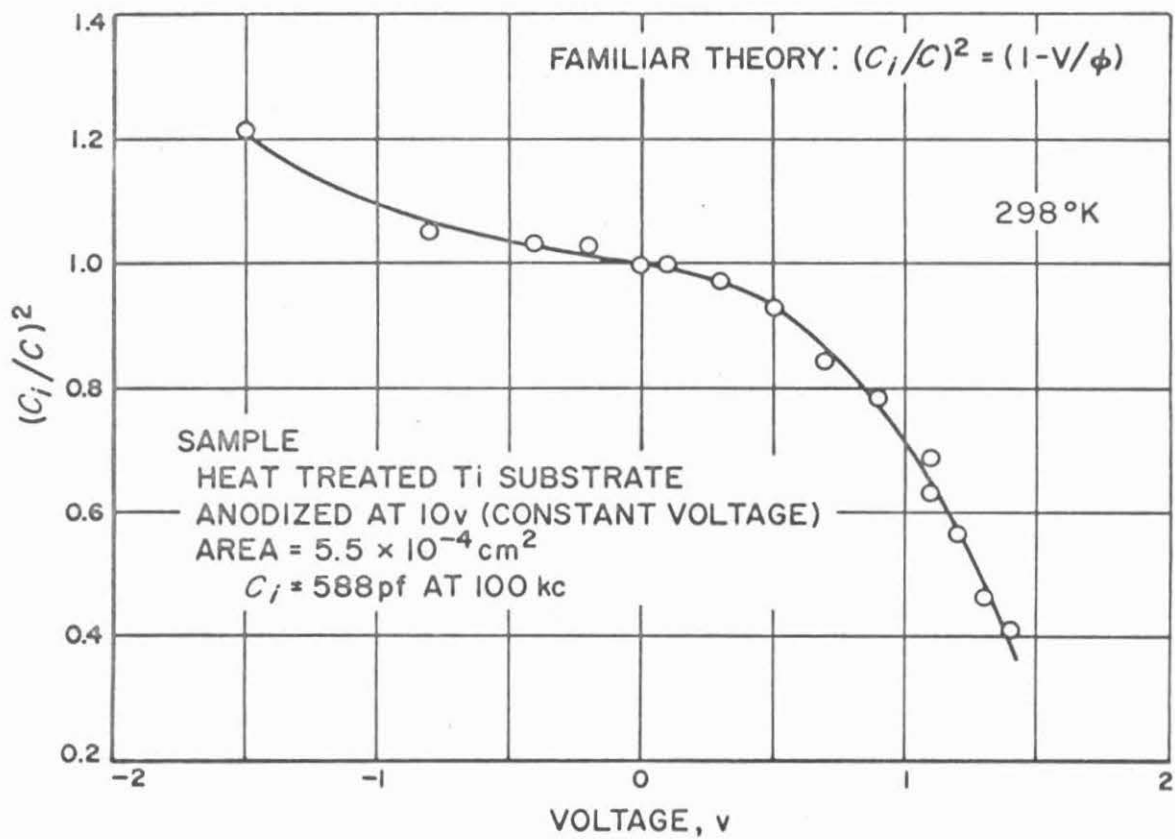


Figure II-3. Dependence of capacitance on dc voltage

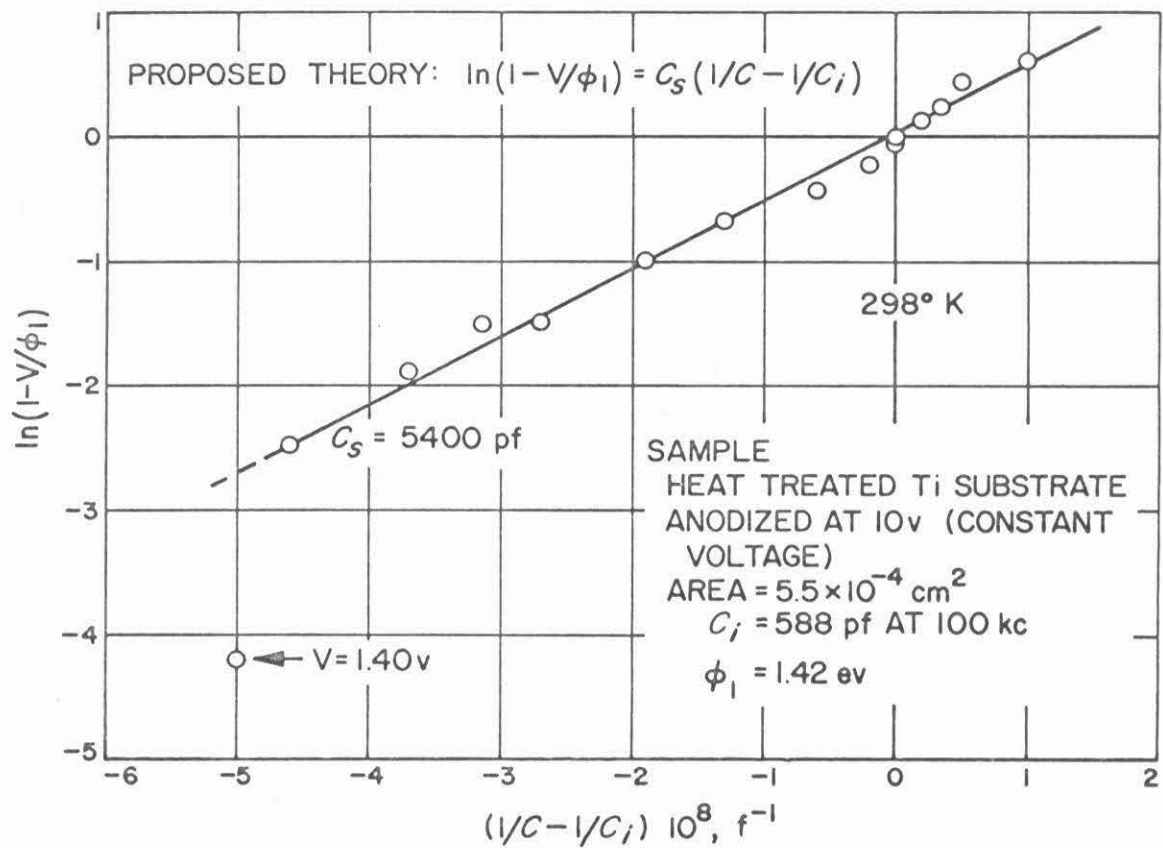


Figure II-4. Linearized plot of capacitance versus dc voltage

samples to gradually recover towards their initial condition following the changes induced during each dc measurement. However, at 77°K the sample would remain in a stable condition determined by the maximum dc voltage previously applied as long as they were maintained at this temperature and the previous maximum voltage was not exceeded.

Fig. II-5 is typical of several samples that were measured in this way. Curve A represents the initial dc characteristic of a previously untested sample measured slowly at increasing currents. Curve B would result when decreasing the voltage from V_B and would remain stable until V_B was exceeded, whereupon a new stable characteristic, curve C would result from the new maximum voltage V_C . Changes of this kind have been reported for other films^(21,22) and have been attributed to a "forming" process that is associated with a redistribution of ions in the oxide film. The effects observed at room temperature were similar except for the fact that the characteristics would not remain stable after forming. In this case it appears that the ions have sufficient thermal energy in the presence of the built-in field to immediately start diffusing back into their original distribution; however, complete recovery is not usually attained. It might be speculated that some precipitation of impurities occurs

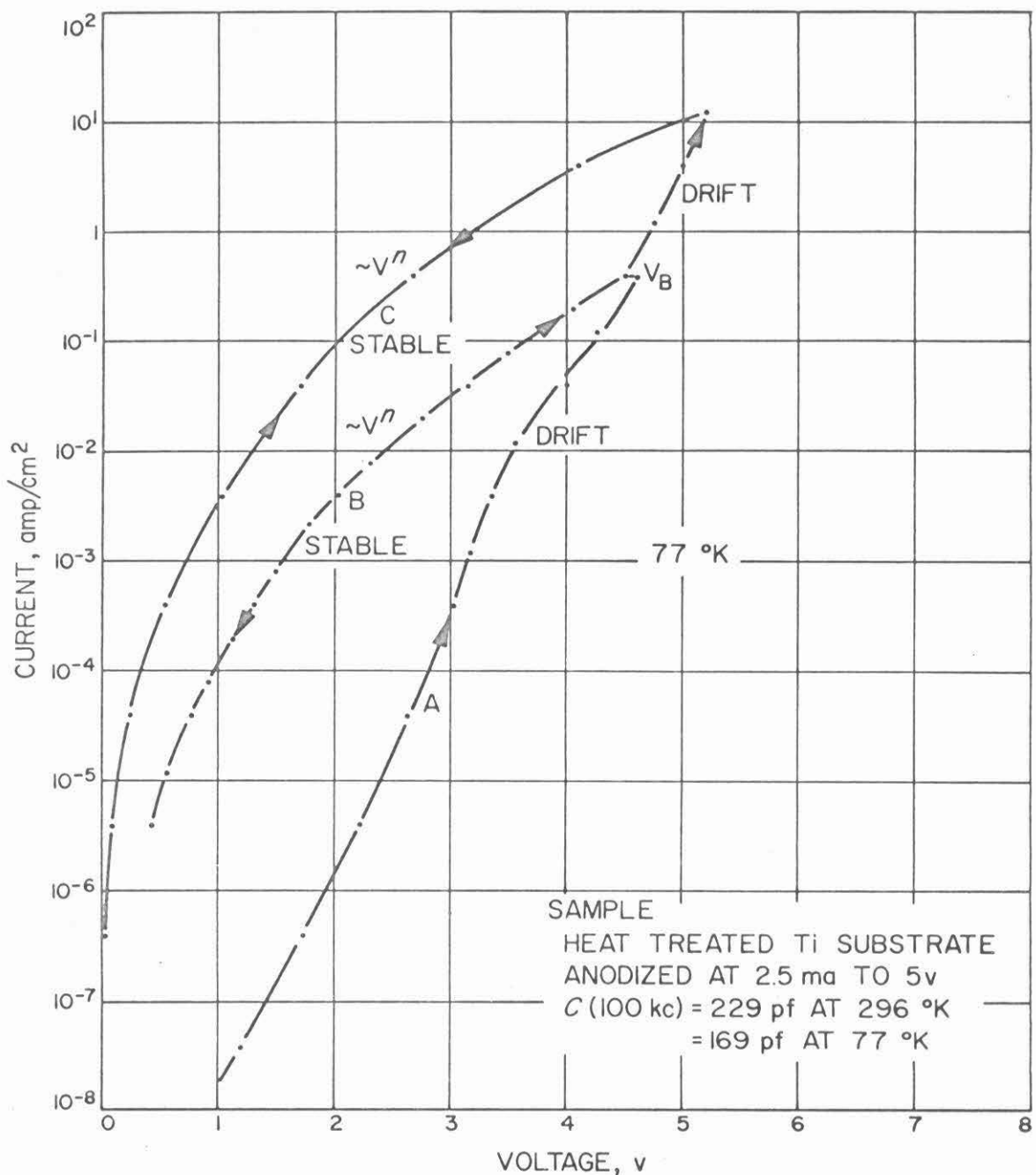


Figure II-5. Electrical forming characteristics

during each forming process in a manner that leaves the sample permanently in a lower impedance condition.

An attempt was made to relate the temperature dependence of the I-V characteristic to this forming process. With a constant positive current applied (10^{-4} amps for example), the sample would appear bi-stable during gradual heating and cooling cycles between 77°K and 296°K. The resulting voltage was observed to switch erratically between a lower value characteristic of the formed sample, meanwhile exhibiting a relatively small variation with temperature, and a higher value characteristic of the unformed sample, at this time exhibiting a much larger variation with temperature. The erratic nature of this process made more detailed measurements impractical.

Samples prepared by anodizing evaporated titanium films at constant voltage also gave characteristics similar to those already described. However in this case, a larger conductance and capacitance per unit area was measured from samples prepared at the same anodization voltage. They also exhibited more uniform characteristics than obtained from the other methods. For this reason, measurements were made on these samples designed to avoid electrical forming effects. For dc currents less than about $\pm 10^{-7}$ amps, the voltages

remained reproducible, with forming appearing at higher dc levels. However, at higher levels it was possible to use voltage pulses of sufficient length to observe an asymptotic limit for the current that preceded the onset of forming, provided the voltage was not too large. When obtained in this way, the current is believed to be representative of the undisturbed oxide film and will subsequently be referred to as I_p . The pulse measurements were made using a Rutherford pulse generator and applying consecutively positive and negative voltage pulses at increasing values while observing the limiting value of current on an oscilloscope. Fig. II-6 gives a typical result measured at room temperature. Measurements made in this way were nearly reproducible providing breakdown had not occurred, and therefore are believed to give the desired results. The direction of rectification is observed to be opposite to that obtained from the dc measurements given in Fig. II-2. Both polarities approach the limiting ohmic dependence at low voltages.

As mentioned previously, the current decay following the normal RC decay is characteristic of some internal resistance of the oxide films and is interpreted to be associated with trapped electrons. Of interest is the current which immediately follows the much shorter external RC decay.

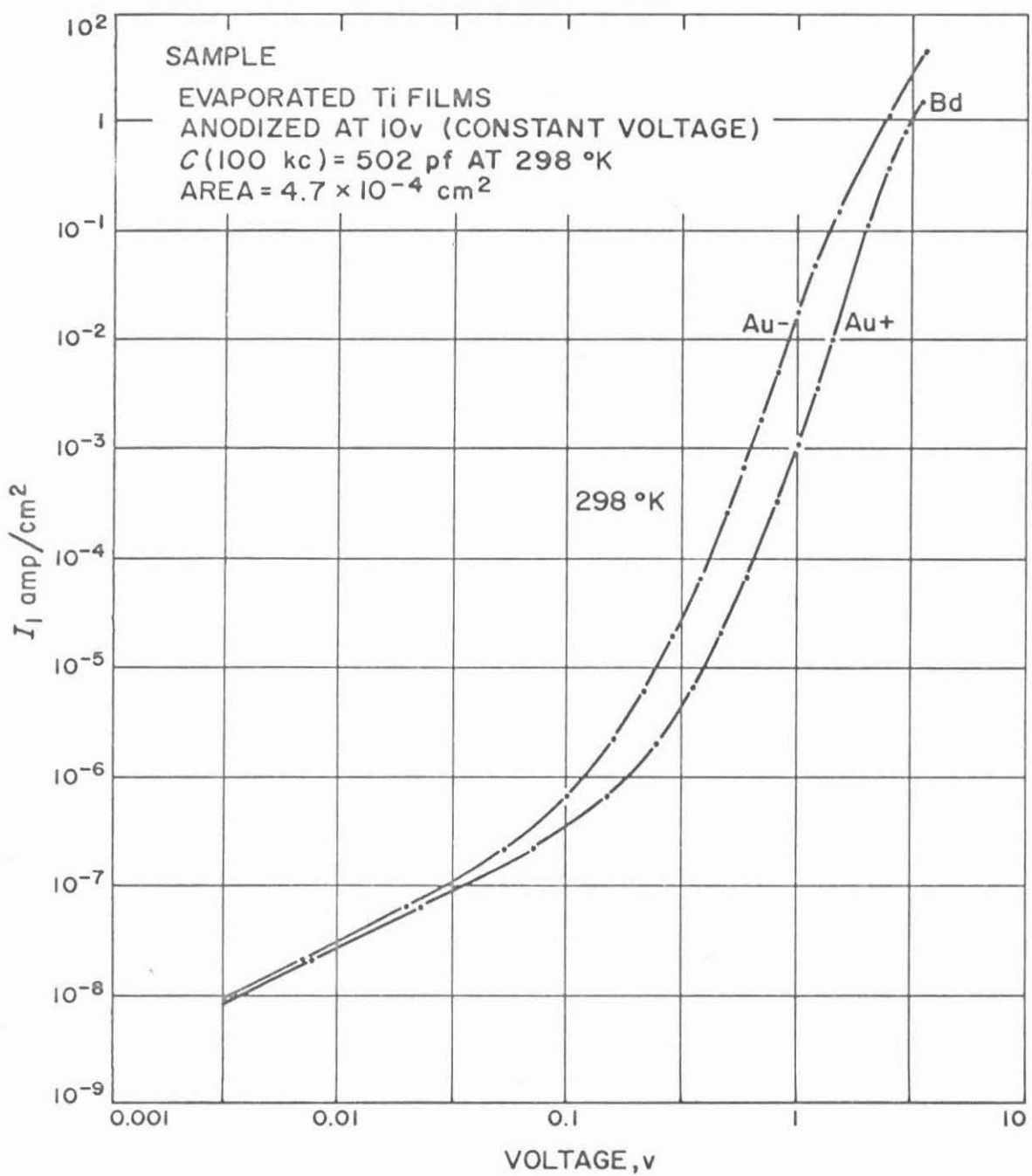


Figure II-6. Current (I_1) versus voltage

This current subsequently referred to as I_0 could then be interpreted to represent the current due to trapped electrons before they readjust to the steady-state distribution. Measurements of this kind were made by balancing out the external RC decay and recording the current and voltage transients on a dual-beam oscilloscope. Figure II-7 illustrates a typical transient response observed. The maximum current in the transient was taken as I_0 and the voltage measured at the same time the maximum occurred. The results obtained in this manner at 298°K for a typical sample are plotted in Fig. II-8 together with the I_1 -V curve measured from the same sample. The I_0 dependence is approximately ohmic and independent of polarity in the voltage range shown. At larger positive voltages the current rise appears at the beginning of the transient response. At the onset of this effect, I_0 must be equivalent to I_1 and correspond to the point where the curves meet. Breakdown usually occurs slightly above this point unless extremely short pulses are used. The capacitance obtained by balancing the RC decay was 285 pf as compared with 462 pf measured on the Boonton bridge at 100 kc. This difference which was typical in all samples measured is consistent with the idea involving a redistribution of trapped electrons and consequently an additional space-charge capacitance.

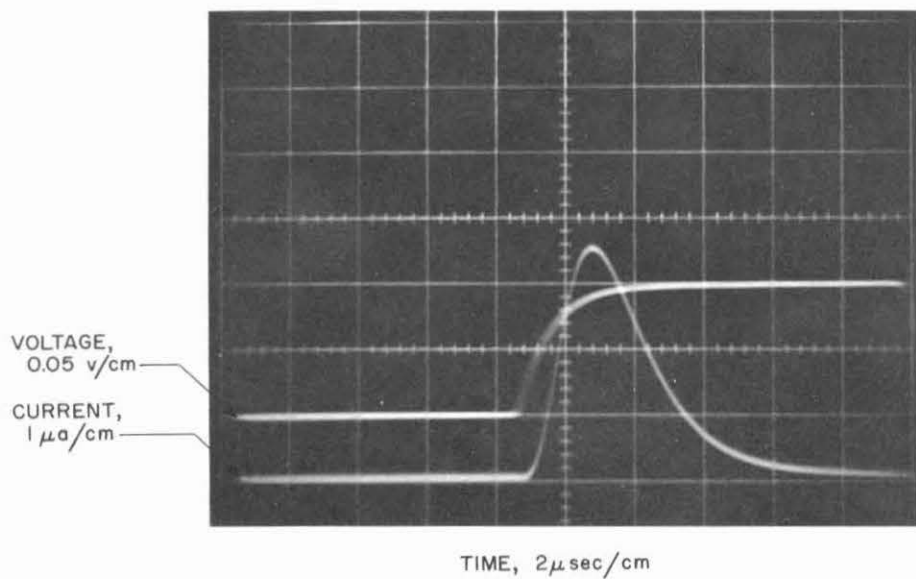


Figure II-7. Typical transient response

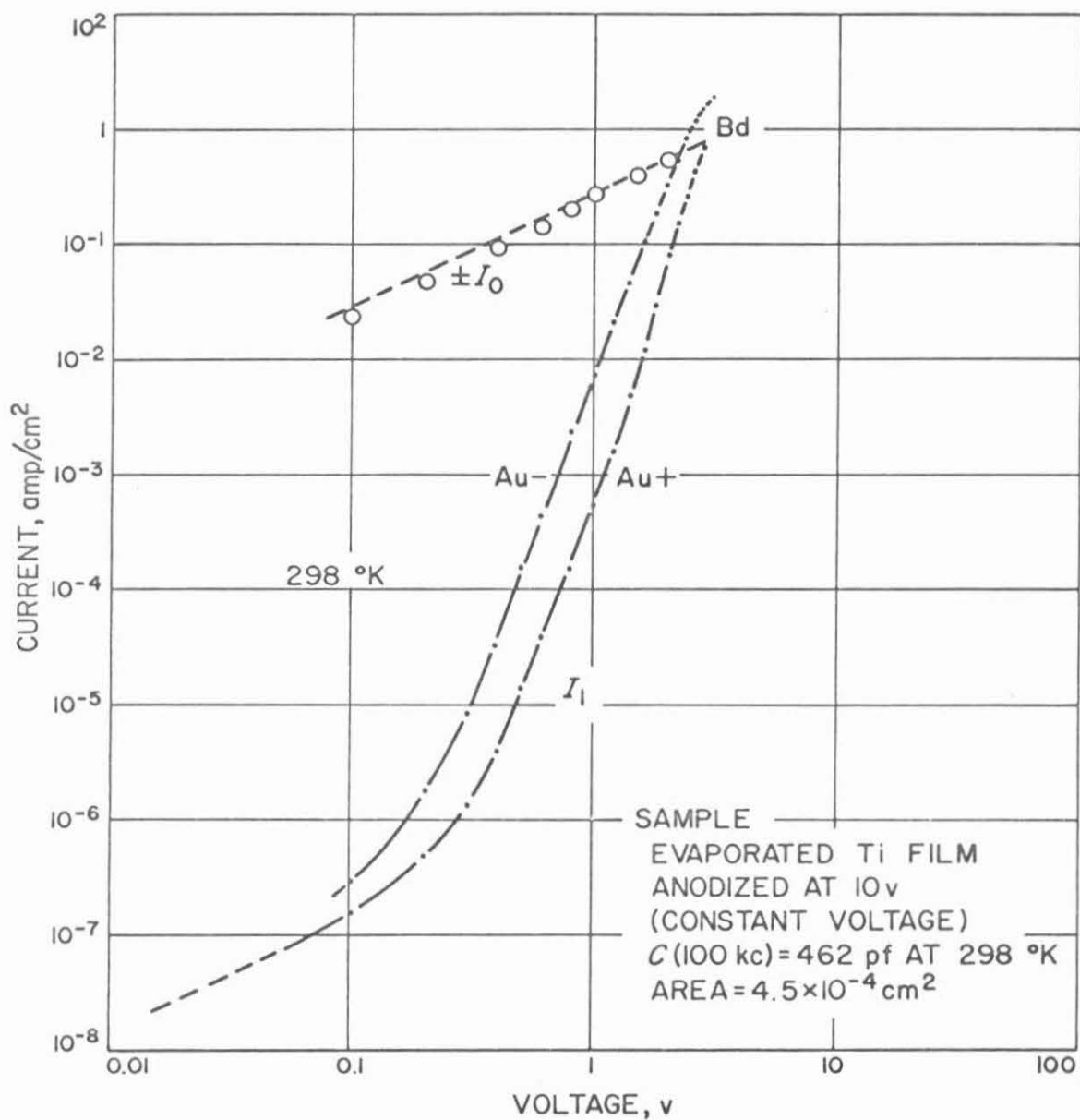


Figure II-8. Current (I_0 and I_1) versus voltage

Measurements of I_0 at both room temperature and at liquid-nitrogen temperature over a wider voltage range are given in Fig. II-9. The capacitance (C_0) obtained by balancing the RC decay at 77°K was 260 pf. As mentioned above, the departures from ohmic behavior occur when the current rise appears at the beginning of the pulse response. The additional current must then be due to the mechanism associated with the current rise, which has been attributed to an ionic origin (forming). The onset of the additional current occurs in this case at approximately one volt at room temperature and ten volts at 77°K. Although this effect has a large temperature dependence, the ohmic region is relatively temperature independent. Measurements attempted at larger negative voltages usually resulted in abrupt breakdowns of the samples and thus no further information could be obtained for this case.

The short circuit photocurrent response of a sample has been measured in order to determine the barrier heights at the contacts as well as the band gap of the oxide. The measurements were made at room temperature with a Gaertner model 1234 monochromator and a Reeder vacuum thermocouple for a calibration reference. The monochromatic light was focussed on a sample prepared with a gold contact

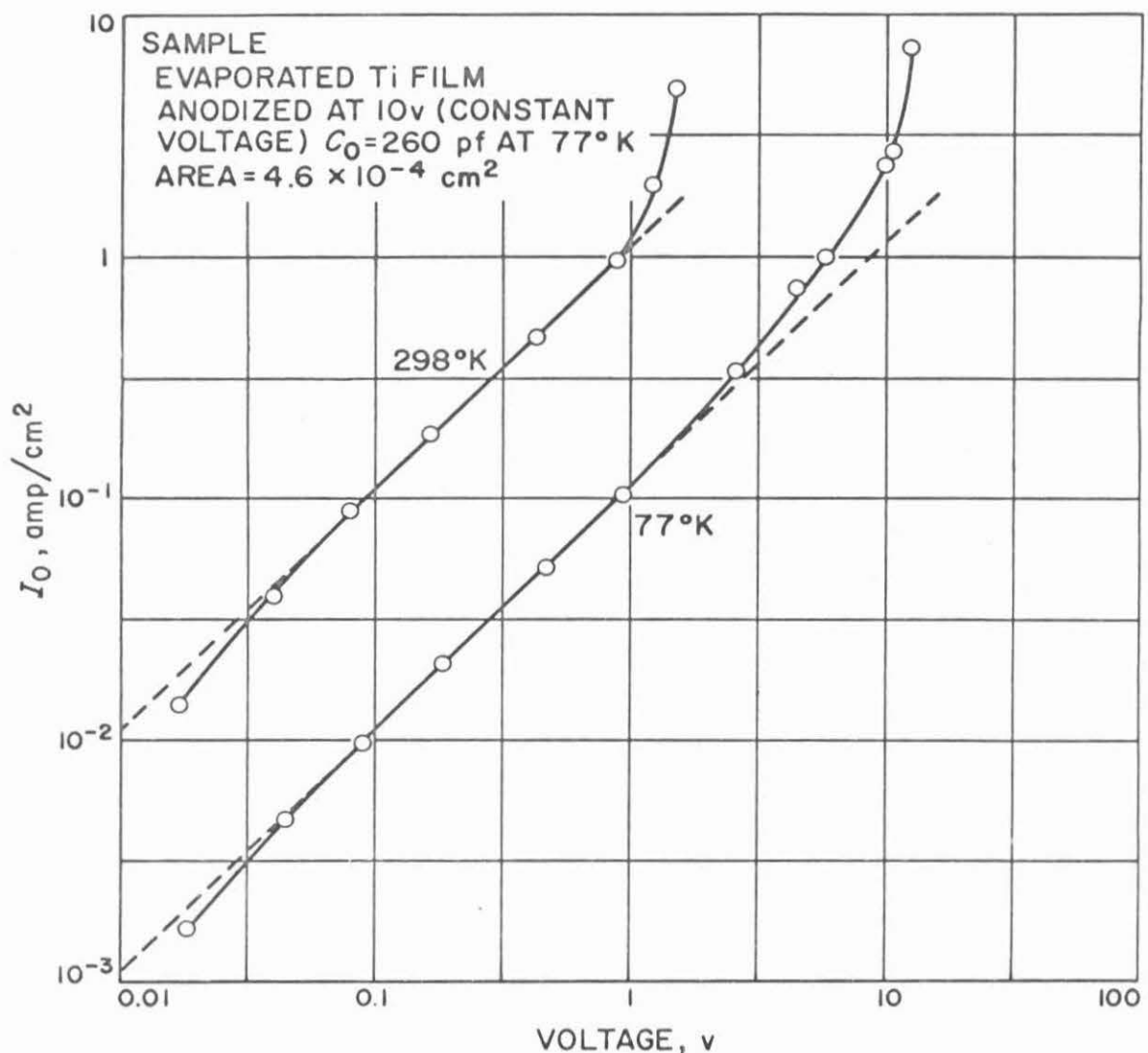


Figure II-9. Initial current (I_0) versus voltage

approximately 500 Å thick as described above, enabling sufficient light to penetrate into the active region of the sample. The response was measured with a narrow-band amplifier synchronized with a 50 cps chopper at the light source. The spectral response R , corresponding to the relative photoelectric energy response per incident photon is commonly plotted as \sqrt{R} vs. $h\nu$ (the photon energy) as a consequence of the well-known Fowler dependence⁽²³⁾

$$R \propto (E - \phi)^2$$

where ϕ is the metal-to-oxide work function. This dependence arises when the photoelectrons assume a zero probability of penetrating the barrier at energies less than ϕ and unit probability for energies greater than ϕ . Cowley⁽²⁴⁾ has considered the case when the probability undergoes a more gradual transition which may be approximated to the next order by a linear dependence of probability on $(E - \phi)$ for energies E not too different from ϕ . In this case one obtains a dependence

$$R \propto (E - \phi)^3$$

suggesting a plot of $R^{1/3}$ vs. $h\nu$. A similar argument may be applied to photoelectrons excited across the oxide energy gap. Gobezi and Allen⁽²⁵⁾ have shown that the above dependence best describes their photo-response measurements

of surface barriers on various semiconductors and offer some alternate possible explanations. Since our experimental results also give better agreement with this dependence, the latter plot is preferred for making the desired extrapolations.

The results obtained from the anodized sample are given in Fig. II-10. The transition energy extrapolated to 3.05 ev corresponds to the energy gap for rutile (see Appendix A and B). The extrapolated value of 1.4 ev is interpreted as the barrier height at the gold-oxide contact. A small reverse response also indicates a barrier height of approximately 1.0 ev which is believed to be due to the titanium-to-oxide back contact. Reverse biasing gave the same value of band gap, but excessive noise at lower energies did not permit a barrier-height extrapolation.

C. Discussion of Results on Anodized Samples

The large hysteresis and time-dependent effects observed in the anodized films have already been interpreted to arise from ionic migration (forming) induced in the oxide film by the applied field. No alternate explanation based upon a purely electronic mechanism can be visualized that might apply to thin films and account for the magnitudes of change and the times involved. On the other hand, the conduction process itself must be predominantly electronic since clearly

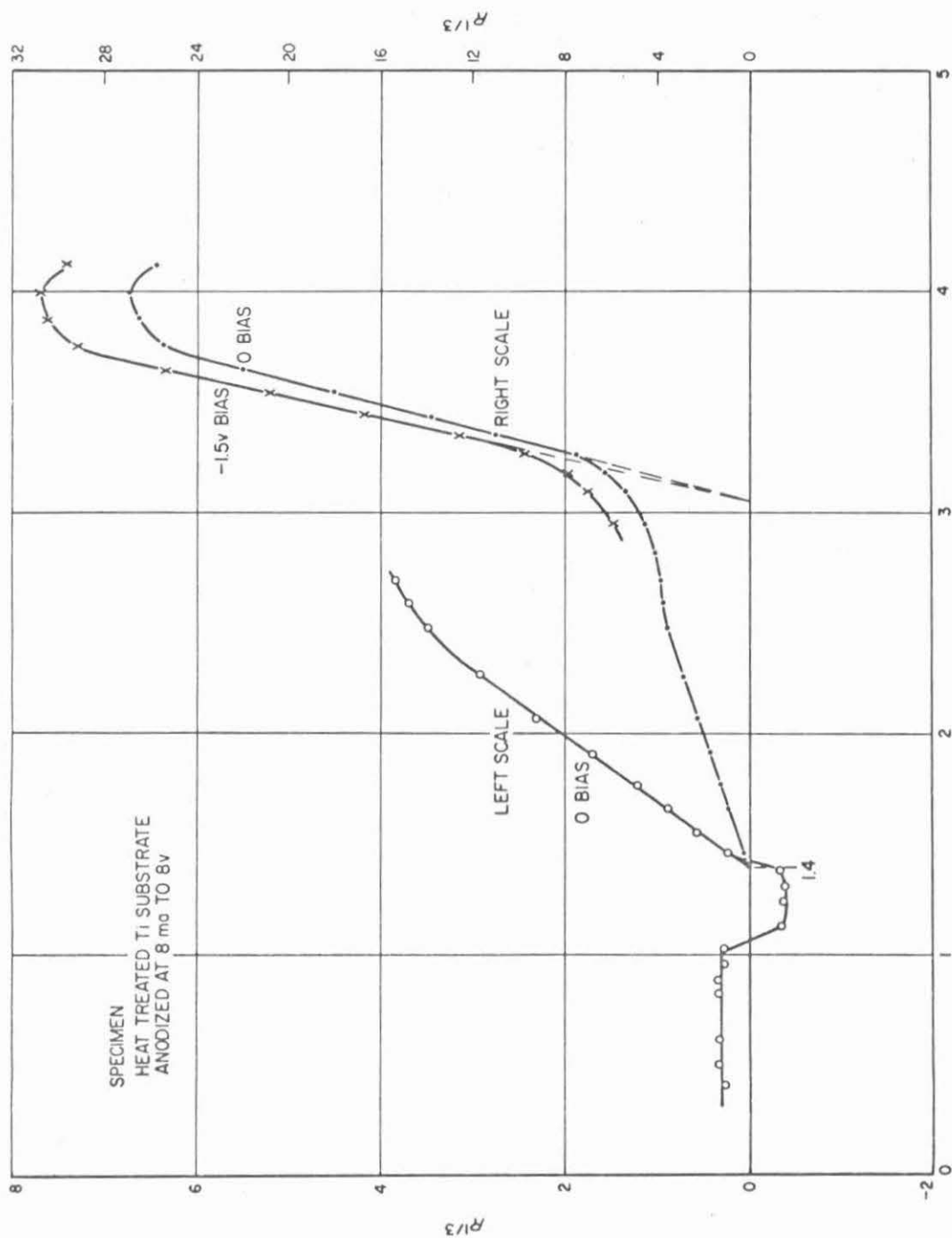


Figure II-10. Photo-response of anodized specimen (Au & Ti contacts)

ionic currents of the required magnitude could not be supported in the thin films for more than an instant without material breakdown. It must be assumed that a limited migration or redistribution of the ions is responsible for large changes in the electronic properties. The effect of the oxide lattice ions is accounted for by the low-frequency dielectric constant, and consequently these additional effects must arise from impurities (or structural defects) in the oxide.

Very large concentrations of impurities are required to have an appreciable effect on the electronic properties of thin films as can be deduced by considering the change in potential introduced in the oxide film by an ionized impurity space-charge (see Section IV A). The requirement for large concentrations of impurities and a correspondingly large space-charge does not seem unreasonable since we are dealing with a highly disordered or amorphous-like structure in the oxide films. Furthermore, impurity concentrations as high as 5 mole percent ($1.6 \cdot 10^{21} \text{ cm}^{-3}$) can be introduced into TiO_2 , and from measurements reported on rutile one concludes that a relatively rapid diffusion of impurities can occur even at moderate temperatures (see Appendix A). Both donor and acceptor type impurities have been observed in rutile, however a natural tendency exists for TiO_2 to be reduced

through the formation of oxygen vacancies which act as donor impurities. Therefore in the absence of large concentrations of acceptors, one would normally expect to obtain an excess of oxygen vacancies and thus an n-type oxide film. In either case, it would not be difficult for a large excess of either type of impurity to enter the thin oxide films during and possibly after their formation. The existence of large densities of defects (of all kinds) also implies many trapping centers and is consistent with the effects already ascribed to traps.

On the assumption that an n-type film is formed in the anodized samples and using the results obtained from the photoresponse measurements, we may deduce a somewhat more specific model of the barrier. The barrier heights of 1.4 and 1.0 ev, interpreted to occur at the gold and titanium contacts respectively, are consistent with the differences in work functions tabulated in the literature. The potential occurring in the oxide as measured from the Fermi level, may appear as illustrated in Fig. II-IIa. It is assumed in this case that the oxide is sufficiently thick, such that the minimum potential approaches a very small value in the interior as determined by the excess concentration of donor type impurities. The positive space-charge then arises from the ionized impurities represented by empty impurity states lying above the

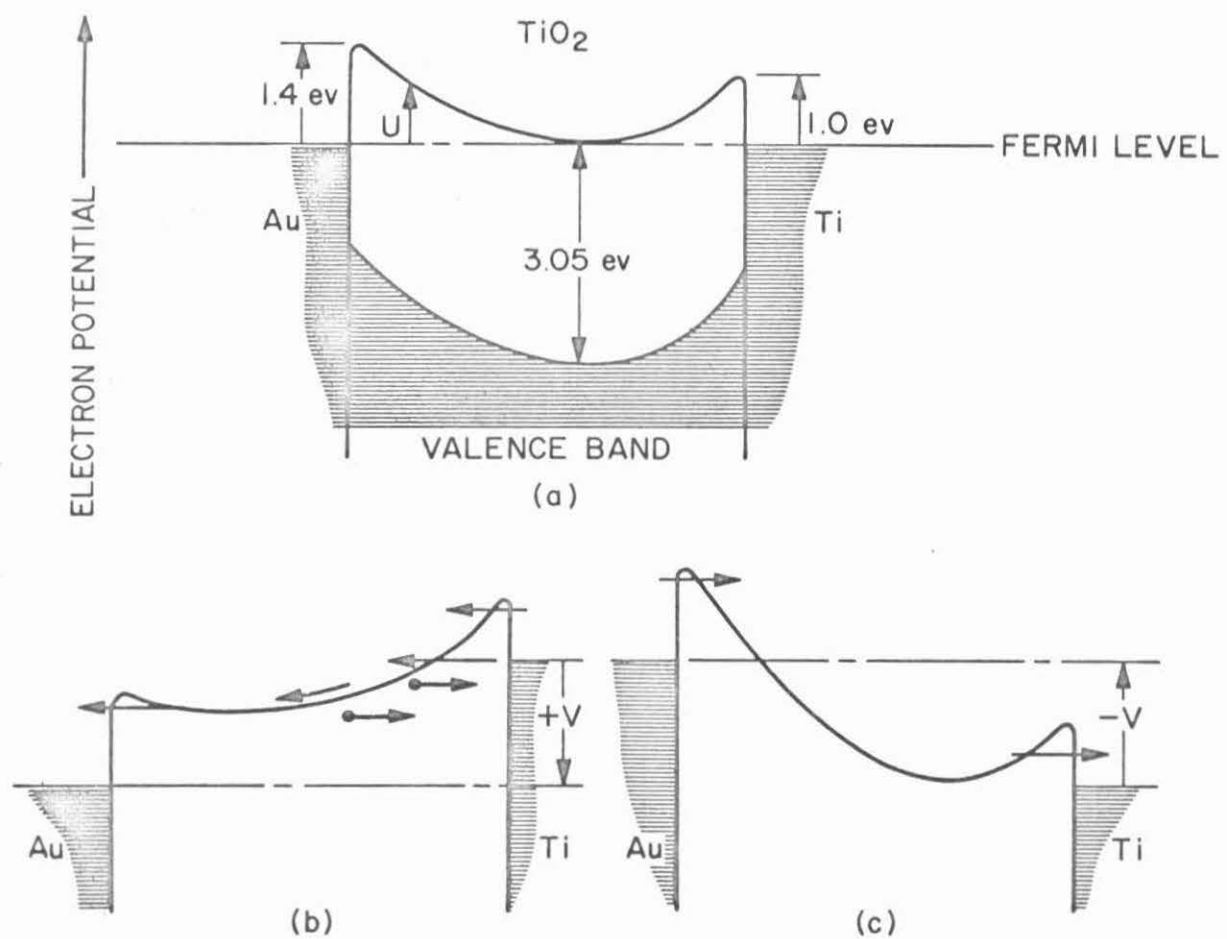


Figure II-11. Representation of proposed barrier: (a) at equilibrium, (b) with positive applied voltage, and (c) with negative applied voltage

Fermi level. From Poisson's equation in one dimension

$$\frac{d^2U}{dx^2} = \frac{4\pi}{\kappa} \rho$$

where U is the electron potential, κ is the static dielectric constant, and ρ is the positive space-charge density of ionized impurities, one sees that a positive curvature in the potential is required which must lead to the kind of barrier illustrated independent of the precise spatial distribution of ionized impurities. Only the detailed shape of the potential barrier will depend on this distribution. The measurements of capacitance, as a function of dc voltage, have already implied that the barriers may possess an exponential shape as will be discussed in detail in Chapter IV. The energy gap of 3 ev requires in the above case a much larger potential barrier for holes, and therefore their effect can be neglected.

When dealing with barriers as represented in Fig. II-11a, we may consider the familiar conduction theories which can apply at metal n-type semiconductor contacts. As mentioned in Chapter I, the two limiting theories involve: (1) electron tunneling through the barrier, and (2) thermionic emission of electrons over the barrier. In case (1), rectification is predicted with the easy direction occurring when the metal contact is at a negative voltage with respect to the semiconductor (oxide interior). This arises because of the

much larger supply of electrons in the metal having energies below the Fermi level as compared with that in the semiconductor. A small temperature dependence is predicted in this case. In case (2), rectification occurs in the opposite direction because of the reduction in the barrier height as seen from the semiconductor under forward bias. In this case the electron supply occurs above the Fermi level and assumes the same type of Boltzmann dependence at either side of the barrier. A large temperature dependence is characteristic of this case.

The experimental results suggest that either limiting case may be approached, depending on the sample history and method of measurement. With a larger barrier believed to exist at the gold contact, the easy direction of rectification should occur for the thermionic case when a positive voltage is applied at the gold contact. This was the situation observed in the dc measurements at room temperature given in Fig. II-2.

The thermionic process also predicts an $\exp(qV/kT)$ dependence in the forward direction. The observed forward dependence can be accurately described by $\exp(41.5V)$ below 1.4 volts, in good agreement with the prediction for room temperature ($q/kT \approx 40$). The reverse

direction is not normally subject to a simple interpretation, particularly in this case where electrical forming effects were present. Because of the forming instabilities, the temperature dependence was not measured directly. However the large temperature dependence observed in the later forming experiments can be related to this case. There appears to be reasonable evidence that a thermionic type of process occurs at the Au contact when electrical forming is allowed to take place under the conditions described.

On the basis of the above discussion the current rise observed at large positive voltages (Fig. II-1) can be interpreted with the help of Fig. II-11b as follows. At large voltages the barrier at the gold contact is suppressed and the current becomes limited by the supply of electrons originating at the titanium contact. Impurity cations drift with the field towards the titanium contact, increasing the width of the Au barrier and reducing the width of the Ti barrier. Emission over the top of the Ti barrier will increase due to the image-force lowering of the barrier height (Schottky emission) as the field due to the additional space-charge increases. Also, tunneling through the barrier will become increasingly important as the barrier narrows. This process must saturate when either the supply of impurity cations near

the gold contact becomes depleted or impurity saturation occurs in the barrier at the titanium contact, providing complete breakdown does not occur first.

For reverse polarity, the opposite process cannot apply until still higher voltages are attained, since nearly the entire voltage drop appears across the larger barrier at the gold contact until the applied field reduces its effectiveness to less than the barrier at the titanium contact. This case is illustrated by Fig. II-11c. Relatively large voltages are required before this condition is reached because of the slow change in the barrier with reverse voltage. A slower variation of current with voltage is therefore also expected in this case, and corresponds to the result given in Fig. II-2. At sufficiently large voltages the onset of ion migration must ultimately be reached. However, as previously stated, complete breakdown always occurred before a current rise could be detected. This may be a consequence of the large fields already existing in the gold-oxide barrier when still higher voltages initiates ion migration from the titanium side. This, in turn, could give rise to an ionic collision-ionization mechanism of breakdown as proposed by Joffé et al⁽²⁶⁾. Also, there exists virtually an unlimited supply of titanium (or oxygen vacancies) at the titanium contact,

The electrical forming experiments performed on samples which were anodized at constant current provide additional evidence of the ionic processes discussed above. In this case it is believed that the barrier at the titanium contact accumulates sufficient positive space-charge during forming to enable tunneling to become the dominant mechanism of electron emission. This is consistent with the temperature insensitivity observed under this condition. The instability observed during temperature cycling is attributed to the competing tendency of the ionized impurities to relax towards their original distribution and thus tending to widen the barrier and causing the electron emission to temporarily revert to more of a thermionic type of mechanism. Apparently, the constant current anodization process results in larger mobilities for the ionized impurities so that the forming process becomes more evident in this case.

In addition to the electrical forming effects already cited for other thin films, similar effects have also been observed with rutile. Observations by Kunin et al⁽²⁷⁾, on both reduced and unreduced rutile with Ag contacts, were interpreted in terms of an electrical generation of donors in the bulk of the crystal. Van Raalte⁽²⁸⁾ has made similar observations on unreduced rutile with Au and Ti contacts but offers an

alternate explanation: the electrons are injected at the cathode gradually filling traps and increasing the density of conduction electrons; the resulting space-charge which would limit the current (scl) is neutralized throughout most of the bulk by holes except at the anode where a negative space-charge is required to support field emission of holes into the bulk. His results appear to support this explanation, however it is difficult to reconcile this model with thin films since unreasonable trapping times would be required in order for the high conductance condition to be maintained for long periods after removing the applied voltage. Experiments were also performed during this investigation on reduced rutile with Au contacts and are described in Appendix B. These experiments also revealed similar forming characteristics.

The results obtained from samples prepared from evaporated Ti films indicate larger impurity concentrations as compared with samples prepared from heat-treated Ti sheet using the same anodization procedure. This conclusion is required to explain the larger conductances and capacitances. Also the reverse direction of rectification suggests a tunneling mechanism. The reduced effect of ion migration or forming is interpreted to be a consequence of the larger impurity concentrations. One might argue on the basis of

impurity saturation; that is, as larger concentrations are reached, the impurities find fewer sites available and therefore must overcome larger barriers in order to move to the next available site. The field-induced drift of ionized impurities would be correspondingly reduced. Complete saturation occurs when all possible sites are occupied and, as mentioned previously, this limit may be as high as $1.6 \cdot 10^{21} \text{ cm}^{-3}$.

In order to attempt a more detailed study of the properties of the films, it is clearly desirable to obtain very stable properties so that a complete set of accurate measurements can be performed on individual samples. The evaporation method described in Chapter III provides such samples as well as offering other advantages.

III. EXPERIMENTS ON EVAPORATED TiO_2 FILMS

A. Preparation of Evaporated Specimens

The fabrication procedure consisted essentially of a sequence of evaporations in vacuum, using masks designed to give the desired configuration. Fig. III-1 illustrates the standard configuration obtained, being composed of an array of crossed metal strips (Au or Al) which contact opposite surfaces of the interlying oxide films. Several samples are obtained from each of the four oxide film thicknesses in this manner, with the extremities of the metal strips providing a convenient place for making soldered connections.

The following sequence of operations was used in the standard procedure: (1) cleaning of the substrate and the materials to be evaporated prior to loading into the vacuum system, (2) vacuum outgassing of the loaded system, (3) evaporation of the first array of metal contacts, (4) deposition of the TiO_2 films, (5) evaporation of the second array of metal contacts, and (6) evaporation of Al_2O_3 protective films (not shown in Fig. III-1). All evaporations were performed without opening the vacuum system in order to avoid any atmospheric contamination at the oxide-metal interfaces. The mechanical movements required for the successive operations,

such as repositioning the masks, changing the evaporation source materials and operating a shutter, were accomplished through two high vacuum movable seals. The substrate ("smoothstrate") and evaporation source materials were cleaned in chromic acid, thoroughly rinsed and boiled in distilled water, and dried with a jet of pure nitrogen gas. Maximum precautions were taken to avoid collecting dust particles on the materials prior to and during loading. The loaded system was out-gassed in vacuum at about 200°C and then allowed to pump for several hours reaching a vacuum of less than $3 \cdot 10^{-8}$ torr before proceeding. A final outgassing of the substrate was performed by heating the substrate to 380°C and allowing it to cool to room temperature just prior to the first metal evaporation.

All evaporations were performed by electron beam bombardment by moving the appropriate source into the target position of the electron beam with the other source materials located out of the way. It was necessary to evaporate the Al or Au contacts out of a tantalum crucible with this method. The contacts were deposited during a period of a few seconds, using a shutter and glass monitor slide to obtain film thicknesses the order of 500 to 1000 Å. The vacuum was less than 10^{-6} torr during these evaporations.

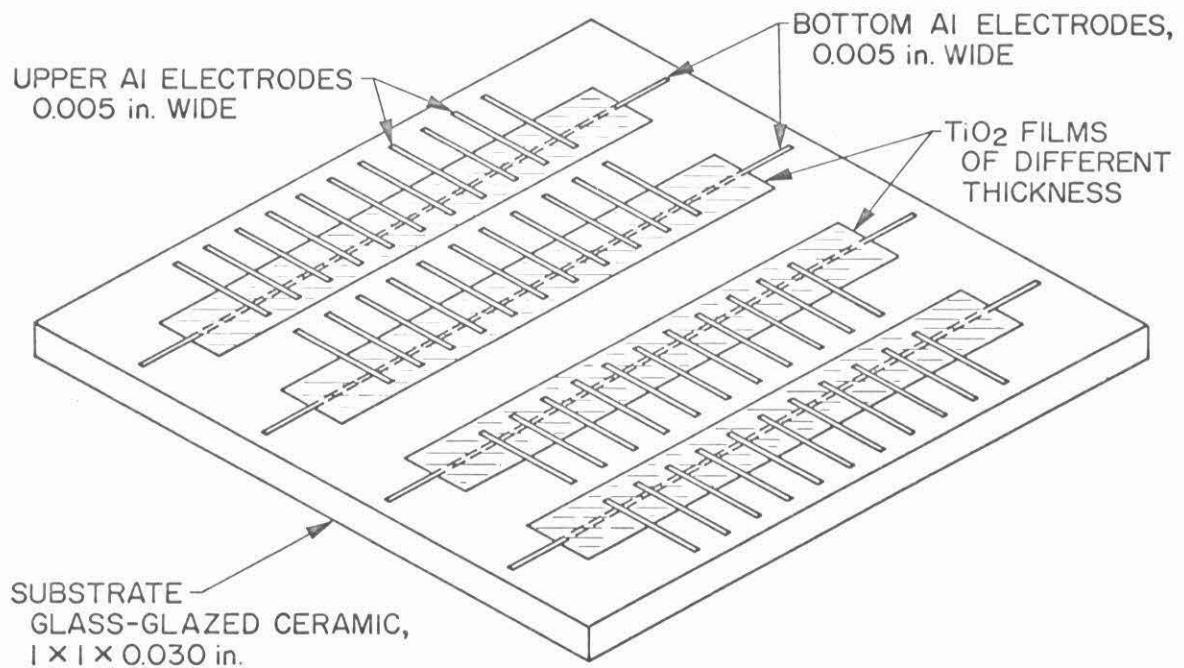


Figure III-1. Configuration for Al-TiO₂-Al thin film samples

The oxide films were deposited by slowly evaporating rutile crystal (TiO_2) in the presence of pure oxygen at a pressure of $4 \cdot 10^{-4}$ torr. The oxygen gas, metered into the system during this evaporation, serves to replace the oxygen which dissociates from the TiO_2 at the temperatures required for evaporation ($\approx 1700^\circ C$). By maintaining a sufficiently slow deposition rate ($\approx .2 \text{ \AA/sec}$), the oxygen gas has time to react with the dissociated molecules being deposited on the substrate and thus form a nearly stoichiometric composition of TiO_2 in the film. The shutter was opened after a steady evaporation rate was maintained and the mask re-positioned at few minute intervals during the evaporation to give the four thicknesses. The thickness and rate were estimated during evaporation by observing color fringes which formed on metal surfaces at fixed locations near the source. Pure titanium was also successfully used in place of rutile as a source. This method was not adopted however, because of difficulties encountered in maintaining a uniform evaporation rate.

The protective film of Al_2O_3 was deposited over the same areas as the TiO_2 films to a thickness of at least 1000 \AA . This served to protect the thin film samples from atmospheric moisture during storage and is believed to insure more

reproducible results. Saphire crystal was found to be a convenient evaporation source of Al_2O_3 . Good insulating films of Al_2O_3 were obtained either with or without the use of oxygen during the evaporation, indicating that no appreciable dissociation of Al_2O_3 occurs at the evaporation temperatures ($\approx 1900^\circ\text{C}$).

The masks were separated from the substrate by approximately $1/16$ in., giving relatively diffuse edges in the evaporated pattern. This is believed necessary in order to avoid appreciable variations in the thickness of the oxide film at the edges of the metal contacts. Fig. III-2 is a photomicrograph showing the area of a typical sample as defined by the overlapping metal strips. The phase contract optics clearly reveals the gradual topological contour at the diffuse edge of the strip. The small blemishes in the film, exaggerated by the phase contrast, were usually related to the original surface of the smoothstrate. Samples exhibiting a minimum of such blemishes were selected for measurements. The active areas of the samples were measured from such photomicrographs, interpreting the effective boundry to lie near the outer part of the diffuse edges.

The evaporation process described makes no attempt at improving the structural order in the TiO_2 films.

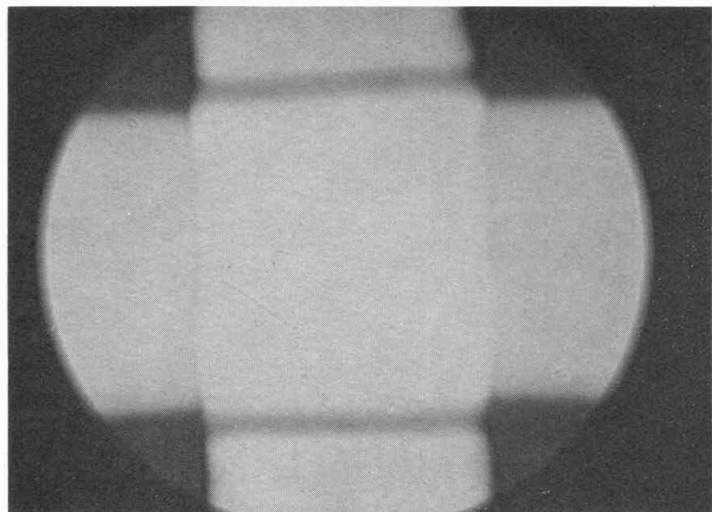
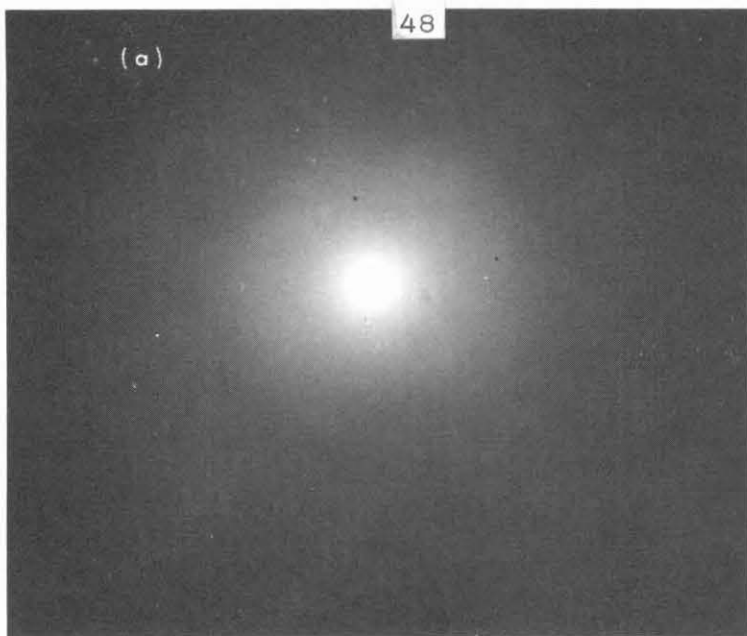


Figure III-2. Phase contrast
photomicrograph of
sample 270X

Rather than introduce new uncertainties associated with an epitaxial process or heat treatment, the intention was to concentrate on the disordered structure one would normally expect from the process described. In order to confirm that the process really gives a highly disordered or amorphous-like structure, an electron transmission diffraction pattern was obtained from an evaporated film. This was accomplished by first preparing a formvar film replica of a smoothstrate surface. Formvar films were stripped from the surface and suspended across small washers that would later fit into the diffraction stage of the electron microscope. The TiO_2 film was evaporated on the formvar films with essentially the same procedure used for making the regular samples, except the film thickness in this case was approximately 500 Å. The formvar was subsequently dissolved away leaving bare films of TiO_2 suspended across the washers. A transmission diffraction pattern obtained from such a sample is shown in Fig. III-3a. The pattern is characteristic of an amorphous-like structure. For comparison a transmission pattern was also made of finely pulverized rutile suspended in a formvar film and is shown in Fig. III-3b. The diffuse rings are the Debye rings which arise from the composite effect of the random orientations of the crystallites of the rutile powder. The rings

(a)



(b)

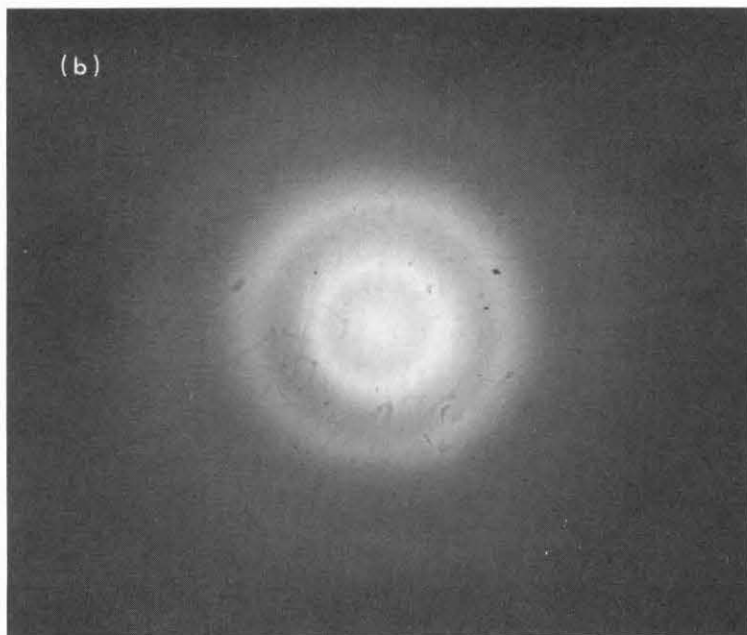


Figure III-3. Electron transmission diffraction patterns: (a) evaporated TiO_2 film, (b) rutile powder suspended in formvar film

are very diffuse because of the small size of the crystallites. The maxima of these rings occur at the same radial positions as inflections in the intensity of the pattern shown in Fig. III-3a for evaporated films. Although this is not evident in the figure, this was carefully checked with microdensitometer traces taken directly from the photographic plates. This relationship suggests that the short range order in the evaporated films is similar to that of the rutile structure. The energy gap measured from anodized films had already suggested that such a correspondence exists.

B. Measurements of Evaporated TiO_2 Films

I. Thickness Measurements. A precise knowledge of the thickness of the oxide film is clearly desirable. In contrast to the anodized films, the evaporated films can be measured directly by an optical interference method, providing they are not too thin. Unfortunately, the range of thicknesses of greatest interest in this investigation falls at the lower limit in sensitivity of the interference method. One reason for concentrating on this range of thickness is due to the fact discussed later that the thicker films exhibited greater electrical forming tendencies which we clearly wish to avoid. Another important reason stems from the ideas discussed in Chapter II involving the influence of ionic space charge layers adjacent

to each contact. It is of immediate interest to investigate these ideas in detail, avoiding if possible any important influences due to a relatively wide oxide interior and correspondingly other possible limiting conduction mechanisms such as described by Mead⁽²⁹⁾. In spite of this constraint it was at least possible to obtain an estimate of the thickness of the thin films by the interference method. A few special specimens were prepared by a modification of the process described in Section IIIA in order to permit a means of making thickness measurements as well as photoelectric measurements to be described later in this section. A single oxide thickness was evaporated on a cover glass substrate in this case, and in addition to the sample contacts, a wider strip of metal was evaporated over an entire edge of the oxide film. No Al_2O_3 overcoat was deposited on these specimens. The thickness measurement was made by multiple beam interference, using a thallium light source (5350 Å) and a half-silvered microscope slide for the comparison plate. Because of some scratching of the specimen surface during this measurement, it was performed after completing all other measurements. The resolution of this method was limited by surface irregularities to about 100 Å.

The thickness of insulating films is commonly

calculated from measurements of capacitance and area, assuming a dielectric constant κ equal to that of the bulk ceramic form of the material. One difficulty in this method arises in assuming the bulk value of κ to apply to thin films, particularly in this case where the accepted value for ceramic rutile is about 100 and there is no guarantee that we are dealing specifically with a rutile structure (over short range) rather than some combination with other structural modifications (anatase or brookite) which have considerably lower values of κ . The other difficulty involves the assumption of a good dielectric which in general is not valid when high impurity concentrations are present such as postulated in Chapter II. This difficulty is evident from the large variations of capacitance with frequency and temperature observed in these films as described later in this section, which clearly makes such a calculation quite arbitrary. However, because of the obvious advantage of this method, measurements were designed which attempt to overcome these difficulties. The capacitance, when measured by balancing the initial RC transient following a voltage step, should lead in the limit of very short times to a value characteristic of an ideal plate capacitor. This would require times short compared with the relaxation time of the electronic charge in the oxide film. However,

evidence will be given which indicates that the relaxation process is characterized by a wide range of time constants extending also to very short times, in general conforming with the ideas discussed in Chapter II. If we can assume that our measurement precedes most of the relaxation process, it may still be acceptable for our purpose. This measurement is considerably improved at lower temperatures where the relaxation times are longer and therefore all such measurements were made at 77°K. The capacitance thus obtained will be referred to as C_0 . The test arrangement used for these and other measurements is described later in this section.

The dielectric constant of the film was still required in order to calculate the thickness of samples from the capacitance and area measurements. This was obtained by preparing a thick oxide film specimen with several large area contacts. The thickness was measured by the optical interference method to be $3020 \pm 100 \text{ \AA}$. From measurements of capacitance as just discussed and the contact areas, the mean value obtained was $\kappa = 27.5 \pm 2.0$. Using this value for κ , the thicknesses calculated from the special samples are compared with those estimated from the interference method as listed by the following:

<u>SPECIMEN</u>	<u>d (CALCULATED)</u>	<u>d (ESTIMATED)</u>
13	204 \AA	$160 \pm 100 \text{\AA}$
15	100	< 100
16	194	140 ± 100
17	457	300 ± 100

The above results indicate no serious inconsistencies although there appears to be a systematic difference. This could be due to either a lower value of κ for thinner films or a systematic error in the interference method. In any case the uncertainties are too large in the thin films to justify a better value of κ . Therefore this value was used for thickness determinations of all other specimens. In these cases, the values calculated were found to vary in a consistent manner with the different film thicknesses deposited on the substrate, as judged by the relative evaporation times.

2. Optical Measurements. The same specimen used for obtaining κ was also used for measuring the refractive index n and the spectral transmission characteristics of the oxide film. In order to measure n , a strip of aluminum film was deposited under the oxide film with its width extending beyond an edge and another strip deposited over the oxide film in a perpendicular sense with its length overlapping the edge. The overlying strip of aluminum film permitted the

measurement of the oxide film thickness in the usual manner, measuring the shift which occurs in the interference fringes at the oxide film edge. At the adjacent region of the edge without the overlying aluminum strip, a shift of the interference fringes occurs because of the phase difference between the light rays which pass through the oxide film before reflection at the aluminum surface compared with the rays which are reflected directly from the aluminum surface beyond the edge of the oxide film. Measurements of the two fringe shifts are sufficient for a calculation of the refractive index. A small correction for the differences in phase shift at the aluminum surface was also included in the calculation. The result obtained is $n = 1.95 \pm .1$ (at 5350 Å).

The spectral transmission characteristics were obtained from an area of bare oxide film on the glass substrate. The measurements were made with the same apparatus described in Section II B for measuring the photo-response. At each wavelength the transmission was measured through the oxide film and glass substrate and also through a clear portion of the glass substrate, the ratio being taken as approximately the optical density of the film. This neglects the effect of the differences in dispersion between the two media on the relative change in the reflection

coefficient. However this becomes important only near the natural absorption frequencies of the media. Since the absorption frequency of glass occurs in the ultraviolet, the result should be applicable up to the first absorption edge of the oxide film. The transmission curve obtained in this way is plotted in Fig. III-4. The transmission above 4 ev is indicated by a dashed line because of the uncertainty introduced by the glass in this range. The maxima and minima occurring in the transmission curve below 4 ev arise from multiple reflections within the film. This permits an independent calculation of n as well as giving its dispersive character. The calculations are made using the familiar relations, $n = m \lambda / 2d$ (maxima) and $n = (m + 1/2) \lambda / 2d$ (minima), where m corresponds to the integral number of internal reflections, λ is the wavelength and d , the film thickness. Fig. III-5 includes the results of these calculations and the value obtained above at 5350 \AA . The agreement is well within the experimental uncertainty. In the same figure are plotted the dispersion relations reported by Devore⁽³⁰⁾ for rutile. Apart from the smaller values of n for the oxide film the dispersive character is quite similar to that of rutile, indicating approximately the same natural absorption frequency. This frequency apparently corresponds to a higher energy

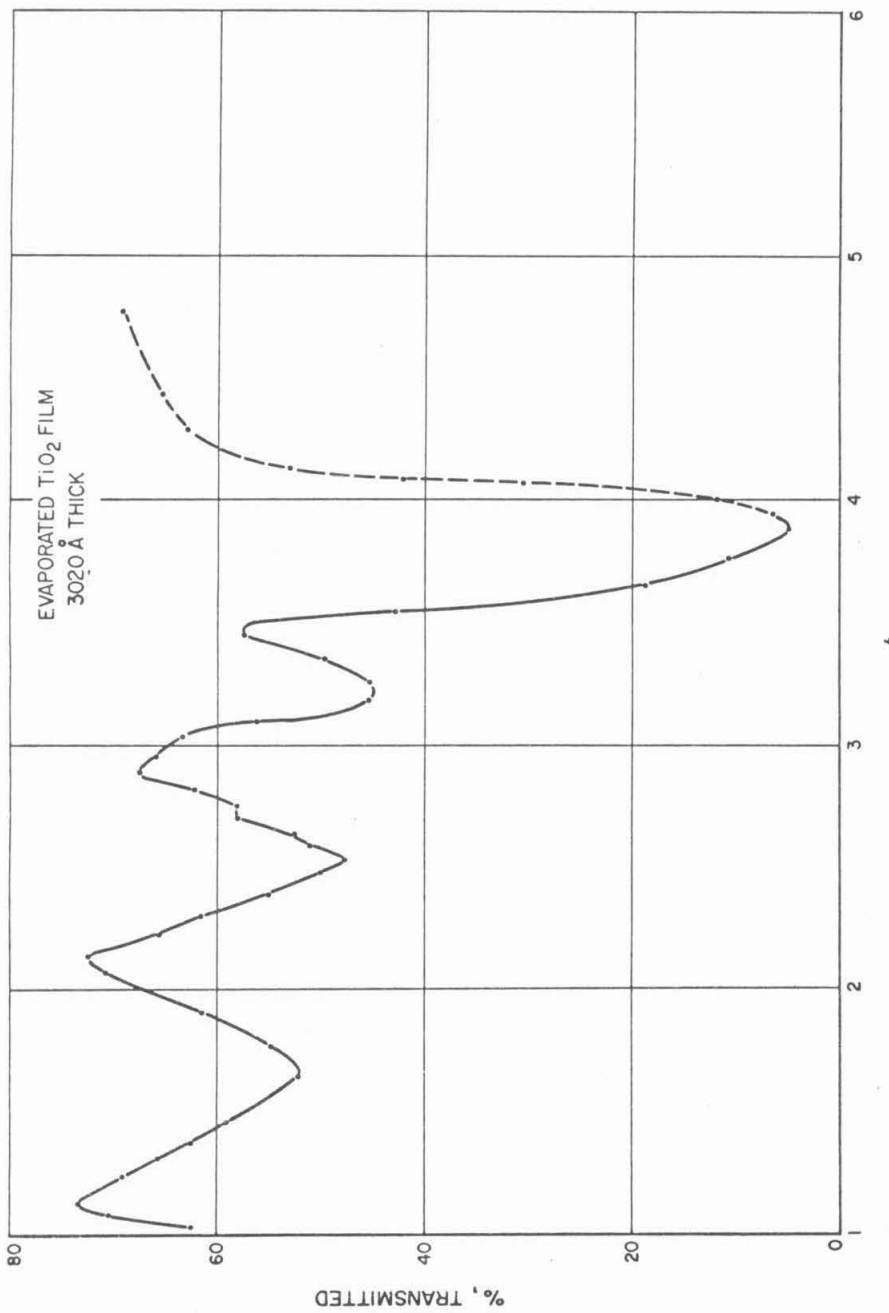


Figure III-4. Transmission through TiO_2 film

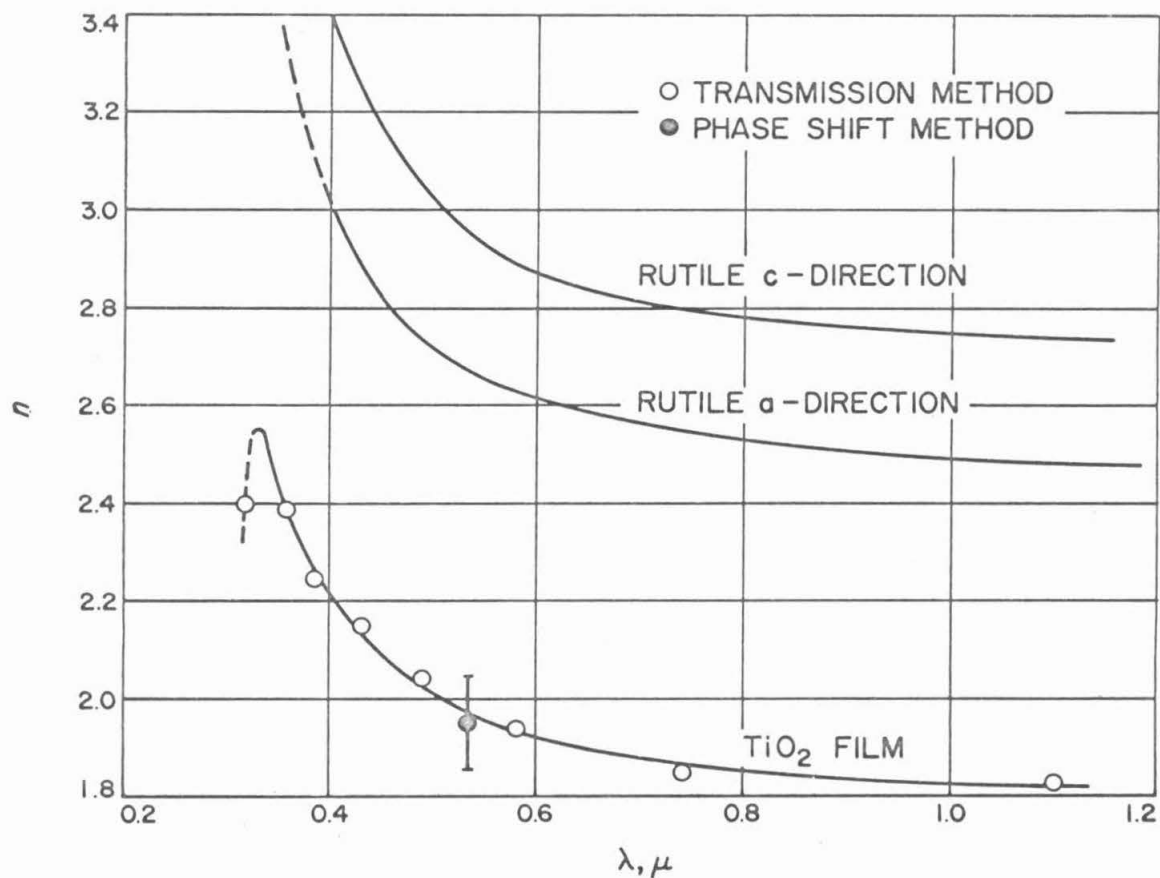


Figure III-5. Refractive index of TiO_2 film

transistion, for example, between the $0^{-2}(2p)$ and $Ti^{+3}(4p)$ bands, rather than to the smaller energy gap of 3 ev (See Appendix A).

3. Photoelectric Measurements. The photoresponse was measured as described in Section II B. The results obtained from specimen #16 having Au contacts are given in Fig. III-6. The two curves represent measurements taken on different days. The extrapolated value of the energy gap 3.15-3.2 ev is somewhat larger than the value of 3.05 ev measured for both the anodized film and rutile. This difference may be attributed partly to the greater uncertainty in the extrapolation but more probably to a systematic error that can be associated with the larger slit openings in the monochrometer that were required for these measurements. The latter would tend to shift the points in the direction of the rapidly increasing response and could account for the difference. The background level can be ignored in the extrapolation from large response levels since in this case it has a negligible effect in the R dependences. The gold contact barrier height is indicated by the 1.45 ev extrapolations, in good agreement with the value 1.4 ev obtained from the anodized sample and rutile (see Appendix B).

The photoresponse was measured from a sample

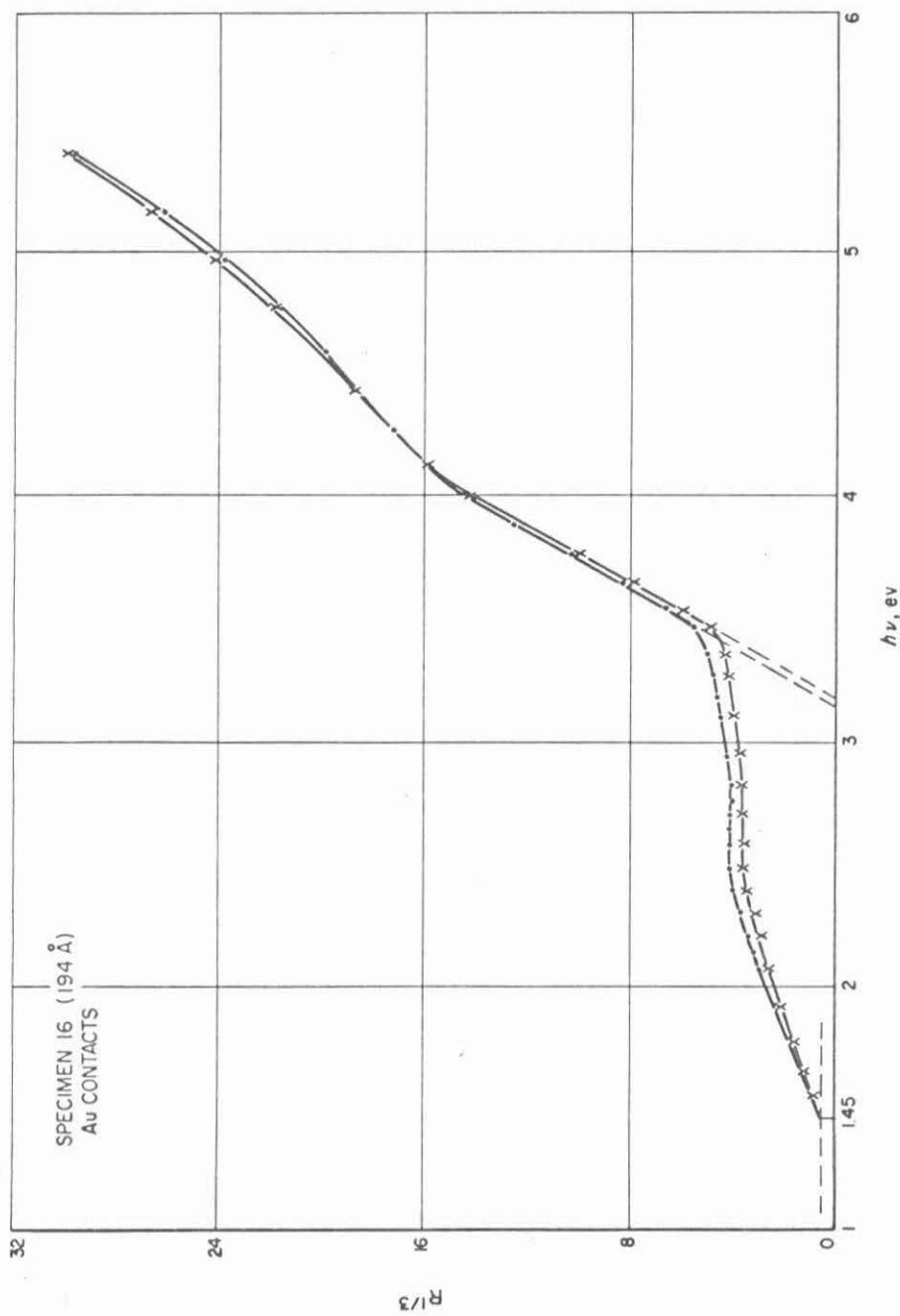


Figure III-6. Photo-response of specimen No. 16 (Au contacts)

with Al contacts from which extensive electrical measurements were also obtained, as described later. Although this sample had a thick protective overcoat of Al_2O_3 , this is not expected to influence the results. The results given in Fig. III-7 were obtained at 0 and $\pm .5$ volts bias (polarity refers to the outer contact). A much larger photo-response is obtained from the contacts in this case which nearly masks the effect of the band gap, indicated by only small indentations in the response near 3 ev. For reasons to be discussed in Section IIIC, the oxide films with Al contacts are believed to be p - type and thus the response below 3 ev can be interpreted in terms of holes excited into the valence band. The much larger response from the contacts in this case is consistent with the general belief that a relatively broad valence band exists compared with a narrow conduction band (see Appendix A).

The large differences with bias can be interpreted in terms of different barrier heights (for holes) at opposite contacts. The zero bias curve can be decomposed into two straight lines (dashed lines) by subtracting the values of R corresponding to the straight line that extrapolates from the foot of the curve from the total R and replotted the new value of $R^{1/3}$. A similar separation of the $\pm .5$ volt curves

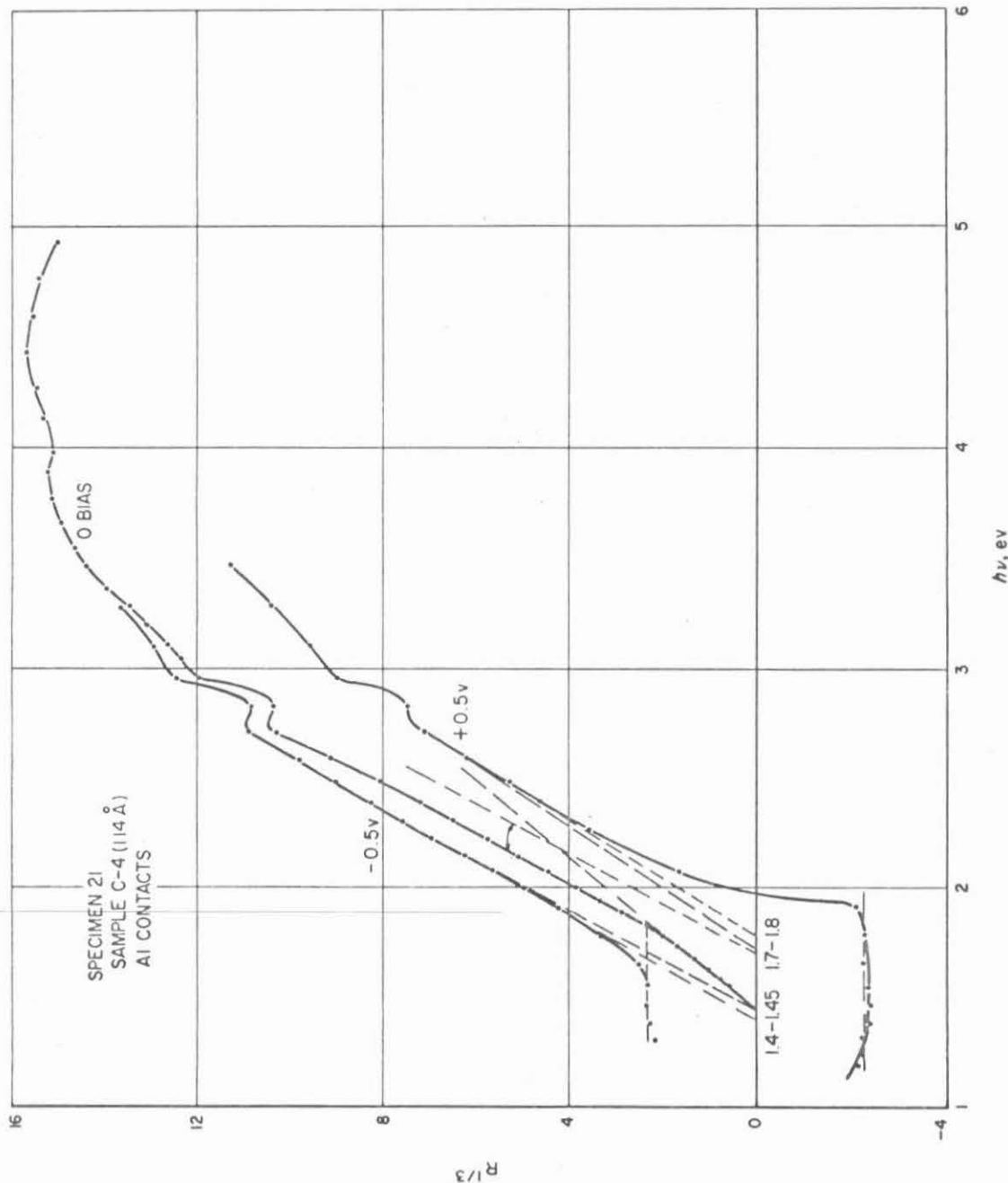


Figure III-7. Photo-response of sample No. 21-C4 (Al contacts)

is accomplished by subtracting the value at the foot (dashed lines) from each total curve. The zero bias curve is then seen to give approximately the same two extrapolations as obtained for each polarity. The barrier heights so determined give approximately 1.4 - 1.45 ev for the underlying contact and 1.7 - 1.8 ev for the outer contact. The response above 3 ev exhibits broad maxima that occur at about the same energies observed for rutile (see Appendix B).

4. Electrical Measurements. The electrical connections were made by soldering 5 mil copper leads with indium to the exposed ends of the evaporated metal strips. Using minimum lengths of these leads, they in turn were soldered to heavier leads a short distance from the sample. The heavier leads were permanently connected to the terminals of a shielded enclosure. In order to minimize thermal emf's during low temperature measurements, the leads were carefully selected as matched pairs and arranged in a symmetrical manner. In some of the earlier measurements the enclosure was a shielded dewar so that the sample could be immersed under liquid N_2 . The temperature dependence was obtained in this case by allowing the liquid N_2 to evaporate and observing the temperature increase by means of a thermocouple attached to the specimen. A gentle flow

of dry N_2 gas was fed into the dewar during this time to prevent condensation of moisture. The latter effect was not completely eliminated at all times and would then result in erroneous leakage currents across the insulation.

A more satisfactory arrangement, used in all later measurements, enclosed the specimen inside a vacuum system. The specimen was clamped against a copper heat sink, using silicone grease to improve the thermal contact. One thermocouple was soldered with indium at the surface of the specimen and another monitor thermocouple attached to the heat sink. The temperature of the specimen was maintained at a constant temperature between 78°K and 296°K by controlling a flow of liquid nitrogen or its cold vapor through the heat sink. Connecting leads from six samples with two common leads were fed through an octal seal in the vacuum base plate to a switching box located just below. Connections to the test apparatus was accomplished with matched pairs of coaxial cables from the two output terminals of the switching box. The leads from the samples were sufficiently short to permit transient measurements to less than 1 μ sec and care was taken to insure negligible leakage in the connections ($< 10^{-14}$ amps).

The evaporated films were typically much less

sensitive to the electrical forming effects observed with anodized films. These effects would appear only at large applied fields, becoming more important at higher temperatures and with thicker films. Both Al and Au contacts were tested, however samples prepared with Al contacts exhibited much better stability and reproducibility than those prepared with Au contacts. For this reason, most of the following results are limited to Al contacts.

The dc I-V characteristics of a thin specimen (#15) with Au contacts are typified by the results given in Fig. III-8. At room temperature the samples were ohmic with breakdown (B_d) occurring consistently at voltages the order of a few tenths of a volt. At 77°K (immersed under liquid N_2) a higher ohmic resistance results, persisting up to a relatively high voltage where it suddenly assumes a high power function of voltage ($\sim V^{14}$). The intersection of the extrapolated ohmic and high voltage dependences occurs at 1.4 volts, the value measured for the barrier height. The initial current I_0 (see Section II B) intersects the dc current at approximately the point of breakdown. The temperature dependence of the current measured from a sample, at .5 volt bias exhibited a slow, approximately parabolic change with temperature to about 170°K, then increasing more

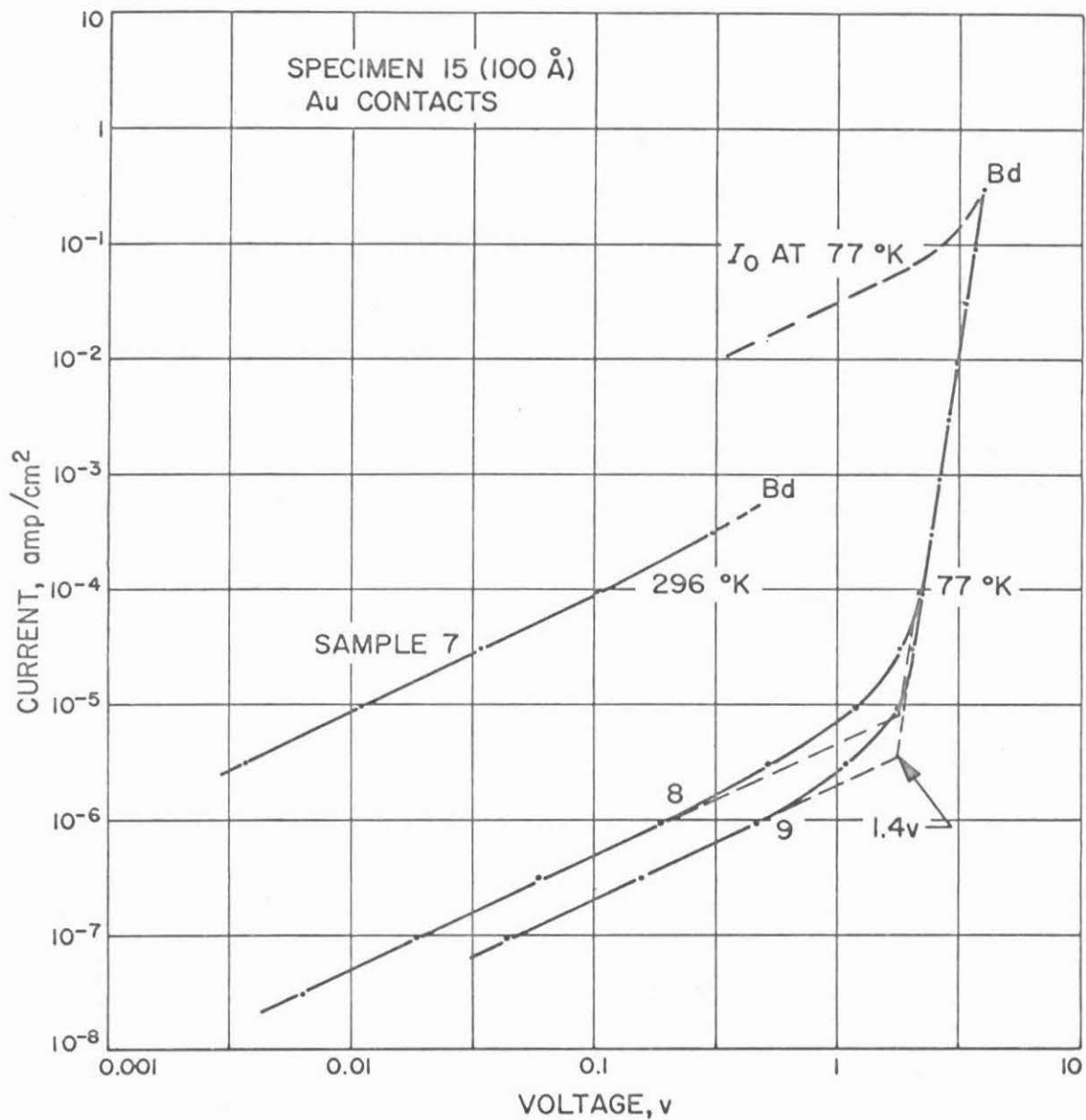


Figure III-8. I-V characteristics of specimen No. 15

rapidly with temperature before breakdown occurred below room temperature.

The dc I-V characteristics of a thick specimen (#17) with Al contacts is typified by the results given in Fig. III-9. Thick specimens such as this exhibited electrical forming tendencies at room temperature and therefore the room temperature data in this case were obtained with voltage pulses by measuring the current asymptote on an oscilloscope, as described for measuring I_1 in Section II B. A standard dc measurement was used at 77°K (immersed under liquid N_2). Breakdown at 77°K was again observed to occur at approximately I_o . The initial current I_o could not be accurately measured at room temperature because of the shorter relaxation times involved. The dc current at .5 volt exhibited a temperature dependence accurately represented by $\exp(-10/kT)$ from 77°K to 296°K.

After subjecting a sample to ac forming at 1.0 volt 100 cps for a few minutes at room temperature, the I-V characteristics would shift to higher voltages, with correspondingly higher resistance at lower voltages. In order to obtain a measurable current at lower temperatures, a 1.0 volt bias was required. The temperature dependence obtained in this case could be represented by $\exp(-.11/kT)$

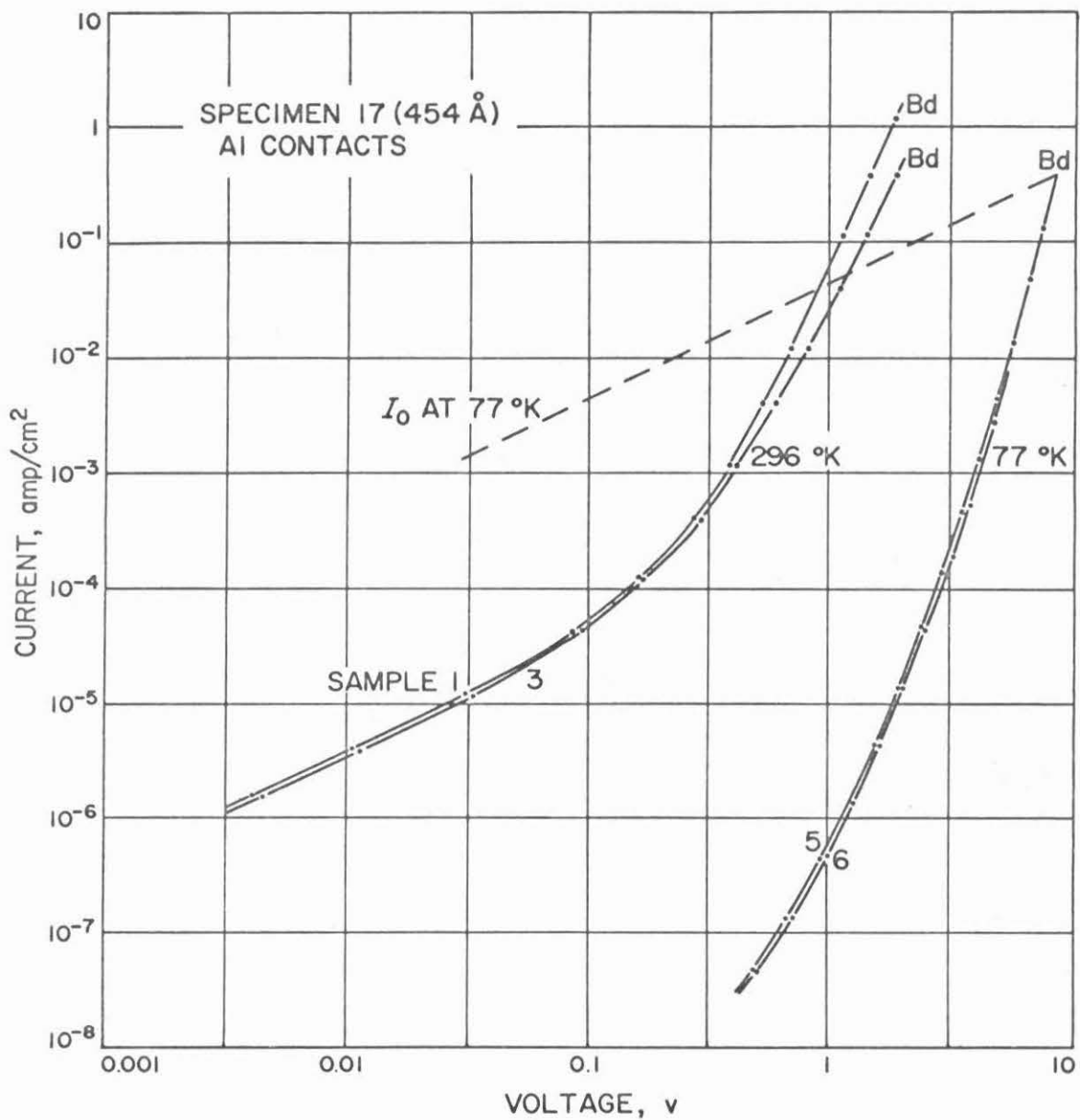


Figure III-9. I-V characteristics of specimen No. 17

below 140°K and $\exp(-.23/kT)$ at higher temperatures.

All subsequent results were obtained from the standard specimens measured under vacuum. The I-V measurements were made on a Keithley 610B electrometer. The I-V characteristics at 296°K and 78°K obtained from samples with various oxide film thicknesses are plotted in Figs. III-10, II, and 12. The letters A,B,C and D represent the successively thicker films deposited on a specimen substrate. No reliable data were obtained from the thinnest film (A) of specimen #21. Figs. III-10 and II illustrate the uniformity of different samples from the same oxide strip, the sample number referring to their sequential order as indexed from one end. A few abnormal samples had been measured and are believed to be related to flaws that were visible under the phase contrast microscope. The measured thicknesses are seen to increase consistently with the sequence of films and the general shift in the I-V curves. The measurements were not in general extended to higher currents in order to completely avoid any forming effects. For reasons discussed previously, it is desirable to examine in more detail the thinner samples. In Figs. III-13, 14, and 15 are plotted complete families of I-V curves at different temperatures, taken from representative samples of

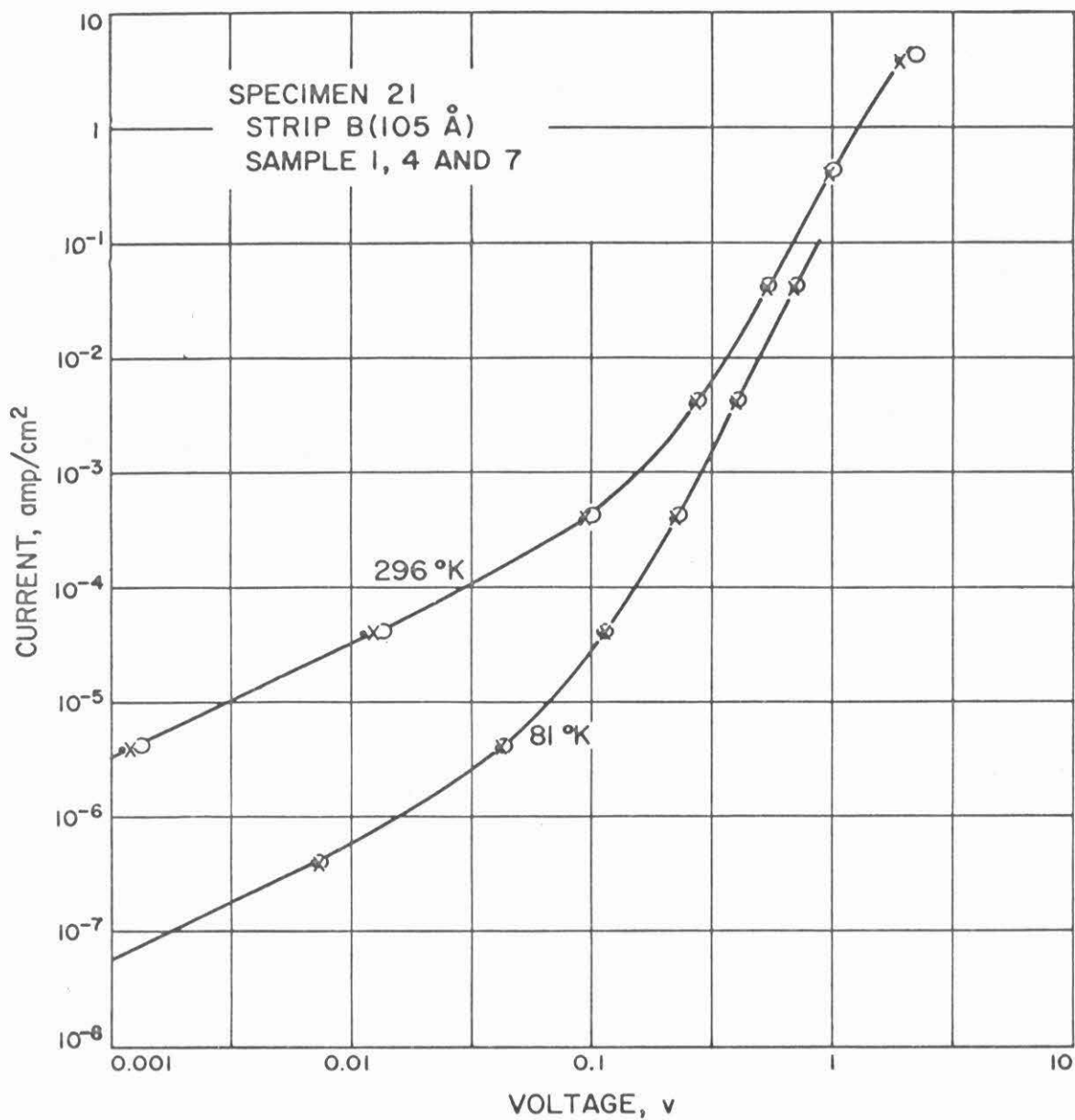


Figure III-10. Comparison of I-V characteristics of No. 21-B

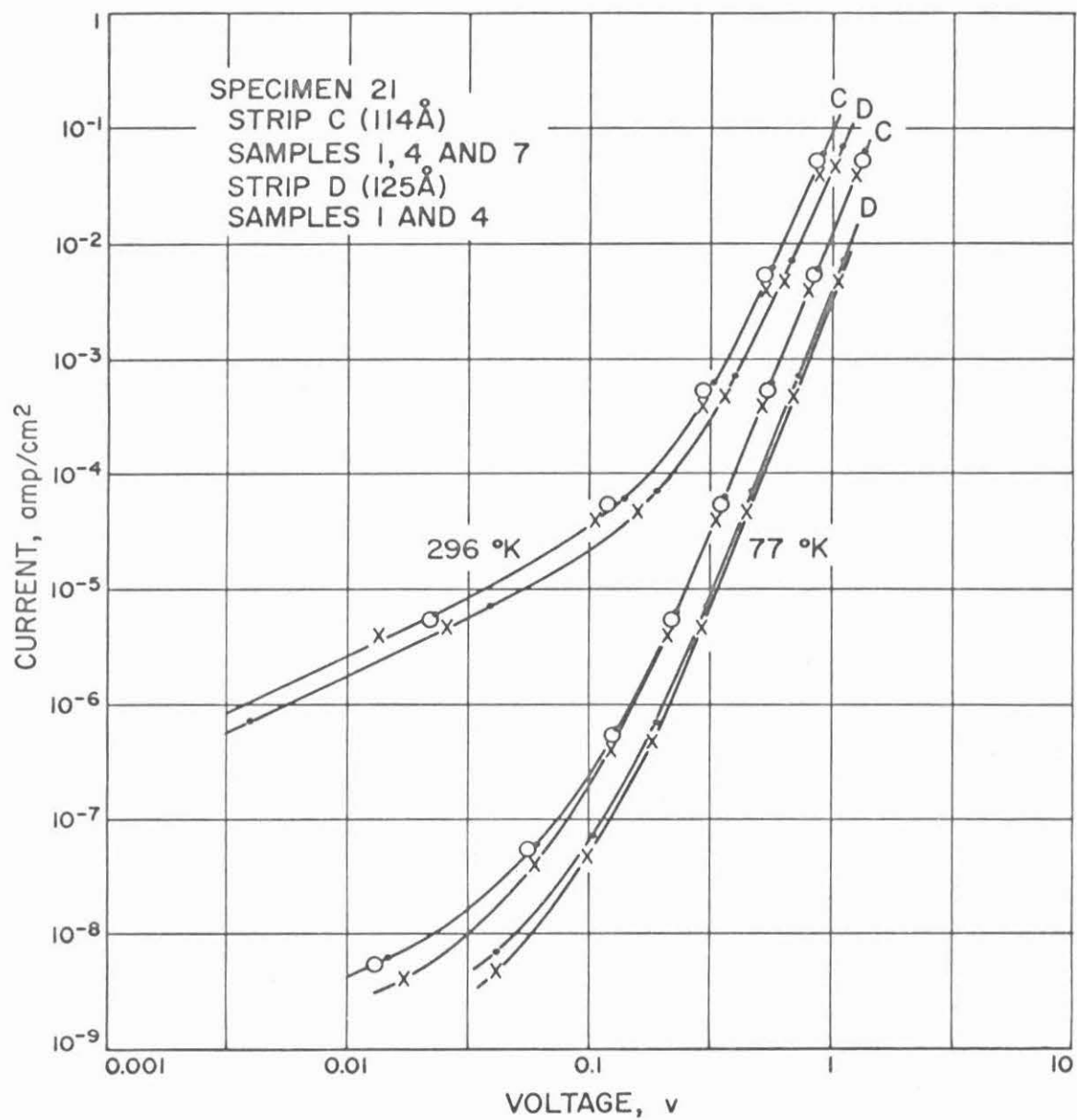


Figure III-11. Comparison of I-V characteristics of No. 21-C and D

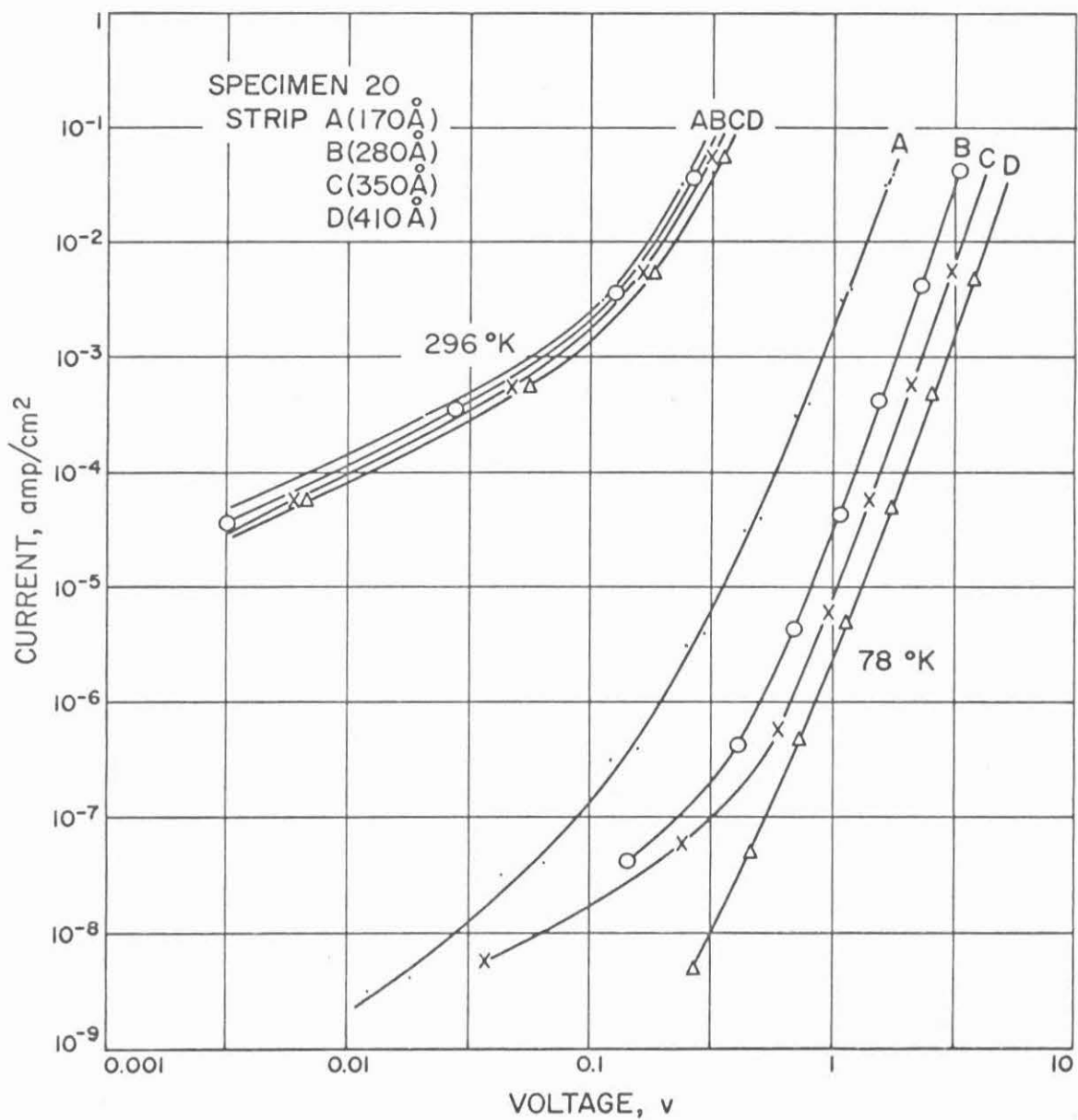


Figure III-12. Comparison of I-V characteristics of No. 20-A, B, C, and D

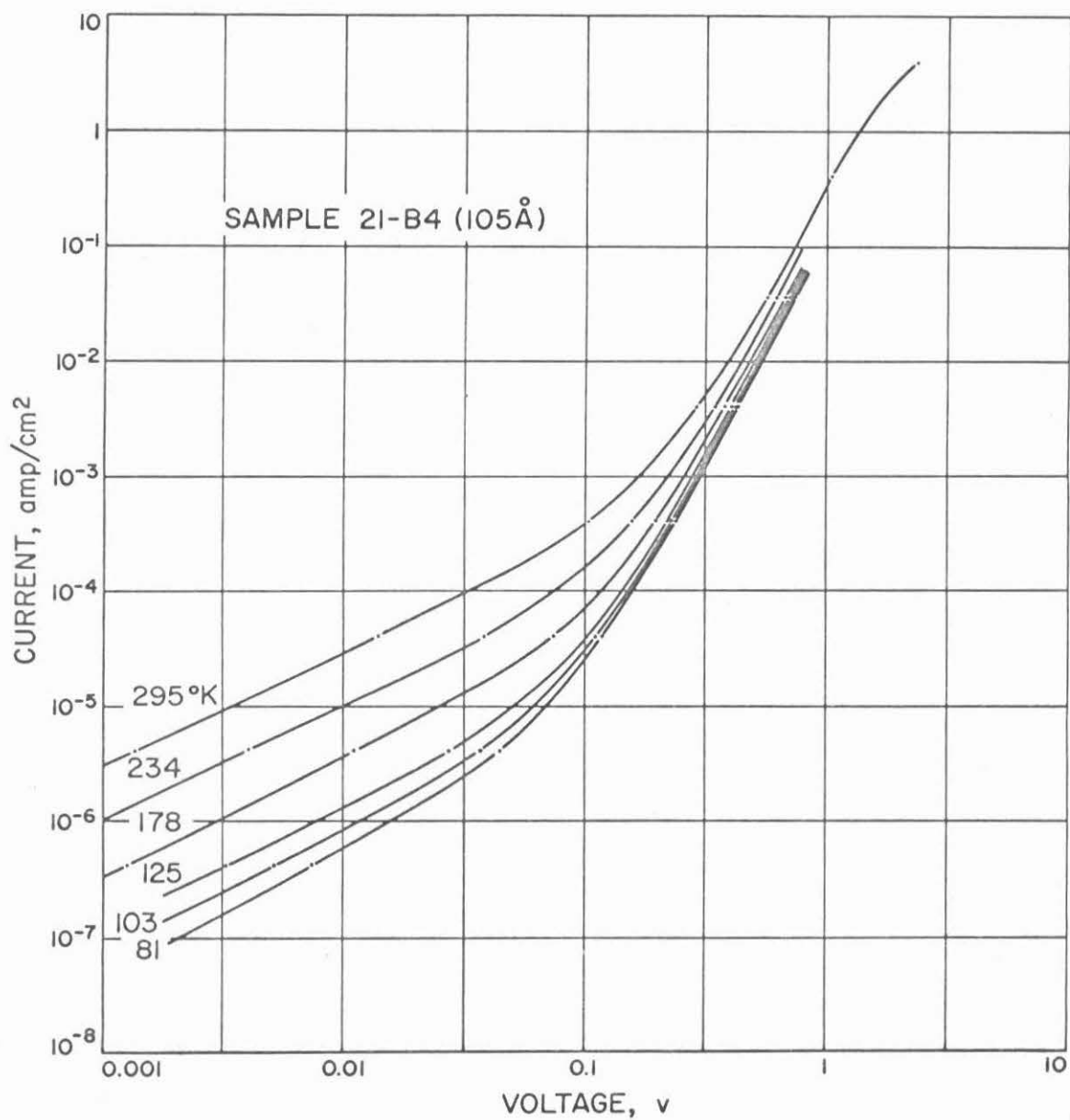


Figure III-13. Families of I-V curves vs temperature of sample No. 21-B4

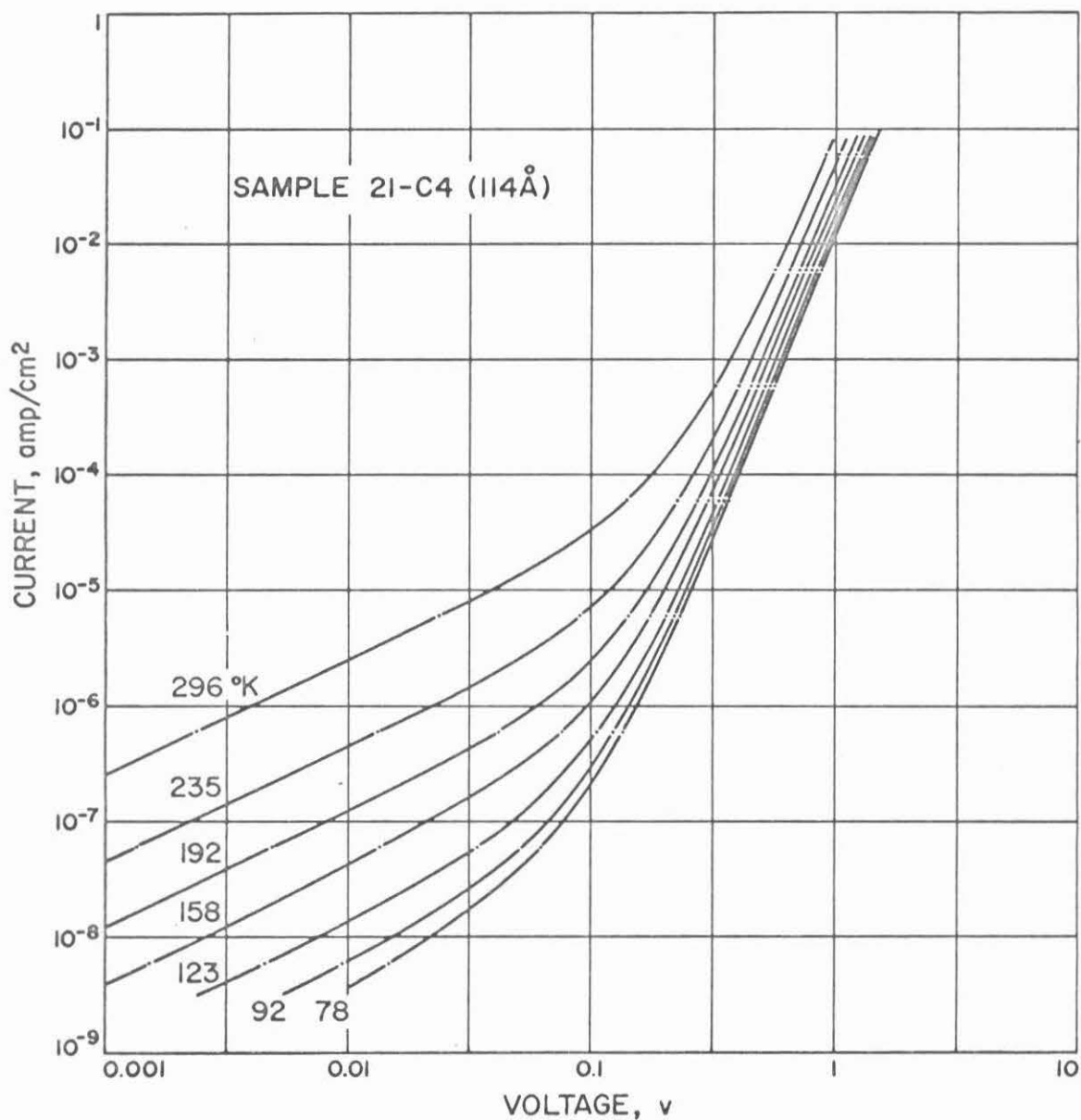


Figure III-14. Families of I-V curves vs temperature of sample No. 21-C4

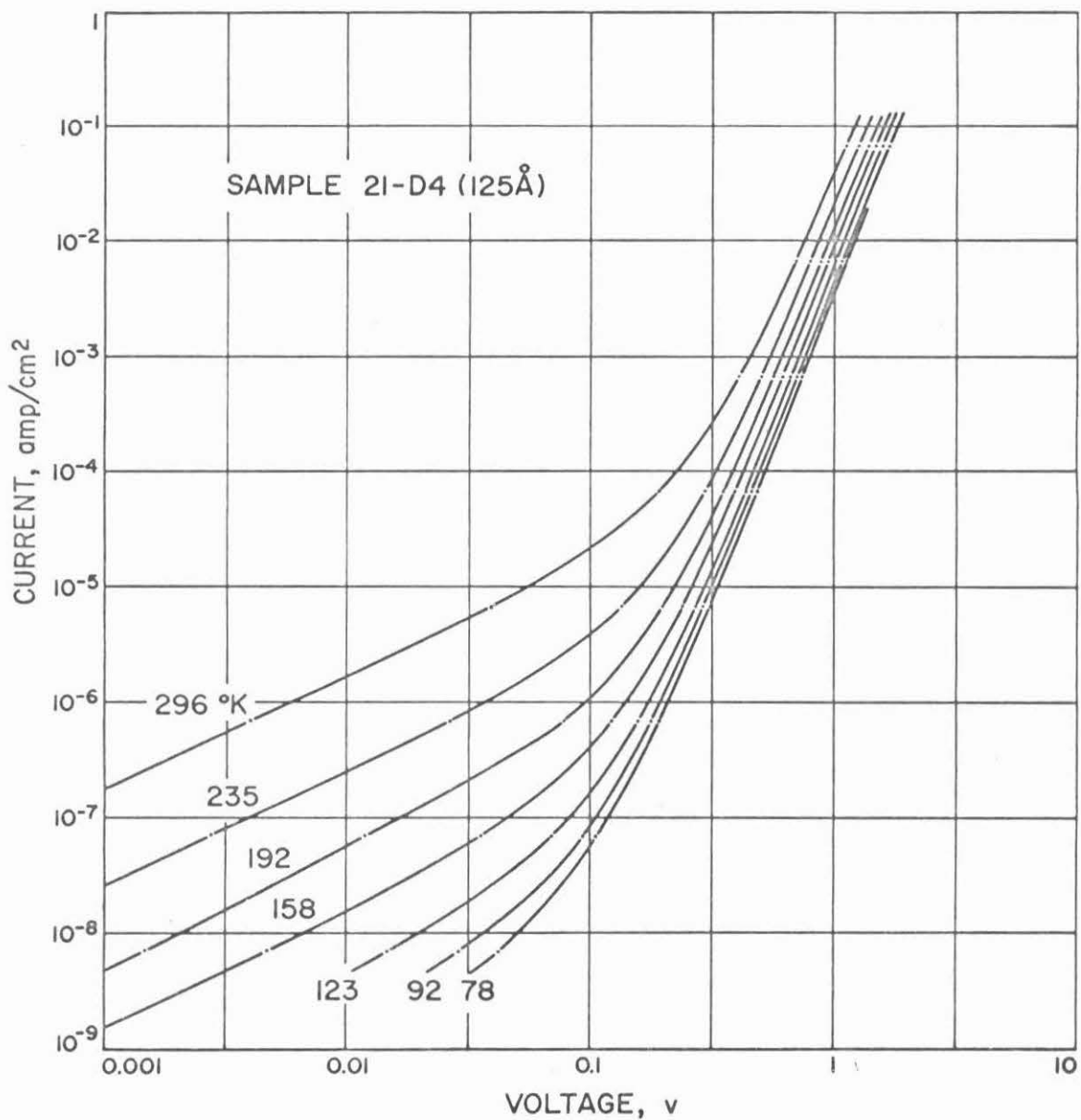


Figure III-15. Families of I-V curves vs temperature of sample No. 21-D4.

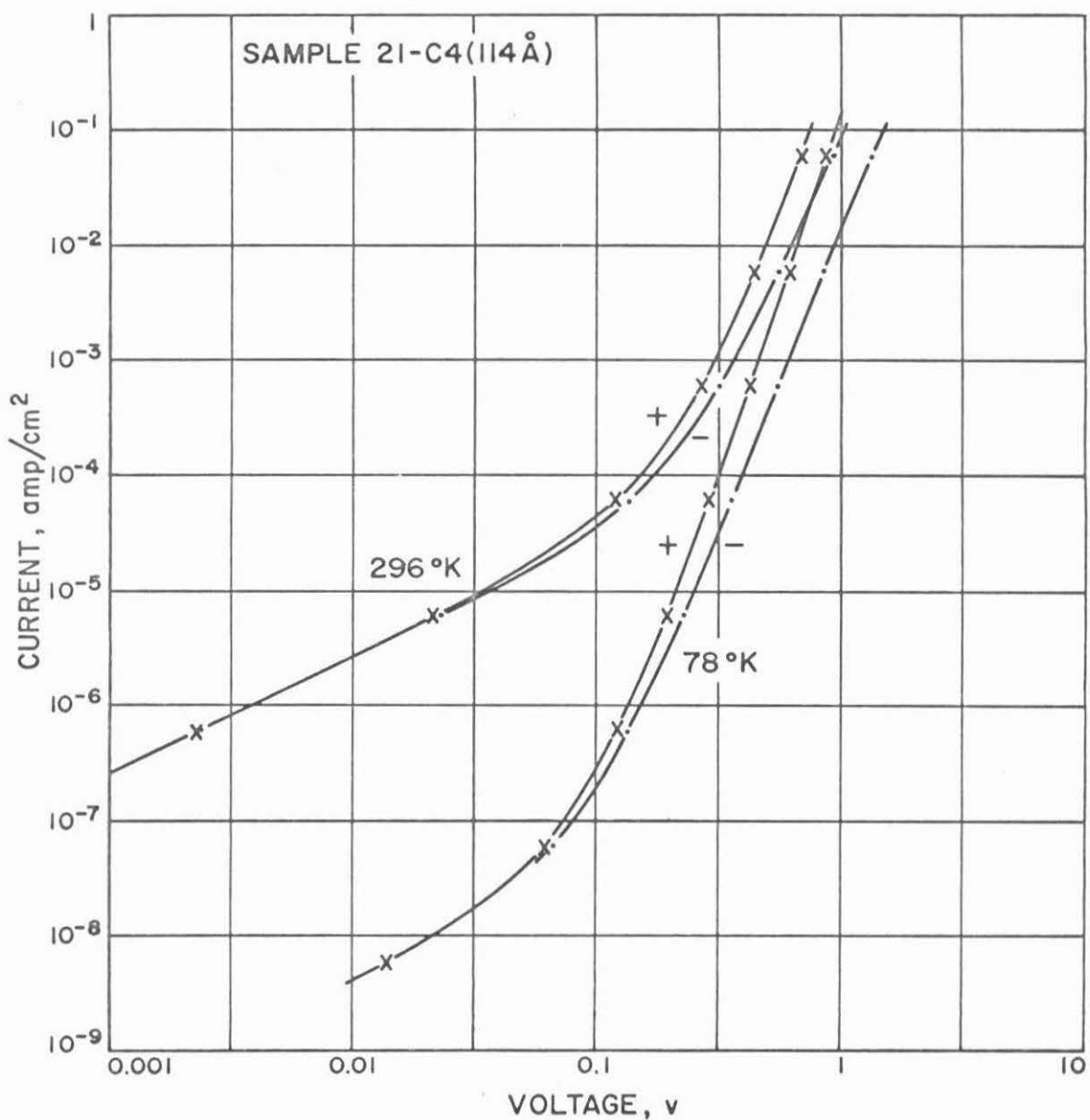


Figure III-16. Rectification characteristics of sample No. 21-C4.

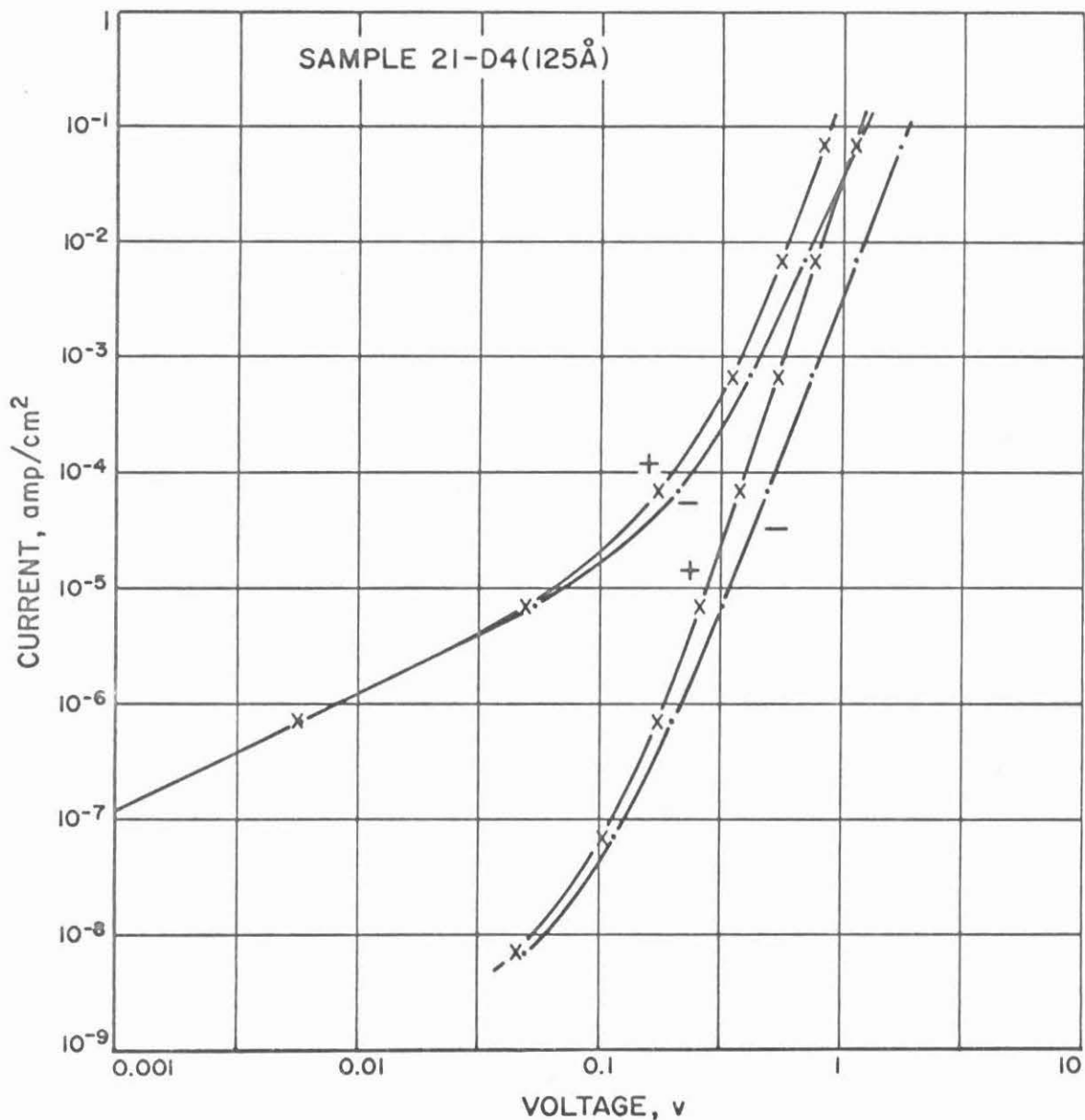


Figure III-17. Rectification characteristics of sample No. 21-D4.

specimen #21, strips B, C and D respectively.

The above results were obtained with negative polarity applied to the outer Al contact. Although both contacts were Al, differences encountered at each contact during the fabrication process result in some rectification. As this became of greater interest during the subsequent analysis a few months after the above measurements were made, some of the measurements were repeated to include both polarities. In Figs. III-16 and 17, both polarities are plotted at 78°K and 296°K for the same samples of C and D (Specimen #21). No significant change from the original characteristics occurred during the intervening time.

Measurements of the capacitance as a function of frequency and temperature were obtained using a Boonton 75C capacitance bridge for frequencies between 5 Kc and 500 Kc and a specially designed bridge for lower frequencies. The results obtained from the same two samples used for the previous data are given in Figs. III-18 and 19. The dashed curve indicates the cut-off effect predicted by a 1000 ohm resistance in series with the limiting capacitance C_o obtained from the pulse measurement. The 1000 ohm resistance represents the approximate value measured for the Al thin film leads. This rather high resistance was a consequence of the

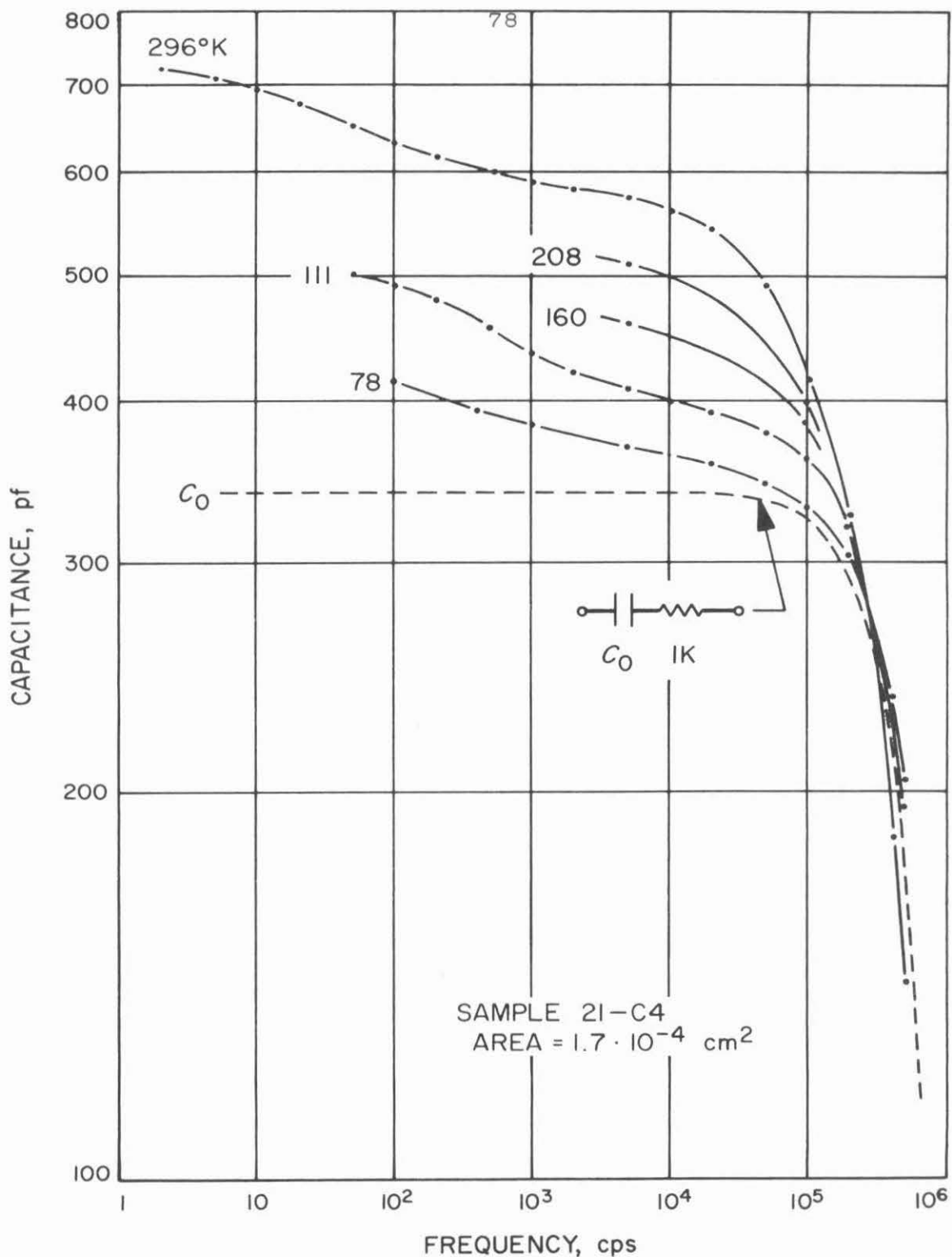


Figure III-18. Capacitance vs frequency and temperature of sample No. 21-C4.

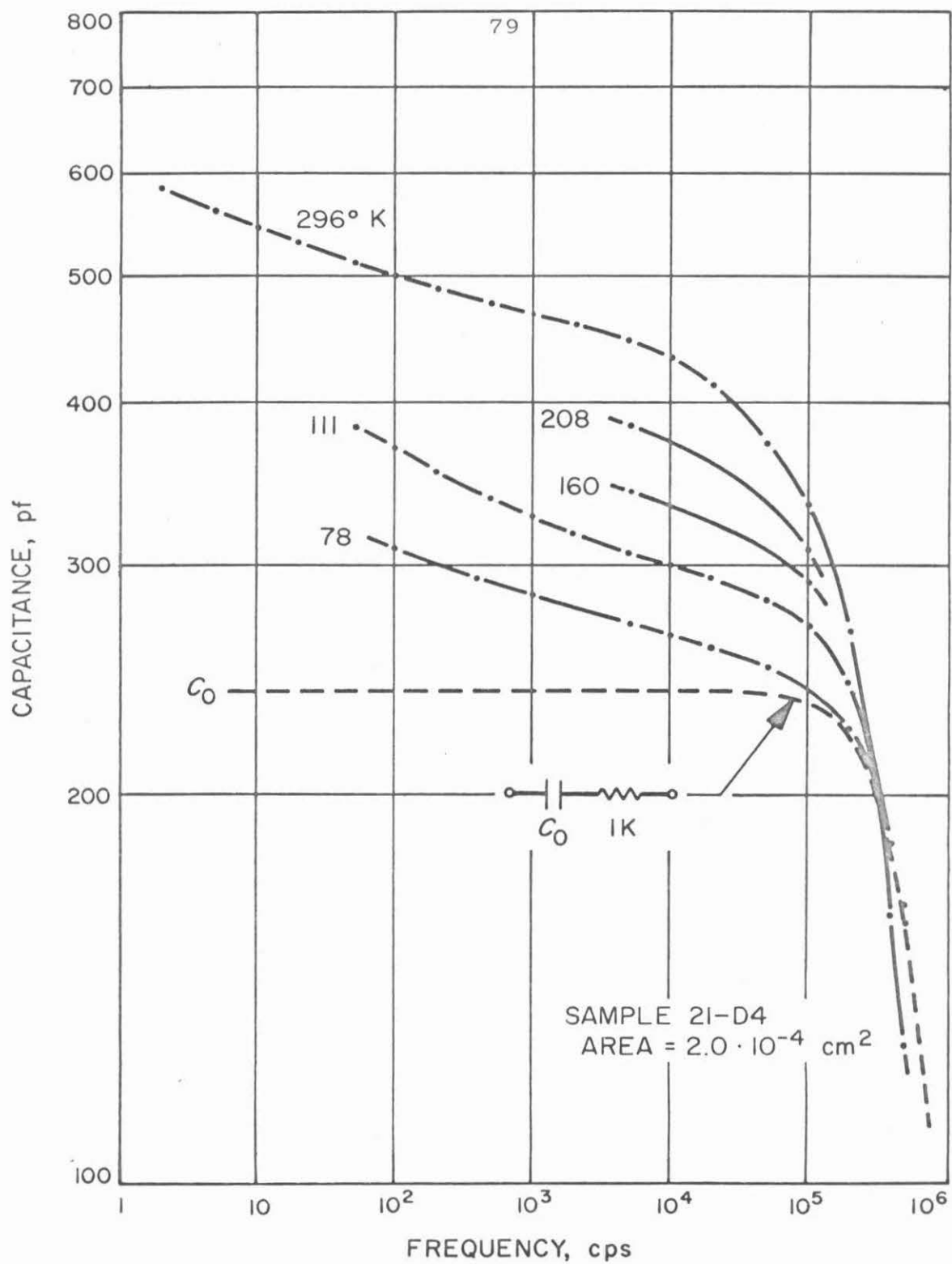


Figure III-19. Capacitance vs frequency and temperature of sample No. 21-D4.

anticipated photo-response measurements requiring Al films about 500 Å thick. The ac conductance was also obtained during the above measurements and is given for the same samples in Fig. III-20. The conductance measured at other intermediate temperatures could not be conveniently included in the figures, but lie smoothly between the plotted curves. The results are again compared with the effect of C_0 in series with 1000 ohm (dashed curves). The 296°K curve asymptotically reaches the same dc value as obtained from Figs. III-14 and 15. The conductance at 78°K could not be measured at lower frequencies but presumably also approaches the dc limit at a much lower value.

The capacitance was observed to also vary with dc voltage. In these samples the variation was smaller at low voltages than observed for anodized samples. Since some electrical forming and eventually breakdown occurred at the highest voltages, the measurements were restricted to other than the selected samples. Fig. III-21 gives the result for a representative sample from specimen #21-C measured at 5Kc on the Boonton bridge at 78°K.

C. Discussion of Results on Evaporated Films

It would be difficult to reconcile the differences between Al and Au contacts simply on the basis of

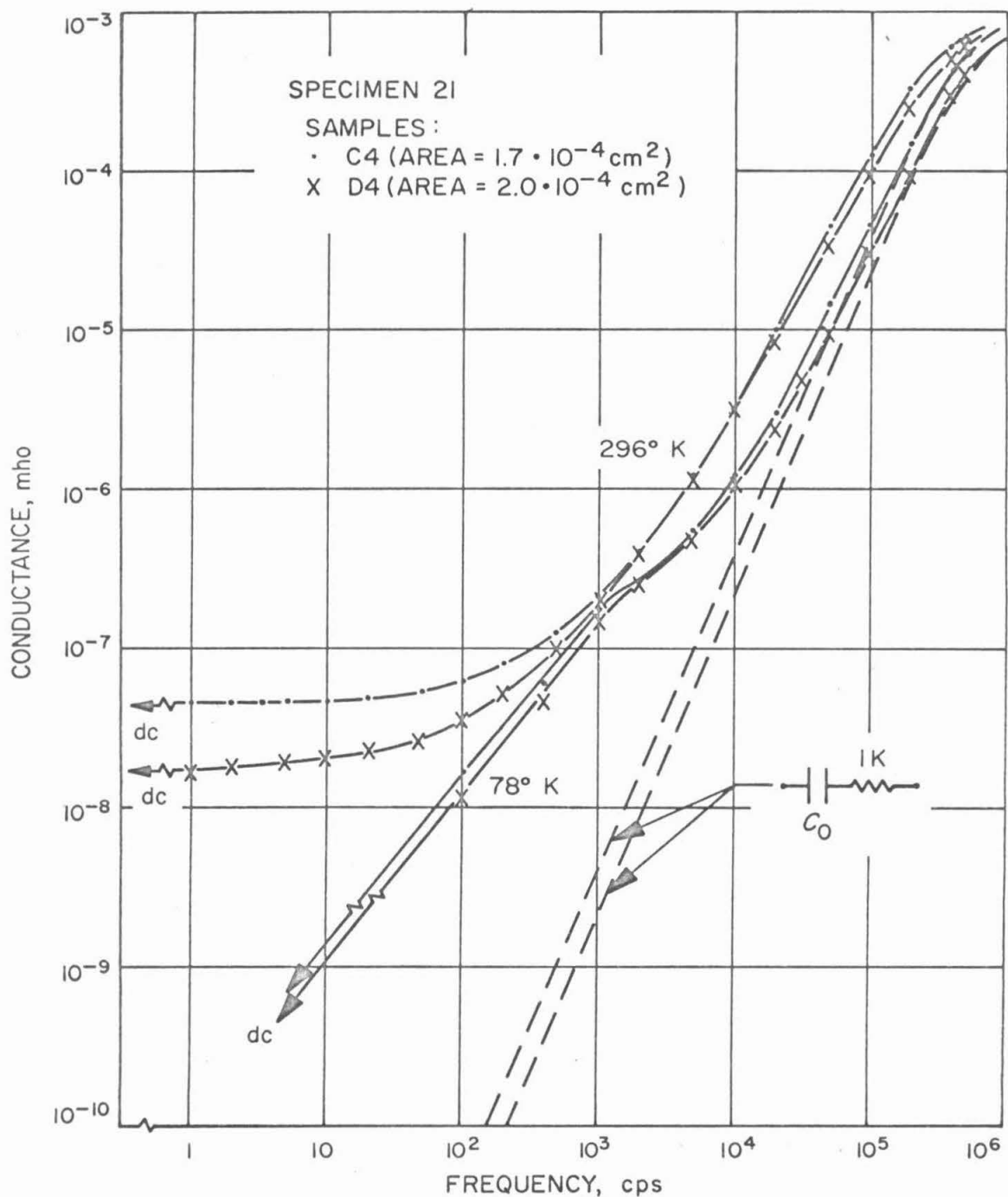


Figure III-20. Conductance vs frequency and temperature for No. 21-C4 and D4.

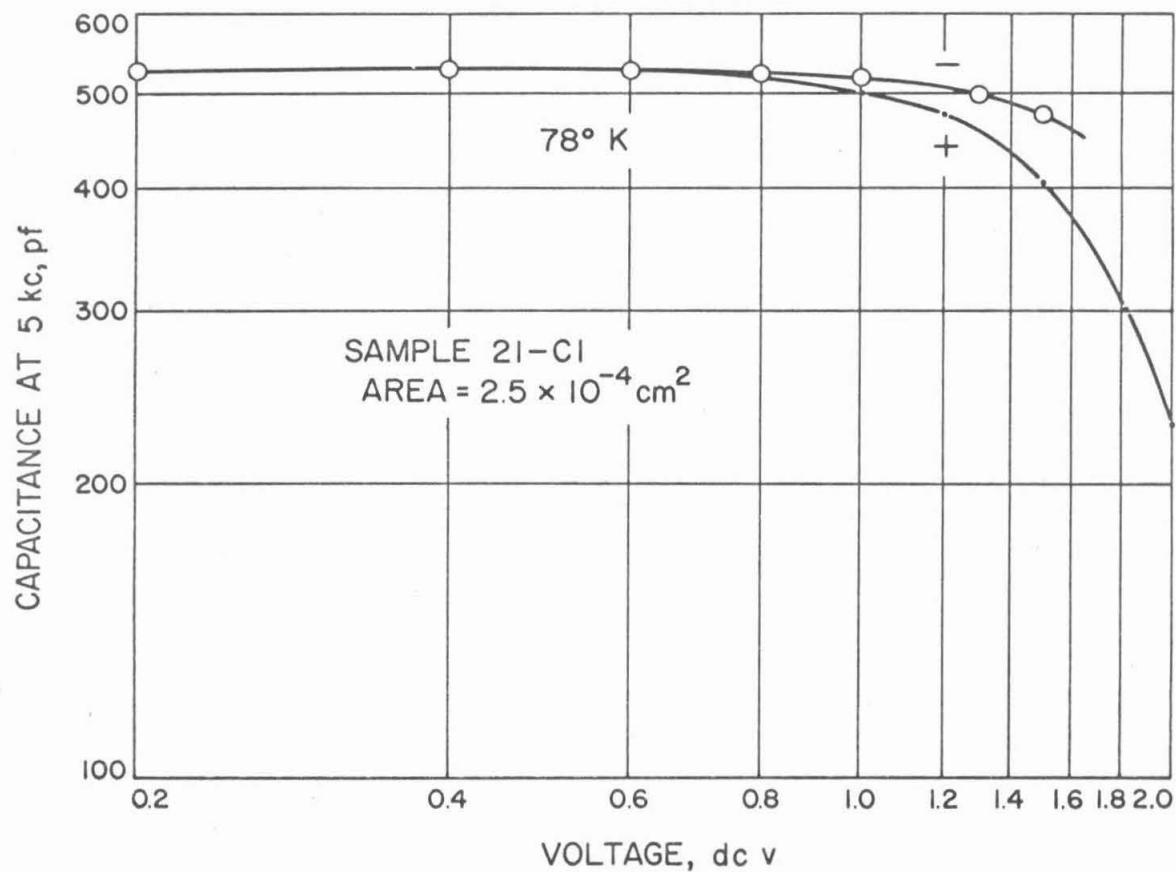


Figure III-21. Capacitance vs dc voltage

corresponding differences in barrier heights. Upon comparing the effect of the different contacts on two samples with similar oxide film thickness (Fig. III-8 and 10), one notes major differences in the I-V dependences although the room temperature conductance is nearly identical. Also there is the very appreciable improvement in the stability of the samples having Al contacts compared with those with Au contacts. The only difference other than the barrier heights that could conceivably be important is the presence of the corresponding Au or Al impurities in the oxide. During the evaporation process, with its associated heat of condensation, one can easily imagine an appreciable diffusion of the metal into the thin oxide films.

It is believed that the presence of Al converts the normally n-type oxide into p-type. Aluminum is known to act as an acceptor in rutile⁽¹⁶⁾, with the Al^{3+} ions occupying Ti^{4+} ion sites, yet p-type rutile is rarely formed because of the strong opposing tendency of reduction that occurs during the normal crystal growth or diffusion process. Aluminum is also commonly used as a stabilizing agent in insulating rutile. There has been evidence for the existence of p-type rutile where iron was the known impurity^(27,31), where Fe^{3+} ions act as acceptors in the same way as Al^{3+} . In our case

the evaporation process may favor the formation of an excess of Al acceptors. One can imagine the Al diffusing through the oxide during the deposition process, compensating for oxygen vacancies as well as continually reacting at the surface with the oxygen vapor and generating additional acceptors. On the other hand, the Au impurities are likely to introduce deep trapping states without affecting the large excess donor concentration introduced by oxygen vacancies.

In both cases we may assume that a large excess concentration of either donors or acceptors results (exact compensation would be very unlikely), and the space charge model discussed in Section IIC would only be changed with respect to the type of carrier (electron or hole) that is involved in the conduction process. If the conduction and valence bands were equivalent (equal effective masses), then clearly no significant differences would result that could not be interpreted in terms of differences in barrier heights. However, it is generally accepted that TiO_2 (both ceramic and single-crystal rutile) has a very narrow conduction band due to a small overlap of the Ti^{4+} 3d states and correspondingly possesses a large effective mass for electrons (see Appendix A). The valence band representing the O^{2-} 2p states is expected to be quite broad, with an effective mass

for holes probably similar to the free electron mass. On the basis of these differences we can account for the observed results.

In the case of the very thin samples with Au and Al contacts (Figs. III-8 and 10), the smaller temperature dependence suggests a tunneling mechanism of conduction especially at low temperatures. However, if one calculates the current from the familiar theory^(II) using the values measured for the oxide thickness and barrier height, the result is many orders of magnitude too small. Even if we allow for conceivably gross overestimates of the thickness (or barrier height), the observed I-V dependence ($\sim V^n$) is quite different than the nearly exponential dependence predicted by this theory. The space charge warping of the potential discussed in Section IIC is capable of accounting for these results as will be demonstrated in Chapter IV. The differences between the Au and Al contacts can be qualitatively understood by the following.

In the case of Au contacts and at low temperatures, the electrons tunneling through the first barrier (adjacent to the negative contact) are trapped by the narrow conduction band in the oxide interior and may lose all their excess energy, reaching thermal equilibrium with the oxide.

Current continuity must be satisfied by electrons tunneling out of the oxide through the second barrier. However since the supply of electrons in thermal equilibrium with the oxide at the dominant tunneling energies is much less than in the metal contact, most of the applied voltage appears across the second barrier until it is nearly suppressed to the fermi-level. Additional voltage then appears across the first barrier and the current increases much more rapidly. The transition voltage therefore occurs at approximately the barrier height as actually observed experimentally. This also corresponds to the transition to the Fowler-Nordheim region⁽³²⁾ for an ideal rectangular barrier, however the current dependence in this case is different. At sufficiently high voltages the effect of the barrier shape is less important and the dependence should approach an $\exp(-B/V)$ form as in the ideal Fowler-Nordheim theory. This also agrees with the results although it is not shown explicitly by Fig. III-8.

In the case of the thinner films with Al contacts (Figs. III-10 and II) and at low temperatures, holes tunneling through the first barrier may not lose all their excess energy in the broad valence band. If the supply

of holes at the dominant tunneling energies at the second barrier is much larger than for equilibrium, the current assumes a different form than that required for electron tunneling. This process which will be treated in Chapter IV predicts the more gradual variation of current with voltage observed.

In thicker films with Al contacts (see Figs. III-9 and I2), the room temperature currents are seen to exhibit quite different values that cannot be correlated with the thickness. This can be understood if specimen #20 (Fig. III-12) has smaller effective barrier heights at the contacts which encourages a thermionic type process at the higher temperatures. At 78°K and at higher voltages the different samples exhibit a more consistent relation to thickness that can be understood in terms of a tunneling process at the contact barriers, but where a larger fraction of the applied voltage is required across the oxide interior with increasing film thickness. On the basis of our model, the holes tunneling into the oxide valence band which lose their energy through collision processes (phonon or impurity) and become trapped before they can tunnel out through the second barrier require an additional voltage across the oxide interior in order to be released at the same rate and

maintain a steady state condition. The shape of the high voltage dependence ($\sim V^n$) remains nearly constant with thickness (compare also with the thinner samples of Fig. III-11) and supports the view that the primary dependence is governed by the barriers at the contacts. In the thinnest samples (Fig. III-10), the I-V dependence exhibits a somewhat smaller slope. This can be understood if the oxide is too thin for the barriers to extend to their normal effective distance from each contact. Alternately, the effect of impurities from the contacts may become excessive in the oxide interior below some critical thickness.

Additional information on the influence of the interior of thicker films was obtained from the experiments described for specimen #17 (Fig. III-9). The activation energies indicated by the temperature dependence are believed to be associated with trapped holes. After ac forming, the larger resistance at low voltage and the increase in the temperature dependence are believed to result from the removal of some of the excess Al acceptor ions. This may occur as Al^{3+} ions are induced by the applied ac field to move out of more stable sites in the oxide, permitting them to diffuse with the assistance of the built-in field to the contacts where they precipitate. The smaller activation energy $E_1 \approx .1$ ev

may be associated with the Al acceptor levels E_A , equaling either E_1 or $2E_1$ depending on the degree of impurity compensation as discussed by Mott and Gurney (loc.cit., pp 156-160). The former applies when the density of excited holes is much less than the density of compensating donors, and the latter when the reverse is true. The larger activation energy $E_2 = .23$ ev, observed above 140°K after forming may be associated with deeper acceptor states. The reduced acceptor concentration would result in less ionic space charge and consequently longer tails in the barriers extending from the contacts. Therefore more of the shallow acceptor states would be depleted of holes, allowing the deeper states to dominate at the higher temperatures. These energies are much too large to result from the usual hydrogenic model of acceptor levels ($\approx .01$ ev). However they may be understood in terms of the large polarization energies associated with the release of trapped holes from the oxide (polaron self trapping). This argument has been used by Frederickse⁽¹⁷⁾ to explain the large donor energies observed in rutile at higher temperatures (typically $\approx .15$ ev).

Without dwelling further on the effect of the interior of the thicker oxide films, we wish to concentrate only on the effects of the contacts. This can be conveniently examined

from the results on the thin film samples of specimen #21. As mentioned above, the results from film B of this specimen indicates that the oxide is too thin to be characteristic of the normal barriers at the contacts. The slightly thicker films, C and D, appear to be ideal for our purpose. These films, represented by the family of I-V curves given in Figs. III-13 and 14 exhibit an appreciable temperature dependence at low voltages that cannot be attributed to a pure tunneling process. However, neither can this temperature dependence be described in terms of distinct activation energies. In Chapter IV it will be shown how the effect of the ionic space charge and its associated barrier shape encourages a thermally assisted tunneling process that predicts precisely this kind of behavior.

The results obtained from measurements of capacitance and conductance as a function of frequency and temperature (Figs. III-18 through 20) can also be interpreted on the basis of the proposed model. The large variation of capacitance with temperature would be very difficult to explain on any other basis. For example, the dependence is much too large to be accounted for by the small temperature dependence of the dielectric constant. The theory derived in Chapter IV predicts an effective barrier width that varies with

temperature, and the corresponding variation of capacitance with temperature will be shown to agree with these results. The sharp cut-off in the frequency dependence has already been attributed to the series resistance of the leads. The frequency dependence of capacitance below its cut-off, can be interpreted on the basis of a redistribution of space charge in the oxide due to trapped holes in the manner discussed in Section II C for trapped electrons in anodized films. It is not possible to use the usual simple model⁽³³⁾ characterized by a single relaxation time for the trapped holes, and accurately describe the observed dependence. A distribution of relaxation times could be chosen that could provide such a description, but this would offer no useful advantage. However, the implications resulting from a distribution of relaxation times are more consistent with our model when we consider the variation of potential with position in the barriers. Trapped holes located at different positions and thus at different energies in the oxide will necessarily find it more or less difficult to shift about under the varying field.

The dependence of conductance on frequency and temperature serves to compliment the capacitance results. The eventual saturation at approximately 10^{-3} mhos near 1 mc is again attributed to the effect of the series resistance. At

lower frequencies, the increase cannot be completely accounted for by the effect of the series resistance but can be interpreted on the basis of the corresponding ac conductance of trapped holes. In Fig. III-20 an inflection appears near 2 kc at 78°K and a corresponding inflection can be detected for the capacitance of the sample in Fig. III-18. This is not as evident in the other sample (Fig. III-19). This can arise if a more prominent relaxation time exists for the trapped holes. On the basis of the idealized model that assumes a single relaxation time we can construct an equivalent circuit such as shown in Fig. III-22. The idealized trapping effect is given by the circuit shown in solid lines within the dashed rectangle (c.f. Ref. 33). Also indicated in phantom lines within the rectangle is the possible extension of the idealized circuit to include a distributed RC network for more accurately describing the sample. Below cut-off ($\omega \ll 1/R_s C_o$) and for $R_1 \gg R_2$, the admittance of the circuit becomes

$$Y = \frac{1/R_2 + (\omega R_1 C_1)^2 / R_1}{1 + (\omega R_1 C_1)^2} + j\omega \left[C_o + \frac{C_1}{1 + (\omega R_1 C_1)^2} \right]$$

where the relaxation time is $R_1 C_1$. Below the characteristic frequency ($\omega = 1/R_1 C_1 \approx 2\pi \cdot 2\text{kc}$) the effective conductance increases from the dc value of $1/R_2$, and above this frequency it saturates at $1/R_1$ (when neglecting R_s). Correspondingly

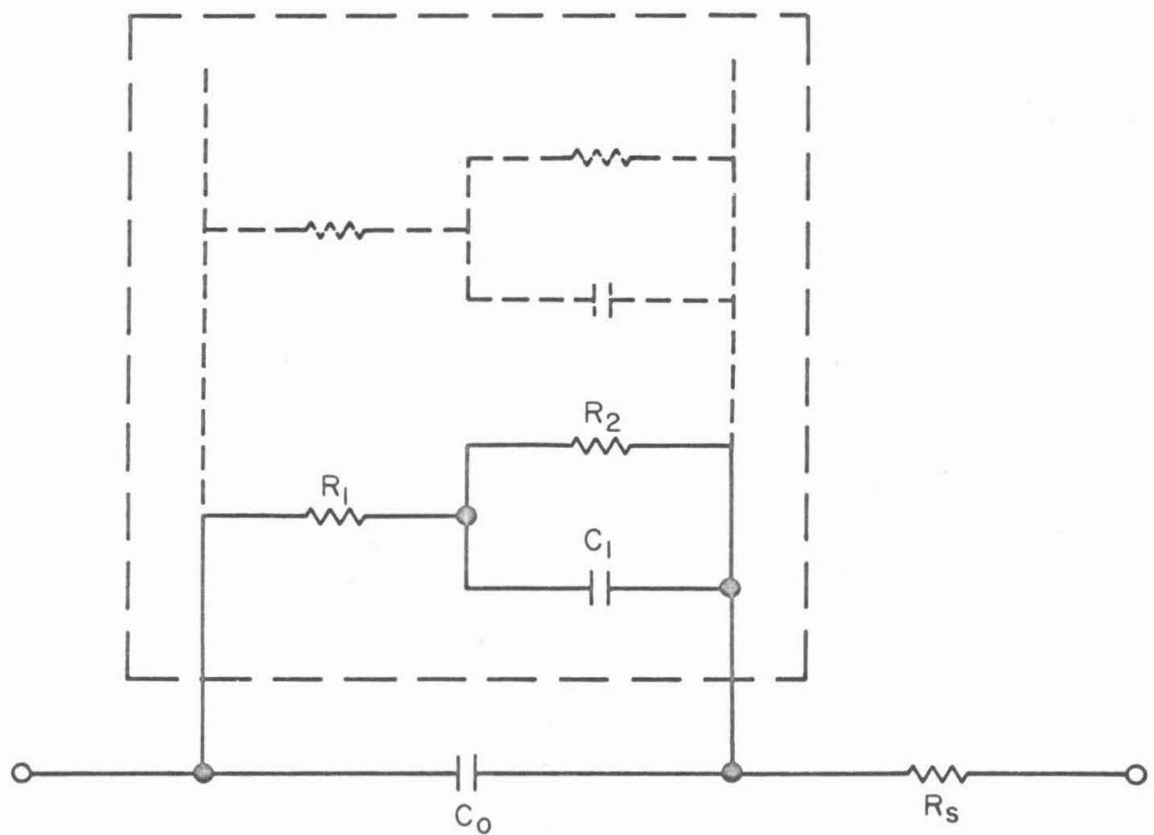


Figure III-22. Equivalent circuit of sample.

the effective capacitance decreases from $C_o + C_1$ to C_o above this frequency. This is in qualitative agreement with the observed dependences, but clearly a more complicated distributed RC network is required for an accurate representation. The pulse measurements for C_o are seen to be consistent with the ac measurements, with the comparison offering some reassurance that the limiting value was nearly reached.

IV. THEORY

A. The Barrier Potential

I. Impurity-Space-Charge Models. In Chapter II we discussed the influence of a large excess of donors in the oxide film (n-type) on the potential shape of the barrier. An equivalent problem is presented in the case of an excess acceptor concentration (p-type) as discussed in Chapter III, when the potential is correspondingly taken for holes. As a matter of convenience, the following treatment will refer specifically to the p-type case.

In order to obtain the barrier potential U (for holes), we start as usual from Poisson's equation in one dimension,

$$\frac{d^2U}{dx^2} = \frac{4\pi}{\kappa} \rho \quad (1)$$

where in this case ρ is defined as the net negative charge density which in general is some function of x , $\rho(x)$. The problem therefore requires a knowledge of $\rho(x)$ which in turn depends on the distribution of ionized impurities.

Single acceptor level with uniform distribution along x . Consider the familiar case in semiconductor theory which deals with a single acceptor level close to the

valence band and the acceptors uniformly distributed in the semiconductor with density N_A . Let the potential* be measured from the Fermi level at the adjacent metal contact, and let $U = -\eta$ at the limit of the space-charge layer ($x = d$). Beyond this layer the positive charge of holes balances the negative charge of acceptors ($\rho = 0$). In the space-charge layer the density of holes decreases as $\exp [-(U+\eta)/kT]$ and becomes negligible when $(U+\eta)/kT \gtrsim 1$ (depletion of holes). Thus, for $U > -\eta$ one can use the approximation

$$\rho \approx qN_A \text{ (constant).} \quad (2)$$

The barrier potential may be evaluated for the general case in which there may be an applied field if we let η include the voltage drop V_1 across the space-charge layer; that is,

$$\eta = V_1 - \eta_0 \quad (3)$$

where $-\eta_0$ represents the equilibrium value of η . We will neglect any resistive effect of the oxide interior beyond the space-charge layer and therefore consider the field in this region to be zero. The boundary conditions

*It is convenient to use potential and energy interchangeably with the understanding that electron volts (ev) is the unit of energy. Thus U may also be understood to represent the energy of holes at the valence band edge measured from the Fermi energy at the contact.

are then

$$\begin{aligned} U(0) &= W \\ U(d) &= -\eta \\ \left(\frac{dU}{dx}\right)_{x=d} &= 0 \end{aligned} \tag{4}$$

where W is the metal-to-oxide work function at the contact. Equation (1) is readily integrated subject to the above conditions, yielding

$$U + \eta = (W + \eta) \left(1 + \frac{x}{d}\right)^2 \tag{5}$$

and

$$d = \sqrt{\frac{\kappa(W + \eta)}{2\pi q N_A}} \tag{6}$$

A similar expression is correspondingly obtained for the opposite contact. Clearly the film thickness must exceed $2d$ in this case. Barriers of this type have been treated extensively⁽³⁴⁾ for more moderate impurity concentrations than considered here, particularly in connection with a thermionic conduction process (Schottky emission, c.f. Chapter I).

Uniform energy distribution of impurity states.

It is unlikely that the above assumptions on ρ should apply to thin films. For example, we can consider the effect of a distribution of acceptor states of density $N(E)$ over a wide range of energies in the forbidden band.

Then clearly ρ must increase with U as correspondingly more states become ionized. Let us assume a uniform distribution of states, defined for convenience by

$N(E) = N_A/W(\text{constant})$. The total density of ionized acceptor states at any x in the barrier must then be proportionate to the height of the valence band above the quasi-Fermi level (imref) at this x . The value of the imref in turn depends on the steady-state transfer of trapped holes in these deep lying states. Since the transfer of trapped holes becomes progressively easier as one moves from the barrier maximum to the tail of the barrier, the inref will correspondingly change more slowly with increasing x , asymptotically approaching its limiting value.

A reasonable approximation is to assume the imref to be constant throughout the space-charge layer, since the error introduced at small x would only become appreciable at very large applied fields. The space-charge density is then approximately

$$\rho \approx \frac{qN_A}{W}(U + \eta) \quad (7)$$

Equation (1) may then be integrated subject to the boundary conditions

$$U(0) = W$$

$$U(x \rightarrow \infty) = -\eta , \quad (8)$$

obtaining

$$U + \eta = (W + \eta) e^{-x/s} \quad (9)$$

where

$$s = \sqrt{\frac{\kappa W}{4\pi q N_A}} . \quad (10)$$

Since a similar expression also applies at the opposite contact, Eq(9) might only be expected to apply when the film thickness w is several times s . When the finite thickness w is accurately taken into account, and for simplicity the contacts are assumed equivalent, one obtains

$$U + \eta = (W + \eta) \frac{\cosh(\frac{x}{s} - \frac{w}{2s})}{\cosh(\frac{w}{2s})} . \quad (11)$$

Thus, for $w/2s > 1$, Eq(11) can be approximated by the simpler expression of Eq(9) applying at each contact, with any small error at the center of the oxide film absorbed in the value of η_0 .

Single acceptor level with exponential distribution along x . If we assume a single shallow acceptor level with the density given by $N_A e^{-x/s}$, as measured from each contact independently, we arrive at essentially the same result given by Eq(9). Such a distribution of acceptors (Al^{3+} ions) can result from a

rate-determined diffusion process that occurs during the formation of the films. For example, consider Fick's diffusion law

$$D \frac{\partial^2 N}{\partial x^2} = \frac{\partial N}{\partial t} \quad (12)$$

where D is the diffusion coefficient of the Al in the oxide under the conditions of formation. If the rate of accumulation of N depends on some rate of reaction R between the Al and the available oxygen, we might write $\frac{\partial N}{\partial t} = RN$.

Eq(12) is then integrated to give

$$N = N_A e^{-\sqrt{R/D} x} \quad (13)$$

where $N(0)$ is defined as N_A to conform with the above.

This result is identical with the required form if we simply let $\sqrt{D/R} = s$.

The Poisson-Boltzmann distribution.

Frenkel⁽³⁵⁾ has discussed how the Debye-Hückel theory of electrolytes can also be applied to solids when under thermal equilibrium with its surfaces (or interfaces). The theory treats the influence of coulombic interactions of ionized impurities under thermal equilibrium which is expressed by the Poisson-Boltzmann equation (in one dimension),

$$\frac{d^2 U}{d x^2} = \frac{kT}{L^2} \sinh \left(\frac{U+\eta}{kT_e} \right) \quad (14)$$

where L is the Debye length and T_e is the equilibrium temperature.* If we let $L = s$, the problem becomes identical to the above when $(U+\eta)/kT_e < 1$; that is, Eq(14) becomes $d^2U/dx^2 \approx (U+\eta)/s^2$ [c.f. Eq(1) and (7)]. For larger values of U (smaller x), Eq(14) predicts a more rapid decrease of U with x . However, the boundary conditions at the surfaces are different during the process of formation and also the attainment of equilibrium is doubtful. In any case, Eq(14) serves to suggest still another possible reason for anticipating barriers similar to the exponential form given in Eq(9).

For lack of more precise knowledge of $\rho(x)$, the subsequent analysis will compare the effect of the exponential barriers of Eq(9) with the usual space-charge barrier of Eq(4). However, the emphasis will be later given to the exponential barriers, primarily because it leads to a better correspondence between the theory and experimental results.

* T_e may refer to some high effective temperature during formation of the film, with the resulting distribution "frozen in" at lower temperatures.

2. Image Force Correction. The effect of image forces at the contacts should also be included in describing the effective barrier potential. The image force correction is approximately

$$U_i = -\frac{q}{4\kappa_0 x} \quad (15)$$

where κ_0 is the optical value of dielectric constant ($\kappa_0 = n^2$) and x is measured from the corresponding contact. [The effect from the opposite contact can be considered negligible for our case, i.e., $q/4\kappa_0 w \ll w$.]

The effective barrier is thus represented by the sum $U + U_i$.

The barrier height ϕ due to the image-force lowering can be determined by evaluating $(U + U_i)$ at the point x_0 , where its derivative is zero. The results obtained for the assumed barriers are

$$\frac{x_0}{d} = \sqrt{\left(\frac{q}{4\kappa_0 d}\right)/2(\phi + \eta)} \quad (16a)$$

and approximately

$$\phi \approx w \left(1 - 4 \frac{x_0}{d}\right) \quad (16b)$$

for the quadratic barriers of Eq(4); and correspondingly,

$$\frac{x_0}{s} = \sqrt{\left(\frac{q}{4\kappa_0 s}\right)/\phi} \quad (17a)$$

and

$$\phi \simeq W(1 - 2 \frac{x_0}{s}) \quad (17b)$$

for the exponential barriers of Eq(9). The above approximations make use of the assumptions $x_0/d, x_0/s \ll 1$, which should be valid in most cases of interest.

3. Effective Barrier Approximations. The effective barrier potential ($U + U_i$) is awkward to use in the form given above. A more useful approximate form may be obtained as follows. For $x > x_0$ the barrier can be nearly represented by the original expression for U if we replace W by ϕ and translate the origin to x_0 . The contribution for $x < x_0$ may be added as a small correction and represented by a parabolic potential fitted at $U(0) = \phi$ and $U(-x_0) = 0$. The errors introduced by these two approximations are in opposite directions and therefore tend to cancel one another. The effective potential then becomes for the quadratic barrier of Eq(4),

$$U \simeq \phi \left[1 - \left(\frac{x}{x_0} \right)^2 \right] \quad \text{for } x < 0 \quad (18a)$$

$$U + \eta \simeq (\phi + \eta) \left(1 + \frac{x}{d} \right)^2 \quad \text{for } x > 0 \quad (18b)$$

where

$$d \simeq \sqrt{\frac{x(\phi + \eta)}{2\pi q N_A}} \quad (18c)$$

and x_0, ϕ are given in Eq(16); and for the exponential barrier of Eq(9),

$$U \approx \phi \left[1 - \left(\frac{x}{x_0} \right)^2 \right] \quad \text{for } x < 0 \quad (19a)$$

$$U + \eta \approx (\phi + \eta) e^{-x/s} \quad \text{for } x > 0 \quad (19b)$$

where

$$s \approx \sqrt{\frac{\kappa \phi}{4\pi q N_A}} \quad (19c)$$

and x_0, ϕ are given in Eq(17).

4. Effect of Statistical Fluctuations. One might also consider the effect of fluctuations in the very narrow barrier due to the discrete nature of the ionized impurities. This is ignored in the classical meaning of $\rho(x)$ which implies a continuous function of x , such as given in Eqs(2) and (7). Henisch⁽³⁴⁾ has suggested the possible limitations of this classical treatment in very narrow barriers that are only a few times thicker than the average spacing of the ionized impurities. However, a continuous function of $\rho(x)$, and correspondingly $U(x)$, clearly exists for describing the statistical average over the entire macroscopic volume of the film. If we were to properly take into account the effect of fluctuations from this average at each increment of area, we would correspondingly have to include the statistical frequency or probability of encountering each fluctuation. When this statistical accounting is carried out, we find that the effect of

fluctuations in reducing the barrier tends to be offset by the associated probabilities describing the frequency of their occurrence.

One way of visualizing this is to consider the limiting case where a local fluctuation results in the complete eradication of the barrier. This limit can occur, for example, when acceptors are found aligned in a chain at each lattice site in the increment of area in question, thus permitting a metallic-like transfer of holes along the chain. If we consider a lattice of normal sites of average spacing a, the probability of not finding a normal site in a chain of length x is given by Clausius' formula⁽³⁶⁾

$$P = e^{-x/a} . \quad (20)$$

We are free to assign acceptor impurities to abnormal sites of this chain if appropriate allowance is made in the value defined for a. Equation (20) may then be interpreted to represent the desired probability for finding an acceptor chain. It may alternately be interpreted simply as the probability of not encountering a normal lattice site (no lattice collisions) and in this sense is equivalent to the usual probability predicted for quantum mechanical penetration of a barrier. The value of $1/a$, which must take into account the presence of the impurities (e.g., acceptors) and the

contacts, is then correspondingly equivalent to the usual attenuation coefficient characterizing the average barrier in quantum theory.

The above argument serves to suggest a similarity between the effect of the average barrier on its penetrability and the effect of local fluctuations. This similarity is characteristic of the familiar "correspondence principle" of quantum theory that states the equivalence between a quantum mechanical and classical description of a system represented in terms of macroscopic averages.

The difficulty in applying this principle to our system arises from the apparent failure of the macroscopic representation in one dimension although in reality we are still dealing with and measuring a macroscopic system (in three dimensions). The question then arises on whether the quantum mechanical effects predicted for our one-dimensional microscopic model should then be valid for our macroscopic system. We can only imply that this is true from the simple argument given above for lack of a rigorous proof. On the other hand, we can turn to the experimental evidence found in similar cases that provides support for this view. For example, the well-known theory of tunnel diodes has very successfully used the classical description

of the barrier in predicting the experimental results, even though the barrier widths in this case may typically represent on the average only two impurity separations. We therefore feel justified in using a classical representation of the narrow space-charge barriers in our proposed model for the TiO_2 films.

B. Transport Theory

1. General Equations. The current density that crosses an arbitrary barrier along the x -direction may be expressed in the general form* [c.f. Eq(13) of Ref. (II)]

$$j = \frac{A}{kT} \int_{-\eta}^{\infty} P(E) \ln \left[\frac{1 + e^{-E/kT}}{1 + e^{-(E+V_1)/kT}} \right] dE, \quad (21)$$

where

$$A = \frac{4\pi m q}{h^3} (kT)^2 = 120 T^2 \text{ amp/cm}^2 \quad (22)$$

is the familiar Richardson's coefficient, $P(E)$ is the transmission probability of the barrier at the energy E , V_1 is the applied voltage across the barrier, and $-\eta$ is the minimum energy allowed. The quantity A/kT times the log term in the integrand is sometimes referred to as the supply function and represents the difference in the flux of holes

*The equations assume that the holes (or electrons) are in thermal equilibrium at each side of the barrier, however the effect of a non-equilibrium distribution of holes in the oxide can be important and is treated in part 3 of this section.

(or electrons) along the x -direction in the range E to $E + dE$ incident from opposite sides of the barrier.

In considering the barrier at the first contact in our model, it is convenient to define $E = 0$ at the Fermi level of the contact. The energy $-\eta$ must represent the edge of the valence band in the oxide, corresponding to the limit of the space charge layer as defined in Section IV A (i.e., $\eta = V_1 - \eta_0$). An additional contribution to the current may result from impurity states in the forbidden band at lower energies. However this "impurity conduction" may be considered to act in parallel with the above process and should normally be negligible except at low voltages and temperatures. The second barrier may be treated in an analogous manner by transforming the energy origin to the Fermi level of the second contact.

The transmission probability can be approximated by

$$P(E) = \frac{1}{1 + e^{\Theta(E)}} \quad (23)$$

where

$$\Theta(E) = \infty \int_{x_{10}}^{x_1} \sqrt{U(x) - E} dx, \quad (24)$$

x_{10}, x_1 are the roots of $U(x) - E = 0$, and ∞ is the factor

$\sqrt{8m^*/\hbar}$ assumed to be constant. Equation (23) represents an extension of the familiar W.K.B. approximation for $P(E)$ [i.e., $P(E) = \exp(-\theta)$] and was used by Murphy and Good⁽³⁷⁾ to describe the effect of energies near the barrier maximum in the case of electron emission from a metal into a vacuum. The expression is exact for an ideal parabolic barrier and therefore represents a good approximation for energies in the vicinity or above the barrier maximum. At slightly lower energies ($E < \phi$), $P(E)$ approaches the familiar form of $\exp(-\theta)$.

One can obtain from Eq(21) the expressions which apply to both limiting cases discussed previously, that is, (1) pure tunnelling and (2) pure thermionic emission. In case (1) the dominant energies occur near $E \approx 0$; thus $\theta(E) \gg 1$ and $P(E) \rightarrow \exp(-\theta)$. The currents may then be evaluated following Stratton⁽¹¹⁾ by using the expansion

$$\theta(E) = b_1 - c_1 E + f_1 E^2 + \dots \quad (25)$$

When $c_1 kT < 1$ and f_1 can be neglected, the integral of Eq(21) converges and gives

$$j = \frac{A}{(c_1 kT)^2} \frac{\pi c_1 kT}{\sin(\pi c_1 kT)} e^{-b_1} (1 - e^{-c_1 V_1}) \quad (26)$$

In case (2) we may use the limits $E/kT \gg 1$, and

$$P(E) \rightarrow 1, \quad E > \phi$$

$$\rightarrow 0, \quad E < \phi$$

which leads to the familiar expression for the thermionic current

$$j = A e^{-\phi/kT} (1 - e^{-V_1/kT}). \quad (27)$$

In most barriers commonly considered, the above two limiting cases [Eq(26) & (27)] represent practical solutions and the intermediate case in which the dominant tunneling energies occur between 0 and ϕ , would only apply over very narrow ranges of voltage and temperature. However, the space charge barriers of Eqs(18) and (19) will in general require a solution to the intermediate case in addition to the "pure" tunneling case of Eq(26).

2. Current for the Intermediate Case. Since this case applies when the dominant energies lie within the range $0 < E < \phi$, we may assume

$$E/kT, \theta(E) \gg 1.$$

Equation (21) then reduces to

$$j = \frac{A}{kT} (1 - e^{-V_1/kT}) \int_{-\eta}^{\infty} e^{-[\theta(E) + E/kT]} dE. \quad (28)$$

The integral may be evaluated by the familiar saddlepoint approximation, that is, by integrating about the energy

in which the bracketed function in the exponent is a minimum. The saddle-point energy E_0 is determined by

$$\left(\frac{d\theta}{dE}\right)_{E_0} + \frac{1}{kT} = 0 . \quad (29)$$

Expanding the function about E_0

$$\theta(E) + E/kT = \beta + \gamma (E - E_0)^2 + \dots$$

where

$$\beta = \theta(E_0) + E_0/kT \quad (30)$$

and

$$\gamma = \frac{1}{2} \left(\frac{d^2\theta}{dE^2} \right)_{E_0} , \quad (31)$$

one obtains the result

$$j = \frac{A}{kT} \sqrt{\frac{\pi}{\gamma}} e^{-\beta} (1 - e^{-V_1/kT}) . \quad (32)$$

The limiting condition for which Eq(32) can be expected to apply is $E_0 > 0$. This is equivalent to the condition

[c.f. Eqs(25) and (29)]

$$c_1 kT > 1 \quad (33)$$

and therefore complements the condition $c_1 kT < 1$ which applies to the case of pure tunneling in Eq(26).

It is useful to compare the results for the two cases as $c_1 kT \rightarrow 1$. From Eq(32) one obtains

$$j \rightarrow A c_1 \sqrt{\frac{\pi}{f_1}} e^{-b_1} (1 - e^{-c_1 V_1})$$

and from Eq(26),

$$j \rightarrow A \left[\frac{\pi c_1 kT}{\sin(\pi c_1 kT)} \right] e^{-b_1} (1 - e^{-c_1 V_1}).$$

We see that the divergent factor $\pi c_1 kT / \sin(\pi c_1 kT)$ from Eq(26) is replaced by the finite factor $c_1 \sqrt{\pi/f_1}$ from Eq(32).

This suggests the following extrapolation between the two limiting cases for $c_1 kT \leq 1$:

$$j = \frac{AB}{(c_1 kT)^2} e^{-b_1} (1 - e^{-c_1 V_1}) \quad (34a)$$

where

$$B = \left[\frac{\sin(\pi c_1 kT)}{\pi c_1 kT} + \sqrt{\frac{f_1}{\pi c_1^2}} \right]^{-1}. \quad (34b)$$

Since $\sqrt{f_1/\pi c_1^2}$ is normally small, its contribution is only important in the vicinity of $c_1 kT=1$. The validity of Eq(34) was confirmed by carrying out a numeral calculation using the saddle-point method with the general expression for the integrand in Eq(21) and assuming reasonable values of f_1/c_1^2 . Similarly Eq(32) was found to represent a good approximation for $c_1 kT > 1$. Equations (32) and (34) are equal at their common limit $c_1 kT=1$.

3. The Two Barrier Problem. The model proposed for the TiO_2 films requires that we consider the effect of two barriers, one associated with each of the two metal contacts. In order to treat this problem we must make certain assumptions on the steady state energy

distribution of holes (or electrons) in the interior of the oxide. We will describe the two limiting extremes one might consider and then propose a third intermediate process which is in complete agreement with our results.

One extreme corresponds to the situation in which the holes tunneling through the first barrier lose all the energy acquired by the applied field to the oxide lattice. The energy distribution of holes may then be described as for thermal equilibrium except for the corresponding change in the (quasi) fermi level in the oxide. The two barriers then act as two independent impedances in series and the applied voltage must divide in the appropriate manner between them. In this case almost the entire voltage will occur across the second barrier until it is sufficiently suppressed by the applied voltage, since the current is limited primarily by the "quasi-equilibrium" supply of holes in the oxide. This was the situation proposed in Chapter II for electrons in the narrow conduction band of n-type oxide films. The problem must in general deal with two simultaneous implicit equations representing the equal currents through each barrier, each a function of its portion of the applied voltage, and the exact solution must then be obtained by numerical or graphical means.

The other extreme corresponds to the situation in which the holes tunneling through the first barrier retain the energy acquired by the applied field during the time required to tunnel through the second barrier. In this case let us represent the supply functions of Eq(21) by generalized functions Y with subscripts added to denote the respective regions. The current through each barrier is then written

$$j_1 = \int_{-\eta}^{\infty} (Y_1 - Y_0) P_1 dE$$

$$j_2 = \int_{-\eta}^{\infty} (Y_0 - Y_2) P_2 dE$$

where only Y_1 and Y_2 retain the usual thermal equilibrium dependence at each contact, that is,

$$Y_1 = \frac{A}{kT} \ln \left[1 + e^{-E/kT} \right]$$

and

$$Y_2 = \frac{A}{kT} \ln \left[1 + e^{-(E+V)/kT} \right]$$

and Y_0 corresponds to the generalized supply function for the oxide interior. Since the steady state condition requires $j_1 - j_2 = 0$, we have

$$\int_{-\eta}^{\infty} [Y_1 P_1 + Y_2 P_2 - Y_0 (P_1 + P_2)] dE = 0 .$$

In this case the integrand must vanish at all E and we

then obtain

$$Y_o = \frac{Y_1 P_1 + Y_2 P_2}{P_1 + P_2}$$

Y_o may then be eliminated from the current equations,

yielding

$$j = \frac{A}{kT} \int_{-\eta}^{\infty} \ln \left[\frac{1 + e^{-E/kT}}{1 + e^{-(E+V)/kT}} \right] \frac{dE}{e^{\Theta_1} + e^{\Theta_2}} . \quad (35)$$

where V is the total applied voltage. This result is directly analogous to the familiar problem of quantum theory which treats the transmission of a particle through an ideal double barrier⁽³⁸⁾. The result of Eq(35) predicts a rapid decrease in the contribution of the second barrier with applied voltage.

We do not believe that either of the above extremes applies in the case of holes entering the oxide. However the holes are likely to lose much of their energy after entering the oxide without necessarily reaching thermal equilibrium with the oxide. In this case let us assume that the supply functions corresponding to the oxide interior in the steady state can be represented by

$$Y_o = \lambda(E) \frac{A}{kT} \ln \left[1 + e^{-(E+\eta)/kT} \right] \quad (36)$$

where the coefficient $\lambda(E)$, which modifies the equilibrium function, varies relatively much more slowly with energy over the range of interest, that is,

$$\frac{kT}{\lambda} \left| \frac{d\lambda}{dE} \right| \ll 1$$

We may then evaluate the current through each barrier about the respective saddle point energies as described previously, but obtained separately for the forward and reverse components of current. We then obtain

$$j_1 = j_{10} - \lambda j_{01} \quad (37)$$

$$j_2 = \lambda j_{02} - j_{20}$$

where we have stipulated the same λ at each of the saddle points corresponding to the reverse component at the first barrier and the forward component at the second barrier.

This is justified since these two saddle points will in general differ only very slightly and $\lambda(E)$ was assumed to vary sufficiently slowly in this range. The continuity condition

$j_1 - j_2 = 0$ then gives

$$\lambda = \frac{j_{10} + j_{20}}{j_{01} + j_{02}} \quad (38)$$

We may then eliminate λ from Eq(37) and obtain

$$j = \frac{j_{10}j_{02} - j_{01}j_{20}}{j_{01} + j_{02}} . \quad (39)$$

In general if $\eta_0 \leq 0$ the intermediate case ($c_1 kT > 1$) will always apply for both current components at the second barrier, j_{02} and j_{20} , as well as the reverse component at the first barrier j_{01} and thus we must always have

$$j_{02} = j_{20} e^{(V-V_1)/kT}$$

$$j_{20} = \frac{A}{kT} \sqrt{\frac{\pi}{\gamma_2}} e^{-\beta_2}$$

$$j_{01} = \frac{A}{kT} \sqrt{\frac{\pi}{\gamma_1}} e^{-(\beta_1 + V_1/kT)}$$

and either

$$j_{10} = \frac{A}{kT} \sqrt{\frac{\pi}{\gamma_1}} e^{-\beta_1} , \text{ for } c_1 kT > 1$$

or

$$j_{10} = \frac{AB}{(c_1 kT)^2} e^{-\beta_1} , \text{ for } c_1 kT < 1 .$$

In most cases of practical interest we can use the approximations *

* β_1 and β_2 are evaluated with respect to the energy zero defined at the Fermi level of the first and second contact respectively as a matter of convenience in applying general equations derived for either contact.

$$\begin{aligned}
 \beta_1 &\simeq b_{10} - \beta_{11}\{T\} - \frac{V_1}{kT} \\
 \beta_2 &\simeq b_{20} - \beta_{22}\{T\} + \frac{V-V_1}{kT} \\
 b_1 &\simeq b_{10} - b_{11}\{V_1\}
 \end{aligned} \tag{40}$$

where b_{10} and b_{20} are constants independent of voltage and temperature, β_{11} and β_{22} are functions only of temperature and b_{11} is a function only of voltage. These approximations are particularly good for the barriers being considered as can be verified from the derivations given later in this section. The current from Eq(39) then becomes for $c_1 kT > 1$

$$j = kT G e^{V_1/kT} (1 - e^{-V/kT}) \tag{41a}$$

and for $c_1 kT < 1$

$$j = G \left(\frac{B}{c_1^2 \sqrt{\frac{8}{\pi}}} e^{b_{11} - \beta_{11}} - kT e^{-V/kT} \right) \tag{41b}$$

where G is the zero field conductance given by

$$G = \frac{A/(kT)^2}{\sqrt{\frac{8}{\pi}} e^{b_{10} - \beta_{11}} + \sqrt{\frac{8}{\pi}} e^{b_{20} - \beta_{22}}} \tag{42}$$

and B is given by Eq(34b). The limiting conductance G is seen to take the form one would expect when considering the two barriers in the zero field limit as two resistors in series. The reverse component in Eq(41b) is

normally negligible whenever the equation is applicable

(i.e., $c_1 kT < 1$).

The voltage across the first barrier V_1 can be determined from the condition that the total space charge in the oxide does not change from its equilibrium value (i.e., no space charge is injected). This condition is implied by the introduction of λ in the above derivation; that is, the supply function at the second barrier depends primarily on the non-equilibrium excess of higher energy holes which has a negligible influence on the total charge density of the holes in the oxide. This condition may be written

$$\int_0^W (\rho - \rho_0) dx = 0 \quad (43)$$

where ρ and ρ_0 correspond to the space charge density of the assumed barriers under an applied field and at equilibrium respectively [i.e., $\rho = (\kappa/4\pi) d^2 U/dx^2$].

Equations (41) and (42) can only apply if the second barrier is not completely suppressed by the voltage, since only under this condition does λ and thus the entire derivation have any meaning. Also when the total applied voltage is greater than the barrier height, direct emission of holes from the first contact over the second barrier, without being trapped in the interior,

becomes increasingly more probable and may become the dominant process. Therefore a practical upper limit on the applied voltage when using Eqs(41) and (42), may be considered to be approximately the barrier height at the second contact.

4. Formulation in Terms of the Proposed Barriers. The relations required in the theory will be subsequently evaluated for each of the proposed barrier potentials given by Eqs(18) and (19). Although the integral defining Θ in Eq(24) may be evaluated exactly for both cases, the initial portions of the two barriers ($x < 0$) given in Eqs(18a) and (19a) normally represent small corrections to Θ which we may approximate by a constant Δ evaluated at $V=E=0$ [we will continue to refer to the main contribution for $x > 0$ as Θ]. The correction Δ has the same form for both cases (with appropriate x_0), giving

$$\begin{aligned}\Delta &= \alpha \sqrt{\phi} \int_0^{x_0} \left[1 - \left(\frac{x}{x_0} \right)^2 \right]^{1/2} dx \\ &= \frac{\pi}{4} \alpha x_0 \sqrt{\phi}\end{aligned}\quad (44)$$

The remaining relations will be treated separately for each type of barrier with subscripts added to distinguish between the first and second contact.

Quadratic Barriers.

Inserting Eq(18b) into Eq(24) we have at the first barrier

$$\Theta_1 = \alpha \int_0^{x_1} \left[(\phi_1 + \eta) \left(1 - \frac{x}{d}\right)^2 - E \right]^{1/2} dx$$

where

$$(\phi_1 + \eta) \left(1 - \frac{x_1}{d}\right)^2 = E + \eta$$

Letting $z = \sqrt{(\phi_1 + \eta)/(E + \eta)} (1 - x/d)$, the integral reduces to

$$\Theta_1 = \alpha \int_1^{\sqrt{(\phi_1 + \eta)/(E + \eta)}} \frac{1}{\sqrt{z^2 - 1}} dz$$

where the parameter T_0 is a characteristic temperature of the oxide defined by

$$kT_0 = \frac{\sqrt{\phi_1 + \eta}}{2\alpha d_1} = \frac{1}{2\alpha} \sqrt{\frac{2\pi q N_A}{\kappa}} . \quad (45)$$

After integrating, one obtains the result

$$\Theta_1 = \frac{\phi_1 + \eta}{kT_0} \left[\sqrt{1 + \frac{E + \eta}{\phi_1 + \eta}} - \frac{E + \eta}{\phi_1 + \eta} \operatorname{sech}^{-1} \sqrt{\frac{E + \eta}{\phi_1 + \eta}} \right] . \quad (46)$$

The other expressions required in the theory for the first barrier [c.f. Eqs(25), (29), (30) and (31)] may be readily evaluated using Eq(46) and are given as follows

[N.B. $\eta = V_1 - \eta_0$] :

$$b_1 = \frac{\phi_1}{kT_0} \left[\sqrt{1 + \frac{\eta}{\phi_1}} - \frac{\eta}{\phi_1} \sinh^{-1} \sqrt{\frac{\phi_1}{\eta}} \right] + \Delta_1 \quad (47a)$$

$$c_1 = \sinh^{-1} \sqrt{\frac{\phi_1}{\eta}} / kT_0 \quad (47b)$$

$$f_1 = 1 / \left(4kT_0 \eta \sqrt{1 + \frac{\eta}{\phi_1}} \right) \quad (47c)$$

$$E_{o1} = \phi_1 \operatorname{sech}^2 \left(\frac{T_0}{T} \right) - \eta \tanh^2 \left(\frac{T_0}{T} \right) \quad (47d)$$

$$\beta_1 = \frac{\phi_1 + \eta}{kT_0} \tanh \left(\frac{T_0}{T} \right) - \frac{\eta}{kT} + \Delta_1 \quad (47e)$$

$$\gamma_1 = \left[4kT_0 (\phi_1 + \eta) \tanh \left(\frac{T_0}{T} \right) \operatorname{sech}^2 \left(\frac{T_0}{T} \right) \right]^{-1}. \quad (47f)$$

The transition between pure tunneling and the intermediate case (i.e., $c_1 kT = 1$ or $E_{o1} = 0$) is given by

$$\eta = \phi_1 / \sinh^2 \left(\frac{T_0}{T} \right) \quad (48)$$

where larger values of η correspond to pure tunneling.

The expression for Θ_2 , with the energy measured from the Fermi level of the second contact, may be obtained directly from Eq(46) by replacing η with $\eta - V$ and ϕ_1 with ϕ_2 , that is,

$$\Theta_2 = \frac{\phi_2 + \eta - V}{kT_0} \left[\sqrt{1 + \frac{E + \eta - V}{\phi_2 + \eta - V}} - \frac{E + \eta - V}{\phi_2 + \eta - V} \operatorname{sech}^{-1} \sqrt{\frac{E + \eta - V}{\phi_2 + \eta - V}} \right]. \quad (49)$$

The other expressions required for the second barrier may be obtained from Eq(49), giving

$$E_{o2} = \phi_2 \operatorname{sech}^2 \left(\frac{T_0}{T} \right) + (V - \eta) \tanh^2 \left(\frac{T_0}{T} \right) \quad (50a)$$

$$\beta_2 = \frac{\phi_2 + \eta - V}{kT_0} \tanh\left(\frac{T_0}{T}\right) + \frac{V - \eta}{kT} + \Delta_2 \quad (50b)$$

$$\gamma_2 = \left[4kT_0(\phi_2 + \eta - V) \tanh\left(\frac{T_0}{T}\right) \operatorname{sech}^2\left(\frac{T_0}{T}\right) \right]^{-1} \quad (50c)$$

Exponential Barriers.

Inserting Eq (19b) into Eq (24) we have at the first barrier

$$\Theta_1 = \alpha \int_0^{x_1} \left[(\phi_1 + \eta) e^{-x/s_1} - E \right]^{1/2} dx$$

where

$$(\phi_1 + \eta) e^{-x_1/s_1} = E + \eta .$$

Letting $z = \sqrt{(\phi_1 + \eta)/(E + \eta)} e^{-x/2s_1}$, the integral becomes

$$\Theta_1 = \frac{\sqrt{\phi_1(E + \eta)}}{kT_0} \int_1^{\sqrt{(\phi_1 + \eta)/(E + \eta)}} \frac{\sqrt{z^2 - 1}}{z} dz$$

where the parameter T_0 is a characteristic temperature of the oxide defined by

$$kT_0 = \frac{\sqrt{\phi_1}}{2\alpha s_1} = \frac{1}{2\alpha} \sqrt{\frac{4\pi q N_A}{\kappa}} . \quad (51)$$

After integrating we obtain the result

$$\Theta_1 = \frac{\phi_1}{kT_0} \left[\sqrt{1 - \frac{E}{\phi_1}} - \sqrt{\frac{E + \eta}{\phi_1}} \cos^{-1} \sqrt{\frac{E + \eta}{\phi_1 + \eta}} \right] . \quad (52)$$

The following expressions are then readily obtained from Θ_1 :

$$b_1 = \frac{\phi_1}{kT_0} \left[1 - \sqrt{\frac{\eta}{\phi_1}} \operatorname{ctn}^{-1} \sqrt{\frac{\eta}{\phi_1}} \right] + \Delta_1 \quad (53a)$$

$$c_1 = \sqrt{\frac{\phi_1}{\eta}} \operatorname{ctn}^{-1} \sqrt{\frac{\eta}{\phi_1}} / 2kT_0 \quad (53b)$$

$$f_1 = \left[\sqrt{\frac{\phi_1}{\eta}} \operatorname{ctn}^{-1} \sqrt{\frac{\eta}{\phi_1}} + 1 \right] / 8kT_0\eta \quad (53c)$$

The saddle point E_{01} is determined by [c.f. Eq(29)]

$$\sqrt{\frac{E_{01} + \eta}{\phi_1}} = \frac{T}{2T_0} \cos^{-1} \sqrt{\frac{E_{01} + \eta}{\phi_1 + \eta}} \quad (54)$$

Since the intermediate case applies only when $\eta \ll \phi_1$,

and thus for all reasonable barriers $(E_{01} + \eta)/(\phi_1 + \eta) \ll 1$,

we may use the expansion

$$\cos^{-1} \sqrt{\frac{E_{01} + \eta}{\phi_1 + \eta}} \simeq \frac{\pi}{2} - \sqrt{\frac{E_{01} + \eta}{\phi_1}}$$

and obtain from Eq(54)

$$E_{01} + \eta \simeq \phi_1 \left[\frac{\pi/2}{2T_0/T + 1} \right]^2 \quad (55)$$

Then to the same approximation we obtain

$$\beta_1 \simeq \frac{\phi_1}{kT_0} \left[1 - \frac{\pi^2/8}{2T_0/T + 1} \right] - \frac{\eta}{kT} + \Delta_1 \quad (56a)$$

$$\gamma_1 \simeq \left(\frac{2T_0}{T} + 1 \right)^3 / \pi^2 2kT_0 \phi_1 \quad (56b)$$

The transition between pure tunneling and the intermediate case (i.e., $c_1 kT = 1$) is given by

$$\tau = 2T_0 \sqrt{\frac{\eta}{\phi_1}} / \sin^{-1} \sqrt{\frac{\eta}{\phi_1}} \quad (57)$$

or $\frac{\eta}{\phi_1} \approx \left[\frac{\pi/2}{2T_0/\tau + 1} \right]^2$

where lower temperatures corresponds to pure tunneling.

The expression for θ_2 , with the energy measured from the Fermi level of the second contact is obtained from Eq(52) by replacing η with $\eta - V$, and changing subscripts, that is,

$$\theta_2 = \frac{\phi_2}{kT_0} \left[\sqrt{1 - \frac{E}{\phi_2}} - \sqrt{\frac{E+\eta-V}{\phi_2}} \cos^{-1} \sqrt{\frac{E+\eta-V}{\phi_2+\eta-V}} \right]. \quad (58)$$

The other expressions required for the second barrier are obtained from Eq(58) as above, with the results

$$E_{02} + \eta - V \approx \phi_2 \left[\frac{\pi/2}{2T_0/\tau + 1} \right]^2 \quad (59a)$$

$$\beta_2 \approx \frac{\phi_2}{kT_0} \left[1 - \frac{\pi^2/8}{2T_0/\tau + 1} \right] + \frac{V-\eta}{k\tau} + \Delta_2 \quad (59b)$$

$$\gamma_2 \approx \left(\frac{2T_0}{\tau} + 1 \right)^3 / \pi^2 2kT_0 \phi_2. \quad (59c)$$

C. Application of the Theory

I. General Considerations. A preliminary comparison of the theory with the experimental results for both the quadratic and the exponential barriers has shown the latter to give much better agreement. Therefore, we will use the theory for the exponential barriers exclusively in the subsequent analysis. Since the experimental results for the thin samples with Al contacts display similar characteristics, we will limit our analysis to a single representative sample (#21-C4). The latter is one of the samples which appears to be consistent with our simplified model; that is, in satisfying the assumption that the barriers associated with each contact extend to their practical limit and that the interior separating the barriers is negligible. We will also provisionally make the additional assumption that the equilibrium potential in the interior η_0 is approximately zero and thus $\eta \approx V_1$. This will be confirmed by the results of the subsequent analysis.

The condition imposed on V_1 by Eq(43) requires that $V_1 = V/2$ if the intrinsic work function W is equal for both contacts as should be the case when both contacts are Al. The differences in barrier heights ϕ_1 and ϕ_2 obtained from the photo-response measurements

must then arise from differences in impurity concentrations adjacent to each contact (interface or surface states). In defining a single characteristic temperature T_o [c.f. Eq(51)] we have already implied that the effective impurity distribution ($\sim N_A$) is essentially the same for both barriers. However, since this does not take into account differences in concentrations in the immediate vicinity of the contacts, no inconsistency is presented by the differences in ϕ . The assumption of constant T_o was made for simplicity and will be shown to represent a good approximation for the experimental results. We will thus use $V_1 = V/2$ in the subsequent analysis. Also since the voltages obtained in the measurements of sample #21-C4 do not exceed the barrier heights, the theory represented by Eqs(41), (42), and (43) should apply in all cases.

The theory is then formulated in terms of two important parameters, ϕ which should relate to the photoelectric measurements and T_o which is adjustable within reasonable limits based on its defining equation. We then wish to show that a single value of T_o can consistently predict the correct dependences of both current and capacitance, each as a function of both voltage and temperature.

2. Current Dependence. The general relations of Eqs(41) and (42) can be simplified further since we can assume $\phi_2 < \phi_1$, from the photoelectric measurements. The larger exponent involving ϕ_1 in the expression for G will always dominate for either polarity. Thus after substituting the appropriate expressions from Eqs(40) and (59) and defining the reduced temperature variable

$$t = \frac{\pi/2}{2T_0/T + 1} , \quad (60)$$

we obtain for the zero field conductance (in mho/cm²)

$$G = 5.6 \cdot 10^6 T_0 \sqrt{\frac{\phi_1}{kT_0}} t^{3/2} \exp\left[-b_{10} + \frac{\pi\phi_1}{4kT_0} t\right] . \quad (61)$$

The intermediate case applies when* [c.f. Eq(57)]

$$\frac{V}{2\phi} < t^2 \quad (62)$$

and becomes

$$j = 2kT G \sinh\left(\frac{V}{2kT}\right) . \quad (63)$$

The pure tunneling case applies when

$$\frac{V}{2\phi} > t^2 \quad (64)$$

* ϕ is used to denote either ϕ_1 or ϕ_2 , where ϕ_2 is to be used when negative voltage is applied at the outer contact (negative polarity) and ϕ_1 with positive polarity.

and becomes

$$j = G_1 B V \exp \left[\frac{\phi}{kT_0} \sqrt{\frac{V}{2\phi}} \operatorname{ctn}^{-1} \sqrt{\frac{V}{2\phi}} \right] \quad (65)$$

where

$$G_1 = 1.14 \cdot 10^6 T_0 \sqrt{\frac{\phi}{\phi}} \frac{kT_0}{\phi} \exp \left[-b_{10} + \frac{\pi(\phi_1 - \phi)}{4kT_0} \right] \quad (66)$$

$$b_{10} = \frac{\phi_1}{kT_0} + \Delta_1$$

and B is given by Eq(34b). We have used the approximation $\operatorname{ctn}^{-1} \sqrt{\frac{V}{2\phi}} \simeq \frac{\pi}{2}$ in the coefficient of Eq(66). In the limiting case at the higher voltages and at 77°K we may assume $c_1 kT < 1/2$ and thus $B \simeq 1$ as can be verified by the results of the subsequent analysis. We then have for this limit

$$\frac{j}{V} \rightarrow G_1 \exp \left[\frac{\phi}{kT_0} \sqrt{\frac{V}{2\phi}} \operatorname{ctn}^{-1} \sqrt{\frac{V}{2\phi}} \right] \quad (67)$$

The nearly V^n dependence exhibited by the experimental results for j in this range suggests that we look for an approximation of this dependence from Eq(67).

One finds that a maximum exists in the theoretical slope n [i.e., $n = d \ln j / d \ln V$], occurring at $V/2\phi = .30$.

The value of the maximum then becomes

$$n_{\max} = 1 + .1775 \frac{\phi}{kT_0} \quad (68a)$$

However a more useful relation which gives a more

effective average near the maximum of the gradually changing n may be given by

$$n \approx 1 + \frac{\phi}{6kT_0} \quad (68b)$$

The slopes measured from sample #21-C4 [c.f. Fig III-17] give $n \approx 6.5$ and 5.4 for the positive and negative polarities respectively and thus $\phi_1/kT_0 \approx 33$ and $\phi_2/kT_0 \approx 26.6$. Thus we have the ratio $\phi_1/\phi_2 \approx 1.24$, which is the proper ratio corresponding to the photo-response measurements from which we may select (within the experimental uncertainty) the values $\phi_1 = 1.75$ ev and $\phi_2 = 1.40$ ev.

We may compare the theory with the experimental data of Fig. III-17 in this range by plotting $\log(j/V)$ versus $\phi \sqrt{V/2} \phi \operatorname{ctn}^{-1} \sqrt{V/2} \phi$ for both polarities. The result given in Fig IV-1 exhibits the predicted linear dependence with the slopes corresponding to $1/kT_0 \ln 10$. We thus obtain more precise values of T_0 which is essentially equal for the two polarities (i.e., 620°K and 630°K), therefore justifying our assumption of a constant T_0 . The values of ϕ/kT_0 estimated from n are seen to compare reasonably well with the more precise values obtained in this way. The value of j/V obtained by extrapolating to the zero of the abscissa must equal G_1 given by Eq(66). The value of b_{10} is thus determined and gives very nearly the same

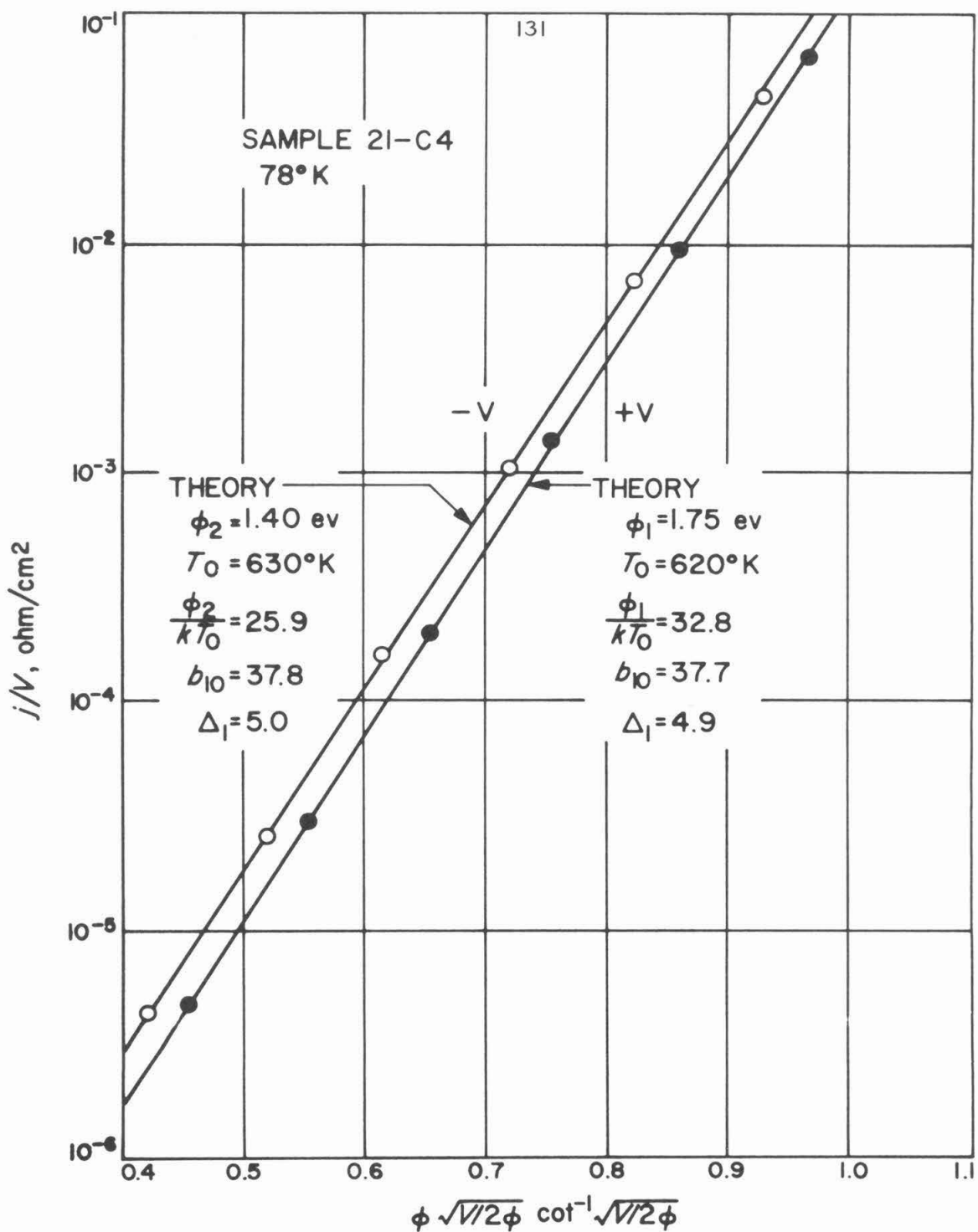


Figure IV-1. Limiting case of pure tunneling-comparison of theory with experiment.

result for each curve (i.e., $b_{10} = 37.8, 37.7$). Since $b_{10} = \phi_1/kT_0 + \Delta_1$, the correction Δ_1 is then obtained, giving 5.0 and 4.9.

The experimental results of Fig. III-15 can be compared with the theory at low voltages given by Eq(63), by plotting the data in the form $j/2kT\sinh(V/2kT)$ vs. V . The result in Fig. IV-2 indicates the predicted constant dependence on voltage except near the transition points $V \approx 2\phi t^2$. The deviation can be partly accounted for by a slight overestimate of the predicted intermediate tunneling current at the transition point. An additional effect may arise from a slight shift in the saddle point energy due to $\lambda(E)$ which was neglected in the theory [c.f. Eq(36)]. This could be interpreted equivalently as an increase in the effective hole temperature at the larger applied voltages leading to deviations such as observed.

The constant asymptotes must according to the theory equal G given by Eq(61). We may then compare the experimental results for G obtained from Fig. IV-2 with the theory by plotting $\log(Gt^{-3/2})$ versus t using the value $T_0 = 620^\circ K$. The result so obtained is given in Fig. IV-3. The deviation of the experimental points at low temperatures from the predicted linear

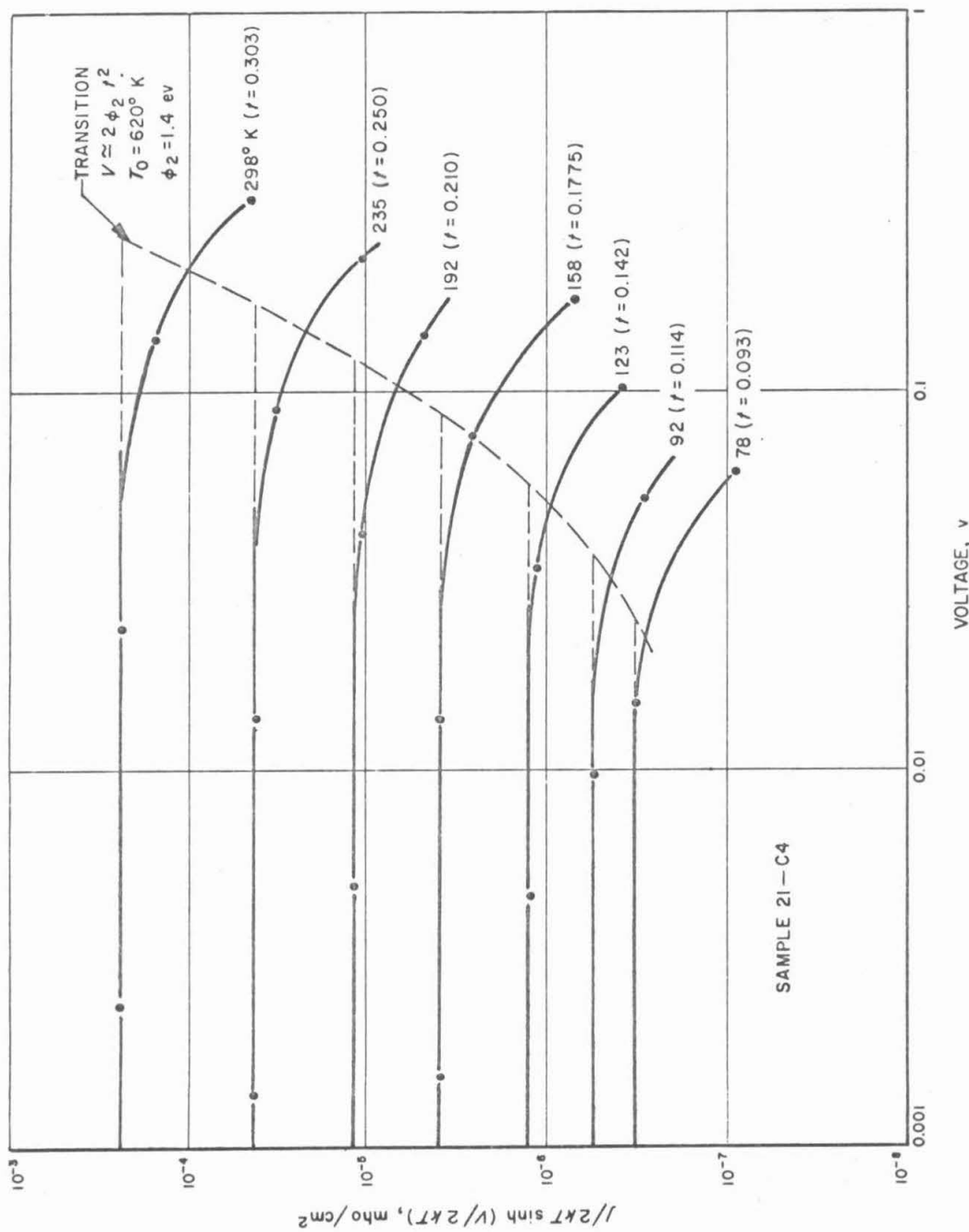


Figure IV-2. Intermediate case at low voltages-comparison of theory with experiment.

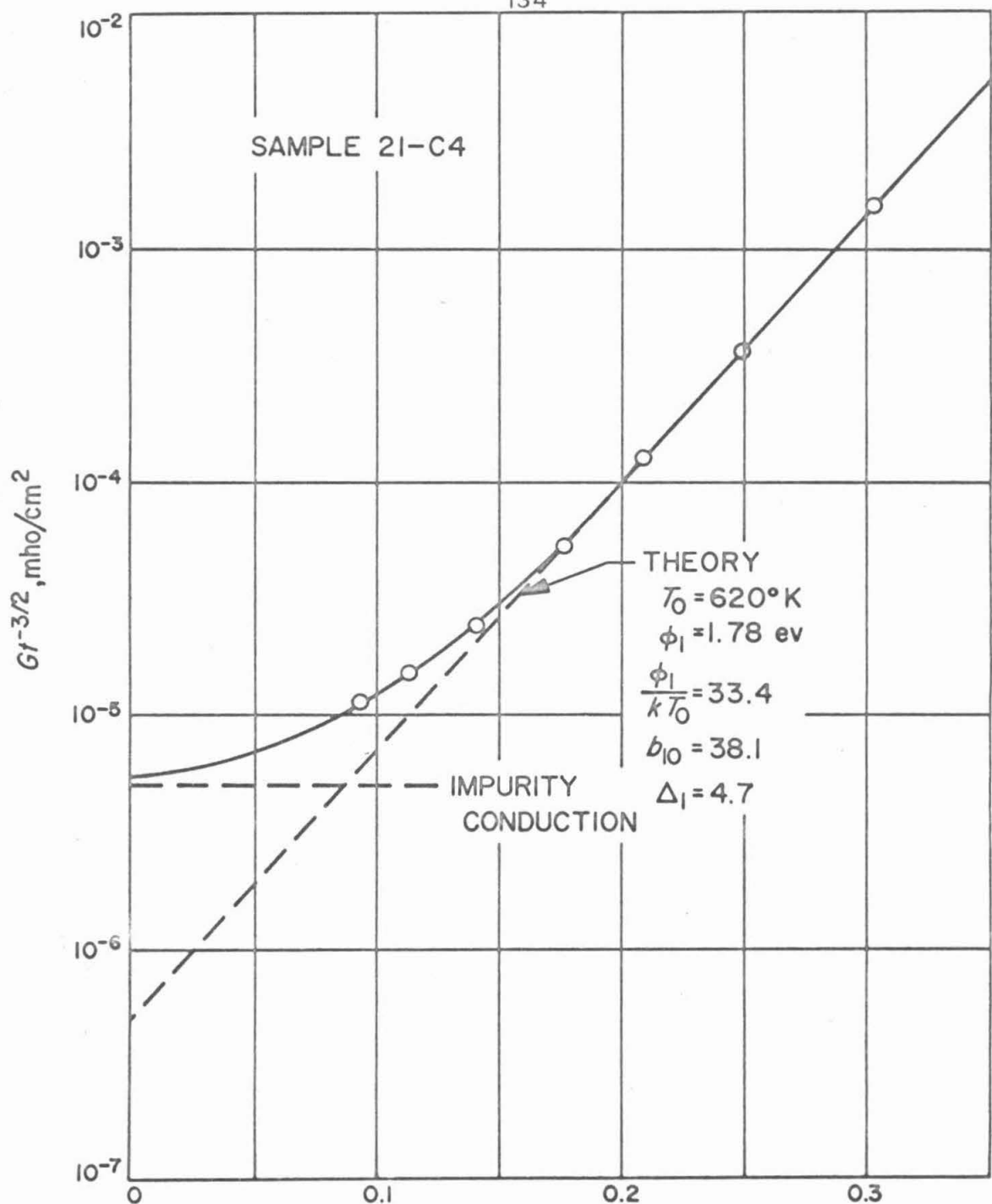


Figure IV-3. Dependence of zero field conductance on temperature-comparison of theory with experiment.

dependence is attributed to tunneling into impurity states (impurity conduction) which was neglected in the theory. By adding an impurity contribution $G_0 t^{-3/2}$ equal to $5 \cdot 10^{-6}$ mhos/cm² to the indicated asymptote, one obtains the solid curve representing a good fit to the experimental points. The theoretical asymptote gives a value of $\phi_1 = 1.78$ ev which is in good agreement with the predicted value of 1.75 ev. Correspondingly, ϕ_1/kT_0 becomes 33.4. The extrapolated value of $Gt^{-3/2}$ at $t=0$ must equal the expression given by Eq(61) and thus we obtain $b_{10} = 38.1$ and $\Delta_1 = 4.7$ which is also in good agreement with the values obtained above. It is interesting to note that the small differences are in the correct direction one would expect from the effect of an additional image force lowering of the barrier height with an applied field, which was neglected in the theory.

The temperature dependence predicted when pure tunneling applies at the higher voltages is given by the coefficient $B \exp \left[\frac{\pi(\phi_1 - \phi_2)}{4kT_0} t \right]$ where B is evaluated for the appropriate barrier [i.e., ϕ_1 for positive polarity and ϕ_2 for negative polarity]. Inserting the appropriate expressions one obtains for -.5 volts,

$$\frac{j}{j_0} = \frac{1.194 \exp(5.15 t)}{\frac{378}{\pi T} \sin\left(\frac{\pi T}{378}\right) + .194}$$

and for + .5 volts,

$$\frac{j}{j_0} = \frac{1.142}{\frac{330}{\pi T} \sin\left(\frac{\pi T}{330}\right) + .142}$$

where j_0 corresponds to the current at $T=0^\circ K$. These relations are compared with the experimental results in Fig. IV-4. Although the observed dependence is somewhat steeper than predicted, a better fit could clearly be obtained by a small adjustment of the parameters. This would hardly be justified in view of other second order effects which have been neglected such as the temperature dependence of the dielectric constant.

The correction Δ_1 may be compared with the expression given by Eq(44) which may be written in the form

$$\Delta_1 = \frac{\pi}{8} \left(\frac{x_0}{s} \right)_1 \frac{\phi_i}{kT_0}$$

where

$$\left(\frac{x_0}{s} \right)_1 = \sqrt{\frac{q \propto}{2 \kappa_0 \sqrt{\phi_i \phi_i}}} . \quad [c.f. \text{ Eqs (17a) \& (51)}]$$

Inserting the values obtained for zero applied voltage and using $\kappa_0 = n^2 = 3.3$ from Fig. III-5 and assuming $m^*/m=1$ (thus $\propto = 1.03(\text{ev})^{-1/2} \text{ \AA}^{-1}$) one obtains

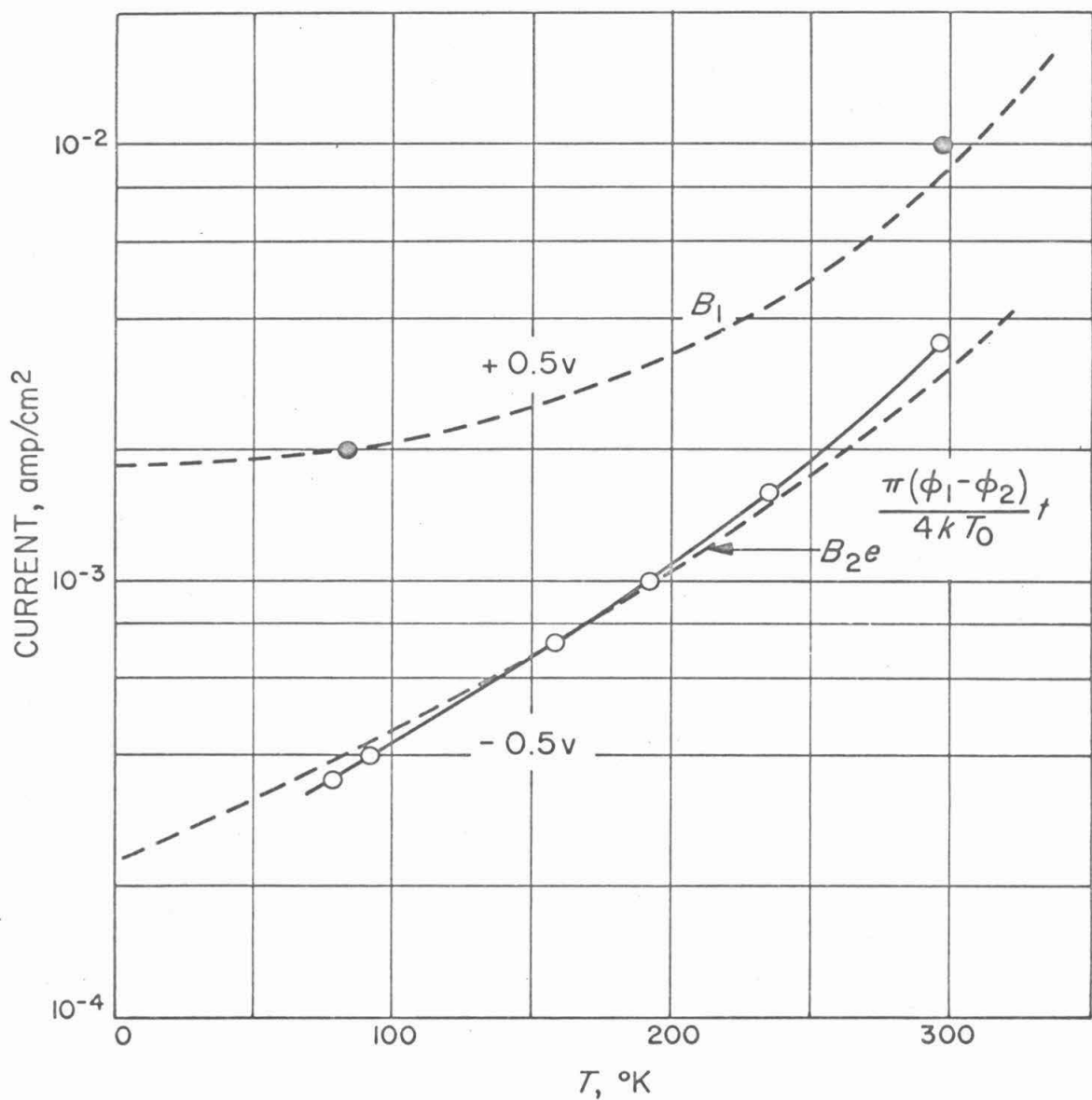


Figure IV-4. Dependence of tunneling current on temperature—comparison of theory with experiment.

$$\left(\frac{x_0}{s}\right)_1 = .228$$

and

$$\Delta_1 = 3.0$$

Therefore the value predicted for Δ_1 by our approximations underestimates the measured values of 4.7-5.0. This is quite understandable if the point made earlier is valid, that is, if a different effective impurity concentration occurs immediately adjacent to each of the contacts, accounting for the different barrier heights. We would then expect a correspondingly larger Δ at the larger barrier than would be characterized by the parameter T_o which is common to both barriers. Alternately, there may be a small contribution from the oxide interior which was neglected and would appear as an effective increase in Δ .

It is of interest to calculate the maximum acceptor concentration N_A from the definition of T_o given by Eq(51). That is if we assume $\kappa = 27.5$, $m^*/m = 1$ and $T_o = 620^\circ K$, we have

$$N_A = \frac{\kappa}{4\pi q} (2\alpha ckT_o)^2 \simeq 1.8 \cdot 10^{21} \text{ cm}^{-3}$$

or about 5.5 mole percent. This corresponds roughly to the saturation concentrations quoted in the literature.

3. Capacitance Dependence. The capacitance may be expressed in terms of the sum of the effective barrier widths in the oxide film, that is

$$\frac{A}{C} = \frac{4\pi}{\kappa} (\Delta x + x_1 + x_2) \quad (69)$$

where C/A is the capacitance per unit area, x_1 and x_2 represent the effective widths of the first and second barrier respectively and Δx represents the total width due to the image force corrections ($\approx 2x_0$) plus any additional contribution of holes trapped in the oxide interior which depends on frequency as discussed in Section III C. We can express x_1 and x_2 by the barrier widths at the saddle point energy from Eq(55), that is

$$U(x_1) - \frac{V}{2} = (\phi_1 + \frac{V}{2}) e^{-x_1/s_1} = \phi_1 t^2$$

or $x_1 = s_1 \left[\ln \left(1 + \frac{V}{2\phi_1} \right) - 2 \ln t \right] \quad (70a)$

and similarly $x_2 = s_2 \left[\ln \left(1 + \frac{V}{2\phi_2} \right) - 2 \ln t \right] \quad (70b)$

where V represents the applied dc voltage with positive polarity corresponding to positive voltage at the first contact (ϕ_1). We have used the intermediate case for the saddle point energy ($\phi_1 t^2$) on the assumption that only small ac voltages are used in measuring the capacitance. The

dc voltage will only affect the steady state barrier shape as indicated by Eq(70), with the dc current acting independent of the small ac fluctuations. The sum $x_1 + x_2$ is nearly independent of dc voltage when the voltage and the difference in barrier heights are not too great. If we write

$$\phi_1 = \phi_o + \Delta\phi$$

$$\text{and } \phi_2 = \phi_o - \Delta\phi$$

and expand to second order terms of $V/2\phi_o$ and $\Delta\phi/2\phi_o$,

we obtain

$$x_1 + x_2 \approx s_o \left[-4 \ln t + \frac{V}{2\phi_o} \left(\frac{\Delta\phi - V}{2\phi_o} \right) \right] \quad (71)$$

where

$$s_o = \frac{s_1 + s_2}{2} \quad (72)$$

Therefore the capacitance changes negligibly with dc voltage when $V/2\phi_o \ll 1$. At dc voltages larger than the barrier height at the negative contact the voltage can no longer be assumed to divide equally between the barriers as assumed for Eq(70), and a greater share of the voltage must then occur across the positively biased barrier resulting in a net increase in the total barrier width. The capacitance will then decrease until the barrier extends across the width of the oxide. This kind of dependence on dc voltage is in qualitative agreement with the result given in Fig III-21. One also observes that the decrease in

capacitance occurs sooner for positive polarity which is consistent with the fact that the larger barrier ϕ_1 occurs at the outer contact. The onset of the rapid decrease in capacitance is seen to occur in the vicinity of the barrier height associated with the negatively biased contact. The limit where the barrier extends across the oxide film could not be reached before breakdown occurred.

In the case of the anodized films with Au and Ti contacts we can expect a larger variation with dc voltage. We have proposed that an electronic conduction process occurs for these samples and that the voltage must divide between the two barriers as with two independent series resistances. Since the barrier at the Au contact was seen to be much more effective than at the Ti contact and therefore dominates until it is nearly suppressed by sufficiently large positive voltages (at the Au contact), we can express the capacitance dependence on voltage in this case approximately by*

$$\frac{A}{C} \approx \frac{4\pi}{\kappa} \left[s_1 \ln \left(1 - \frac{V}{\phi} \right) + \Delta x_0 \right]$$

where Δx_0 is the total effective barrier width at zero

*The change in sign of V corresponds to the electron conduction process for this case.

applied voltage. A more convenient form is

$$\ln\left(1 - \frac{V}{\phi_i}\right) = C_s \left(\frac{1}{C} - \frac{1}{C_i}\right) \quad (73a)$$

where $C_s = \frac{\kappa A}{4\pi s_1}$ (73b)

and $C_i = \frac{\kappa A}{4\pi \Delta x_0}$ (73c)

is the capacitance at zero applied voltage. In Fig. II-4 we have plotted the data in the form corresponding to Eq(73) using the average value obtained for the Au barrier height (i.e., $\phi_i = 1.42$ ev). The predicted linear dependence agrees within the experimental uncertainties, with the expected deviation occurring when $+V$ approaches ϕ_i . From the measured value of the slope, $C_s = 5400 \text{ pf}$, and using $\kappa = 27.5$ and $A = 5.5 \cdot 10^{-4} \text{ cm}^2$, we calculate from Eq(73b) $s_1 = 10.7 \text{ \AA}$. It is interesting to compare this value with that obtained from the above results for sample #21-C4. From the definition of T_o given by Eq(51).

$$s = \frac{\sqrt{\phi}}{2\alpha k T_o}$$

and assuming $m^*/m=1$, one calculates $s_1 = 12.1 \text{ \AA}$ and $s_2 = 10.9 \text{ \AA}$. The similarity in the values of s for different kinds of samples is required by our model in order to describe reasonable barriers, consequently these results are

also encouraging.

The temperature dependence of the capacitance at zero dc bias is also predicted by Eqs (69) and (70) for the samples with Al contacts. This may be expressed in a more convenient form by

$$t = \exp \left[\frac{\Delta x}{4s_o} - \frac{\kappa}{16\pi s_o} \frac{A}{C} \right] \quad (74)$$

where s_o is defined in Eq(72). The experimental data taken at 5 kc (see Fig. III-18) is plotted in Fig. IV-5. The semi-log plot of the results exhibits the predicted linear dependence with the slope giving

$$\frac{s_o}{\kappa} = .328 \text{ \AA}$$

Using the values of s_1 and s_2 given above for $m^*/m = 1$, we have $s_o = 11.5 \text{ \AA}$ and thus obtain $\kappa = 35$. This is in reasonably good agreement with the value $\kappa = 27.5 \pm 2.0$, since the uncertainty in the area alone is easily $\pm 10\%$ and of course we have assumed $m^* = m$. There is also the possibility that the value 27.5 may have been reduced by a lower dielectric constant in the interior of the thick oxide film used in the measurement.

The value of $\Delta x/4s_o$ may be obtained from the position of the curve and gives at 5 kc, $\Delta x/4s_o = .97$.

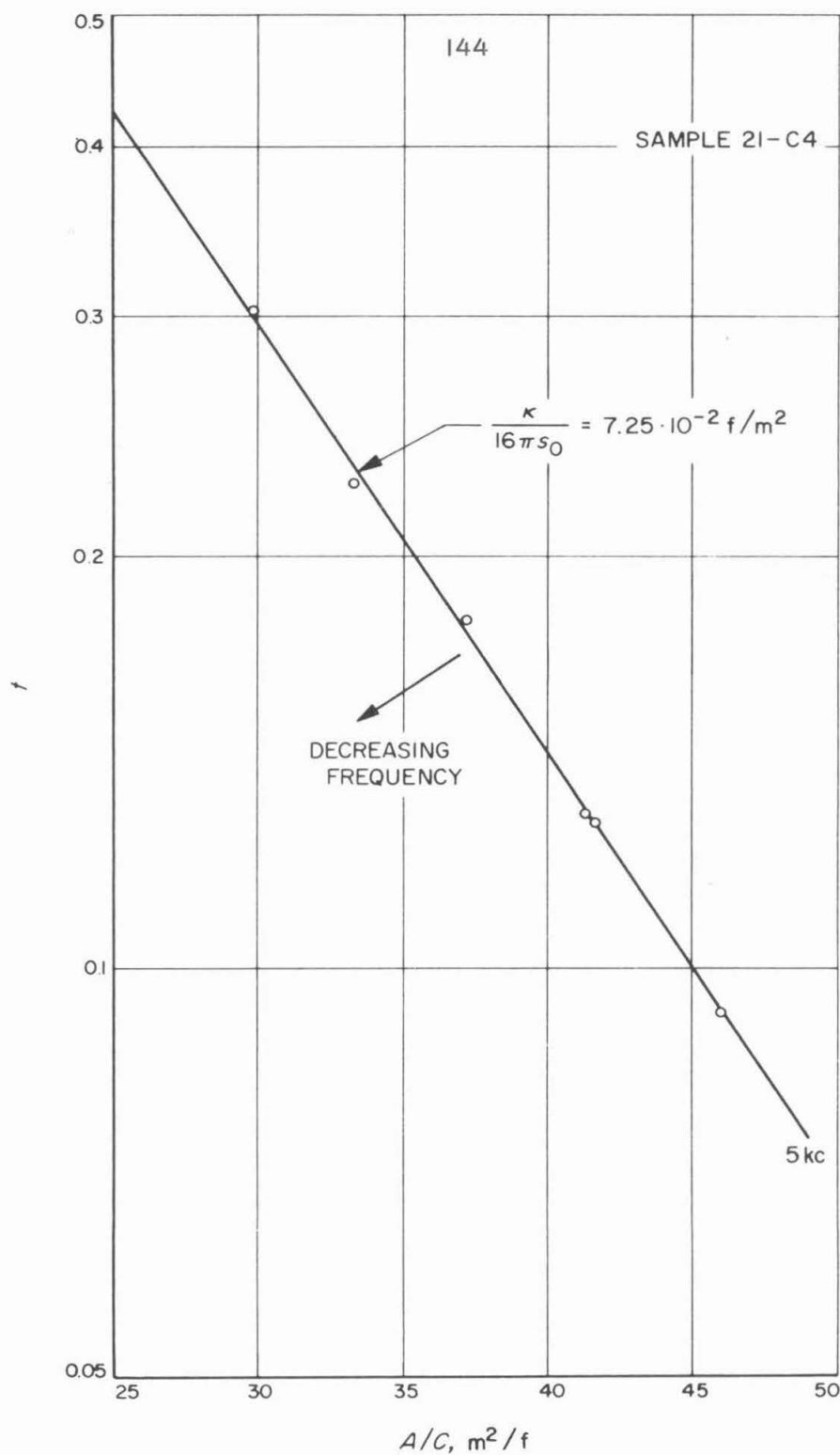


Figure IV-5. Dependence of capacitance on temperature-comparison of theory with experiment.

This value decreases with decreasing frequency as indicated by the corresponding increase in capacitance (see Fig. III-18) which we have related to the effect of trapped holes. In the dc limit we would predict that $\Delta x/4s_0$ should approach $x_0/2s_0 \approx .15$. The results are quite consistent with this prediction, especially since the values obtained depend on the difference of two larger quantities and become very sensitive to the error in the area measurement.

V. CONCLUSIONS

The electrical properties of thin TiO_2 films have been interpreted in terms of a physical model that considers the effect of large impurity concentrations on the shape of the barrier potential. If we consider only the general features of such barriers before making any specific assumptions on the impurity distribution in the oxide, we are able to arrive at a qualitative understanding of a variety of results that would defy explanation on the basis of the usual model of insulating films. For example the electrical forming effects observed in anodized films are readily understood in terms of the change occurring in a narrow space charge barrier as the distribution of ionized impurities is disturbed by the applied field. Similarly one can qualitatively interpret the I-V characteristics and the capacitance variation on the basis of the general model. A more specific model was required in order to formulate a quantitative description of the properties.

In formulating a quantitative theory we have treated two different barrier shapes (quadratic and exponential) that arise on the basis of certain assumptions concerning

the distribution of ionized impurities. The two kinds of barriers may in a sense be considered limiting cases for the impurity distribution so that the analysis of the experimental results provides us with a means of evaluating the kind of distribution that actually occurs in the barrier. We have found that the theory formulated in terms of the exponential barriers is in good agreement with the experimental results, and therefore conclude that the actual barriers can be very nearly represented by an exponential form. In Section IV A we have offered three possible physical reasons for predicting barriers of this kind which are essentially indistinguishable on the basis of our results. However the sensitivity of the barrier to the contact metal (Au or Al) suggests that the most important reason may be associated with a rate-limited diffusion process from the contacts. On the other hand, this effect does not exclude the possibility of a Poisson-Boltzmann type of distribution. Furthermore the impurity states may also be distributed over different energies in the forbidden band (the third possible reason) in addition to either or both of the other possibilities and still obtain the same kind of barrier.

A serious difficulty discussed^(7,34) in connection with the early interpretations of a tunneling-type process

at metal-semiconductor contacts involves the extreme sensitivity of the barrier resistance to its effective width. This is readily resolved in terms of our model since we have considered the barrier only in terms of the interaction between the oxide and the metal contact and the maximum impurity concentration that occurs in the oxide. The analysis of our experimental results has indicated that the impurity distribution is determined by the saturation concentration of impurities (acceptors) at the contact and therefore it does not depend in a sensitive manner on the precise conditions for its formation or the total thickness of the film. The effect of film thickness has been interpreted in terms of an additional effect in the oxide interior which we have successfully avoided in our detailed treatment of the experimental results by an appropriate choice of samples.

In order to obtain a consistent description of our results we have concluded that the evaporated titanium oxide films with Al contacts must be p-type. This conclusion is of particular significance in view of the fact that it is ordinarily difficult to obtain p-type rutile in bulk form. For samples prepared with Au contacts we have offered more qualitative arguments that indicate that the oxide films in this case are probably n-type.

A key device introduced in the development of the theory involves the treatment of the energy distribution of holes in the p-type oxide films under applied voltage. By introducing an unknown multiplier λ that only modifies the equilibrium distribution at higher energies in a reasonable manner and eliminating λ from the equations under steady state conditions, we arrive at explicit relationships for the current and capacitance as a function of voltage and temperature. The success of the theory in describing the experimental results leaves little doubt as to the validity of this approach. We therefore suggest that this approach may also be useful in other two barrier problems where intermediate transitions of an indeterminate nature are involved in the steady state process.

Finally, our TiO_2 films which were shown to be essentially amorphous, exhibited properties that could be related to rutile. We therefore are inclined to believe that the short range structural order of the films is essentially that of rutile. However, this relationship cannot be carried too far, since the large degree of disorder in the film could easily permit a similar relationship to other structural modifications of TiO_2 (anatase and brookite). In this respect the values measured for the dielectric constant and refractive

index of the films are more consistent with the lower values reported for the other crystalline forms of TiO_2 .

APPENDIX A

PROPERTIES OF RUTILE

Rutile is the most stable crystalline form of TiO_2 .

Other forms (anatase and brookite) are irreversibly converted to rutile when heated between 700 and 920°C. The crystal structure of rutile is in the tetragonal class with lattice constants $a = 4.5937 \text{ \AA}$ and $c = 2.9581 \text{ \AA}$. The structure may be considered composed of slightly distorted TiO_6 octahedra with one pair of Ti-O bonds being slightly longer than the other two pairs (1.94 and 1.99 \AA). The bonding forces often considered to be ionic (based on Ti^{4+} and O^{2-} ions), have been shown to also possess an appreciable covalent contribution⁽¹⁶⁾.

The energy band structure may be considered in terms of the electronic configurations of the ions. The filled 2p levels of the O^{2-} ion are broadened to form the valence band. The normal electronic configuration of the titanium atom is $(4s)^2(3d)^2$ outside its argon core, and the conduction band is generally believed to arise from the unfilled 3d levels of the Ti^{4+} ions, with the 4s levels forming a broad band at higher energies. Morin⁽³⁹⁾ has also

indicated on the basis of orbital theory that the 3d band may also be split into narrow $d\epsilon$ and $d\delta$ bands. In accounting for the observed low mobilities in rutile, it is generally believed that the 3d levels overlap slightly to form a narrow 3d conduction band and not extending to the much broader 4s band. There still remains some question about the band structure although extensive experimental results have been reported.

The reported measurements of the band gap vary considerably and we can only attempt to give our interpretation. Cronemeyer⁽⁴⁰⁾ obtains from conductivity measurements, taken over a wide range at higher temperatures, two well defined activation energies which are interpreted in terms of energy gaps of 3.05 and 3.7 ev. From optical transmission measurements, he obtains an energy gap of 3.03 ev. From photoconductance of reduced rutile, he obtains energy gaps in the range of about 2.8 to 3.0 ev, the value increasing with decreasing temperature. The evidence suggests that the 3d band occurs at about 3.05 ev above the valance band, with the 3.7 ev energy possibly associated with the $d\delta$ or 4s band, and the 2.8 to 3.0 ev energies, with a donor impurity band.

Most of the results reported by other investigators can be related to one of the above values or some combination of them. For example, Rudolph⁽³¹⁾ reports 3.12 ev; Earle⁽⁴¹⁾ 3.4 ev; and Sandler [see Ref (16)] 2.8 ev. Although the optical absorption edge in thick rutile crystals is consistently observed near 3 ev, the optical dispersion reported by De Vore⁽³⁰⁾ and others indicates a higher natural absorption energy above 4 ev that may relate to the influence of the broad 4s band. This is consistent with the reflectance peaks at 4.0 and 4.13 ev reported by Nelson and Linz⁽⁴²⁾ from oriented single-crystal rutile for directions perpendicular and parallel to the c-axis respectively. The optical absorption edge for thin polycrystalline films was also found by the above authors to occur near 3.9 ev, with similar results reported by Cronemeyer⁽⁴⁰⁾ and also obtained in this investigation (see Section III B). It would appear that the absorption due to the narrow 3d band which is important in relatively thick crystals becomes less important in thin films and one then observes the stronger absorption due to the much broader 4s band. Conductivity measurements at high temperatures reported by Hauffe [see Ref (16)] indicate an energy gap of about 3.9 ev that may similarly

relate to the greater importance of the broad 4s band at high temperatures. Our measurements on rutile described in Appendix B are also consistent with the above interpretation of the band gaps occurring near 3 and 4 ev, corresponding to the 3d and 4s conduction bands respectively. In addition the photo-response measurements also suggest an additional impurity band at about 2.8 ev.

The conductivity of rutile is usually generated by a reduction process, which is commonly believed to form oxygen vacancies, each of which may act directly as a donor center or alternately cause two adjacent Ti^{4+} ions to convert to Ti^{3+} donor sites. Grant⁽¹⁶⁾ has summarized the effects of various other impurities investigated which can be classified as either donors (e.g., W, P, Sb, V, Ta, Nb) or as acceptors (e.g., Al, Fe, Ga, Y). The latter have been characterized by their ability to compensate for donors, however p-type rutile also has been observed under certain conditions^(27,31). The impurity concentrations generally tend to saturate at a few mole per cent, and Ehrlich⁽⁴³⁾ has determined the maximum concentration of oxygen vacancies before structural changes occur to be 5 mole per cent. Although no detailed information has been found in the literature on the diffusion constants, the

conditions reported for obtaining uniformly reduced rutile samples^(40,44) indicate large values for the diffusion constant of oxygen vacancies in rutile, that is, the order of $3 \cdot 10^{-8} \text{ cm}^2/\text{sec}$ at 350°C and $10^{-5} \text{ cm}^2/\text{sec}$ at 800°C , and thus an activation energy the order of .8 ev. These values are consistent with the large effects of ionic drift observed in rutile under applied fields.

The dielectric constant of rutile is given as 173 for the c-direction and 89 for the a-directions. The average of 117 compares with values the order of 100 measured for ceramic rutile. Similarly ceramic rutile exhibits electrical properties comparable to single-crystal rutile, with electron mobilities for reduced specimens measuring the order of $.1$ to $1.0 \text{ cm}^2 \text{ volt}^{-1} \text{ sec}^{-1}$. The additional scattering due to grain boundaries in ceramics appears to be masked by the strong coupling of electrons with the polar modes of lattice vibrations (polarons). Correspondingly large effective masses are usually quoted for reduced rutile ranging from 1 to 1000 times the free electron mass but more commonly indicated to be the order of 25. This is consistent with a narrow 3d conduction band, the very large values possibly representing the larger polaron mass. Although extremely large donor concentrations are usually produced in reduced

rutile (e.g., in excess of 10^{20} cm^{-3}) the material is not degenerate, exhibiting distinct activation energies centering around .1-.2 ev at higher temperatures and the order of .01 ev at very low temperatures. The large values of activation energies cannot be interpreted in terms of the usual hydrogenic model of donor states but may be interpreted by the polaron self-trapping energy as discussed by Frederikse⁽¹⁷⁾. The low energies may be associated with the true binding energy of the donors. The polaron effect is strongly related to the coupling constant α_p as discussed by Fröhlich⁽⁴⁵⁾. If one uses the values of 50μ for the restrahlen wave length, as measured by several investigators, and the refractive index of about 2.5, one obtains $\alpha_p \approx 4(m^*/m)^{1/2}$. If α_p is greater than about 6, strong coupling occurs accompanied by a very large polaron mass. Thus one can easily expect a strong polaron effect in reduced rutile since m^*/m is believed to be greater than 2.

APPENDIX B

EXPERIMENTS ON RUTILE

Single crystal rutile purchased from Linde Air Products was sliced into specimens approximately $.1 \times .2 \times 1.0$ cm, with the c-direction parallel to their lengths. The specimens were reduced at 650°C in H_2 for ten minutes. The resistivity of the reduced specimens was approximately 2 ohm-cm, and comparing this with published data, the carrier concentrations at room temperature are estimated to be the order of $10^{18} - 10^{19} \text{ cm}^{-3}$ and donor concentrations greater than 10^{20} cm^{-3} . The specimens were prepared with Au contacts by immediately evaporating a thin film of Au ($\approx 500 \text{ \AA}$) on surfaces freshly exposed after fracturing the specimen in a vacuum. A true cleavage could not be obtained, but a smooth surface was exposed when the specimens fractured, lying approximately along a plane perpendicular to the c-axis. The areas of the gold contacts were defined after the evaporation by carefully scraping the Au film away from the boundary of the desired area. The opposite contacts were made by soldering indium to the other surfaces of the specimen. They introduced no detectable contact resistance at room

temperature.

The photo-response from the Au contact was measured with -1.5 volts applied at the contact. The results are plotted in Fig. B-1 in the manner described in Section IIB. The large response extrapolates to 3.05 ev, the value believed to represent the energy gap from the valance band to the 3d conduction band. A second peak above 4 ev may arise from the additional contribution from the 4s band. Direct observation of the energy gap to this band is partially masked by the effect of the lower 3d band but appears to be in the general vicinity of the suspected value of about 4 ev (see Appendix A). The tail in the response which extrapolates to 2.8 ev is believed to represent transitions to a donor band. The small response at lower energies is interpreted to arise from electrons excited from the Au contact into the conduction band of the underlying rutile crystal, and thus the extrapolation to 1.4 ev gives the barrier height at the Au contact. This is in close agreement with the results obtained from both anodized and evaporated TiO_2 films with Au contacts (see sections IIB and IIIB).

The capacitance at 100 kc was measured at room temperature as a function of dc voltage. The capacitance

exhibited considerable drift with time unless the sample was first electrically formed by applying a sufficient positive dc voltage at the Au contact for several minutes. The results obtained from a sample at room temperature after forming at +.5 volts for 15 minutes are plotted in Fig. B-2. The usual theory of a metal-semiconductor barrier gives the dependence $(A/C)^2 = \frac{8\pi}{\kappa}(V_o - V)/qN_D$ where N_D is the donor concentration and V_o is the built in potential at the barrier equal to the barrier height less the equilibrium potential at the limit of the space charge region, (i.e., $V_o = \phi - \eta_o$). Thus the result gives the predicted linear dependence of $(A/C)^2$ vs. V with the intercept equaling 1.35 ev, consistent with the measured barrier height. The difference would predict $\eta_o \approx .05$ ev which is quite reasonable, although the experimental accuracy does not permit this result to be taken too seriously. The electrical forming is believed to cause positively ionized donors to drift out of the space charge region into the interior of the specimen, correspondingly reducing the concentration N_D at the tail of the space charge region. From the slope of the dependence the effective donor concentrations N_D is estimated to be approximately $6 \cdot 10^{17} \text{ cm}^{-3}$ which is considerably less than the average value for the crystal but is consistent with the

forming process proposed.

Optical transmission measurements were obtained from a polished slice of unreduced rutile, sliced 1 mm thick perpendicular to the c-axis. The result indicated a sharp absorption edge at 3.06 ev in agreement with the results obtained by other investigators and the value believed to be the energy gap (to the 3d band). No effects of a donor band at lower energies could be detected in this case. A small residual transmission barely detectable above the noise persisted out to approximately 4 ev and may have been related to the 4s band.

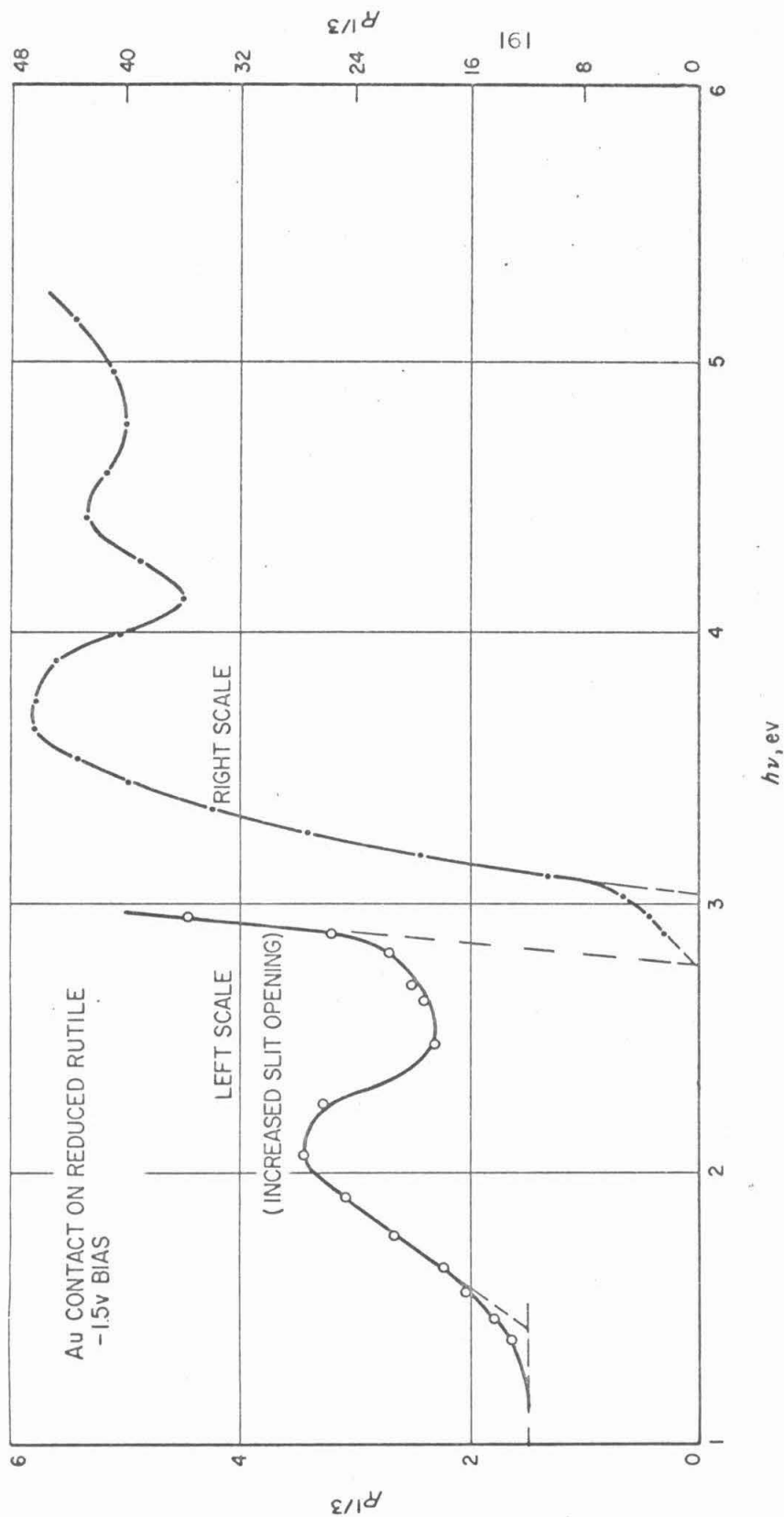


Figure B-1. Photo-response of rutile (Au contact).

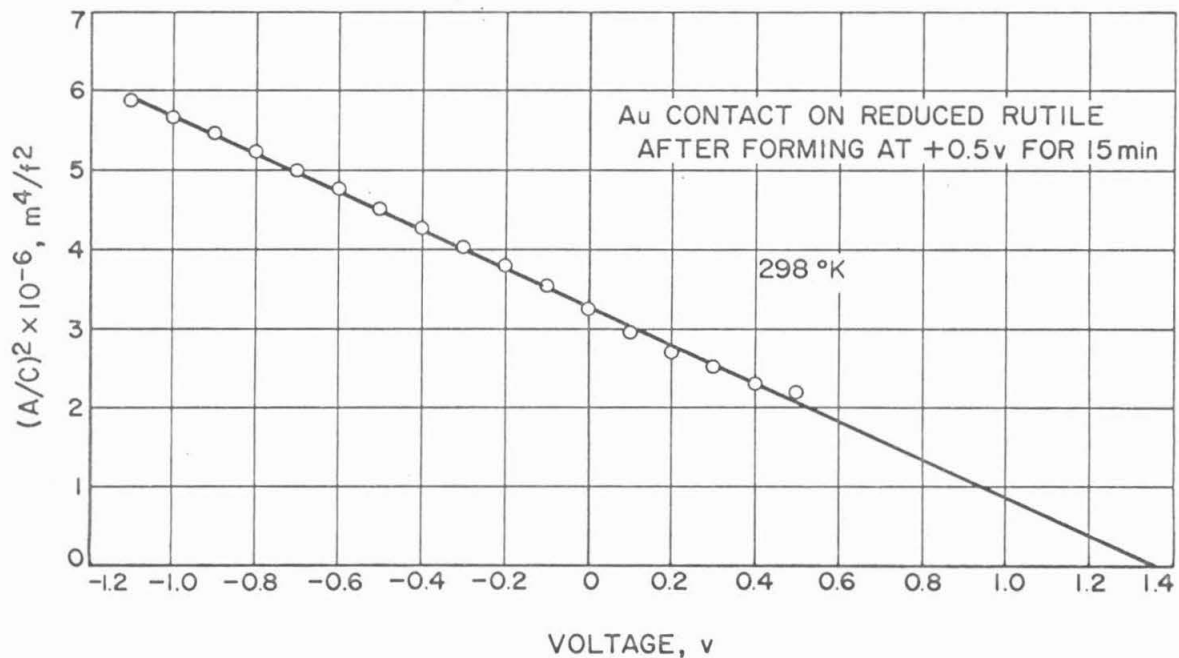


Figure B-2. Dependence of capacitance on dc voltage.

REFERENCES

1. A.Schuster, Phil.Mag. and J.Science 48, 251 (1874).
2. J.Frenkel, Phys.Rev. 36, 1604 (1930).
3. A.H.Wilson, Proc.Roy.Soc. (London) A136, 487 (1932).
4. L.Nordheim, Zeits.f.Physik 75, 434 (1932).
5. J.Frenkel and A.Joffé, Phys.Zeits.d.Sowjetunion 1, 60 (1932).
6. W.Schottky and F.Waibel, Naturwiss. 20, 297 (1932); W.Schottky and W.Hartmann, Zeits.f.techn.Physik 16, 512 (1935); Naturwiss.24, 558 (1936).
7. N.F.Mott and R.W.Gurney, Electronic Processes in Ionic Crystals, Dover Publications, New York (1964); pp. 176 - 185.
8. C.A.Mead, J.Appl.Phys. 32, 646 (1961).
9. I.Gaiever and K.Megerle, Phys.Rev. 122, 1101 (1961).
10. J.G.Simmons, J.Appl.Phys. 34, 1793 (1963).
11. R.Stratton, J.Phys.Chem.Solids 23, 1177 (1962).
12. T.E.Hartmann and J.S.Chivian, Phys.Rev. 134, A1094 (1964).
13. M.McCall, Electron Current through Thin Mica Films, Phd Thesis, Calif.Inst.Tech., Pasadena, Cal.(June'64).
14. N.F.Mott, Proc.Roy.Soc. A171, 27 (1939).
15. W.Schottky, Zeits.f.Physik 13, 367 (1939).
16. F.A.Grant, Revs.ModernPhys. 31, 646 (1959).

17. H.P.R.Frederikse, *J.Appl.Phys.* 32, 2211 (1961).
18. L.E.Hollander, Jr. and P.L.Castro, Report LMSD-894803, Lockheed Missiles and Space Div., Sunnyvale, Calif.
19. L.Young, Anodic Oxide Films, Academic Press, London (1961).
20. A.Rose, *Phys.Rev.* 97, 1538 (1955).
21. S.R.Pollack, W.O.Freitag and C.E.Morris, *Journal Electrochem. Soc.* 1, 96 (1963).
22. D.Meyerhofer and S.A.Ochs, *J.Appl.Phys.* 34, 2535 (1963).
23. W.G.Spitzer and C.A.Mead, *J.Appl.Phys.* 34, 3061 (1963).
24. A.M.Cowley, Tech.Rept.No. 0414-1, Electron Devices, Stanford, Calif. (May 1965).
25. G.W.Gobezi and F.G.Allen, *Phys.Rev.* 137, 245 (1965).
26. A.Joffé, T.Kurchatoff, and K.Sinelnikoff, *J.Math.Phys.* 6, 133 (1927).
27. V.Ya.Kunin, Yu.N.Sedinov, and A.N.Tsikin, *Sov.Phys.-Solid State* 5, 2028 (1964).
28. J.A.vanRaalte, *J.Appl.Phys.* 36, 3365 (1965).
29. C.A.Mead, *Phys.Rev.* 128, 2088 (1962).
30. J.R.DeVore, *J.Opt.Soc.Am.* 41, 416 (1951).
31. J.Rudolph, *Z.Naturforsch.* 14a, 727 (1959).
32. R.Fowler and L.Nordheim, *Proc.Roy.Soc. (London)* A119, 173 (1928).

33. R.S.Muller, Physics of Semiconductors, (Proc. 7th Intern. Conf., Paris), Academic Press, London (1964); p.631.
34. H.K.Henisch, Rectifying Semi-Conductor Contacts, Oxford Univ. Press, London (1957); Ch.7.
35. J.Frenkel, Kinetic Theory of Liquids, Oxford Univ. Press, London (1946); p.38.
36. Ibid; p.127.
37. E.L.Murphy and R.H.Good,Jr., Phys.Rev. 102, 1464 (1956).
38. D.Bohm, Quantum Theory, Prentice Hall, New York (1952); pp. 283 - 288.
39. F.J.Morin, Bell System Tech.J. 37, 1047 (1958).
40. D.C.Cronemeyer, Phys.Rev. 113, 1222 (1959).
41. M.D.Earle, Phys.Rev. 61, 56 (1942).
42. C.W.Nelson and A.Linz, Tech.Rept. No. 184, Laboratory for Insulation Research, Mass.Inst.Tech., Cambridge, Mass. (Dec.1963).
43. P.Ehrlich, Z.Elektrochem. 45, 362 (1939).
44. R.G.Breckenridge and W.R.Hosler, Phys.Rev. 91, 793 (1953).
45. H.Fröhlich in Polarons and Excitons, Ed.C.G.Kuper and G.D.Whitfield, Plenum Press, New York (1963).